LEACHING KINETICS
OF
SYNTHETIC HEAZLEWOODITE

Y. Zaayman
Hons. B.Sc. (PU for CHE)

Dissertation submitted in partial fulfilment of the requirements for the degree *Magister Scientiae* in Chemistry at the North-West University

Supervisor: **Dr. G. Lachmann (North-West University)**
Co-supervisor: **Prof. O.S.L. Bruinsma (North-West University)**

Potchefstroom
2004

CONTENTS

SUMMARY

The sources of base metals are mainly in the form of oxides or sulphides, of which the sulphides are predominantly present in South Africa. These metals are intergrown platinum group and base metals in the form of alloys and sulphides. In order to produce high grade saleable metals, it is necessary to effectively separate the base metals from the precious metals.

By means of a hydrometallurgical process, that is leaching, metals can selectively be extracted from ores. The mechanism of leaching can be described by oxidation-reduction and acid-base reactions.

During this study, the leaching of a synthetically prepared heazlewoodite (Ni_3S_2) nugget was investigated. The parameters that were studied during the thermal leaching investigation are:

- different acids;
- different temperatures;
- nitrogen and oxygen;
- copper(II) and iron(III) ions.

The influence of these parameters is discussed. It was found that the leaching rate appears to be dependant on the orientation of the crystals. The leaching process is partly an oxidation process, which is enhanced by the addition of strong oxidants. This was seen by the high leaching rates yielded by nitric acid. Oxygen and iron(III) also accelerated the dissolution process. Leaching rates were typically in the order of 0.87 ± 0.02 $mg.m^{-2}.s^{-1}$ in 0.5 $mol.dm^{-3}$ H_2SO_4 under an oxygen atmosphere. This rate increased to 12.4 ± 0.20 $mg.m^{-2}.s^{-1}$ and 15.8 ± 0.13 $mg.m^{-2}.s^{-1}$ in the presence of Fe(III) and Cu(II) ions under an oxygen atmosphere, respectively.

Two activation energies were calculated from the thermal data. These values were found to be 28.2 $kJ.mol^{-1}$ for the initial leaching rate, and 45.75 $kJ.mol^{-1}$ for the final leaching rate. These values are indicative of a surface chemical rate determining step.
The two electrochemical methods used to investigate the oxidation-reduction reaction were cyclic voltammetry and chronopotentiometry.

It was found that the dissolution rate determining processes occurred between 0.25 and 0.55 V (v. SHE). Results showed that irreversible oxidation-reduction processes control the electrochemistry of heazlewoodite. Since the oxidation-reduction processes are not the only reactions occurring, the presence of acid-base reactions complicated the description of the dissolution process. A qualitative description of the voltammograms, as well as an empirical model describing the leaching process, is given. In this model the formation of an inert layer is described, which forms by the oxidation of the nickel sulphide surface. The dissolution of the layer in acid was slower than the dissolution of the Ni_3S_2, which resulted in a decreased leaching rate.

OPSOMMING

Die bronne van basis metale is hoofsaaklik in die vorm van oksiede en sulfiede, waarvan die sulfiede oorheersend in Suid-Afrika gevind word. Hierdie metale is 'n mengsel van platinum groep en onedele metale in die vorm van allooie en sulfiede. Om hoë gehalte metale te produseer is dit noodsaaklik om die onedele metale op 'n effektiewe wyse te skei van die edelmetale.

Deur middel van 'n hidrometallurgiese proses wat loging genoem word, kan metale selektief uit erts geëkstraheer word. Die meganisme van loging kan beskryf word deur oksidasie-reduksie en suur-basis reaksies.

In hierdie studie is die loging van 'n gesintetiseerde heazlewoodite (Ni_3S_2) knopie ondersoek. Die parameters wat bestudeer is gedurende die termiese logings ondersoek is:

- verskillende sure;
- verskillende temperature;
- stikstof en suurstof;
- koper(II) en yster(III) ione.

Die invloed van hierdie parameters word bespreek. Vanuit die resultate wil dit voorkom of die logings tempo afhanklik is van die oriëntasie van die kristalle. Die logings proses is gedeeltelik 'n oksidasie proses wat versnel word deur die byvoeging van sterk oksideermiddels. Bogenoemde was duidelik vanuit die hoë logingstempo wat gelewer is deur salpetersuur. Suurstof en yster(III) het ook die oplosproses versnel. Logings tempo's was tipies in die ordegrootte van 0.87 ± 0.02 mg.m^{-2}.s^{-1} in 0.5 mol.dm^{-3} H_2SO_4 onder 'n suurstof atmosfeer. Die tempo het toegeneem na 12.4 ± 0.20 mg.m^{-2}.s^{-1} en 15.8 ± 0.13 mg.m^{-2}.s^{-1} in die teenwoordigheid van Fe(III) en Cu(II) ione in 'n suurstof atmosfeer, respektiewelik.

Twee aktiveringsenergieë was bereken vanuit die termiese data. Vir die aanvanklike logingstempo was 'n aktiveringsenergie van 28.2 $kJ.mol^{-1}$ bereken, terwyl 'n waarde van 45.75 $kJ.mol^{-1}$ vir die finale logingstempo verkry is. Hierdie waardes dui op 'n chemiese oppervlak snelheidsbepalende reaksie.

Die twee elektrochemiese metodes wat gebruik is om die oksidasie-reduksie reaksies te bestudeer is siklovoltammetrie en chronopotensiometrie. Daar is gevind dat die snelheidsbepalende oplosproses voorkom tussen 0.25 en 0.55 V (v. SHE). Resultate het getoon dat onomkeerbare oksidasie-reduksie prosesse die elektrochemie van heazlewoodite beheer. Die teenwoordigheid van suur-basis reaksies asook oksidasie-reduksie reaksies, bemoeilik die beskrywing van die oplosproses. 'n Kwalitatiewe beskrywing van die siklovoltammogramme, asook 'n empiriese model wat die logings proses beskryf, word gegee. In hierdie model word die vorming van 'n inerte lagie beskryf, wat vorm gedurende die oksidasie van die nikkel sulfied oppervlak. Die oplostempo van die lagie in die suur is stadiger as die oplostempo van Ni_3S_2, wat 'n afname in logingstempo veroorsaak.

CHAPTER 1

INTRODUCTION

1.1 BACKGROUND

Economically important base metals like cobalt, nickel and copper occur as sulphide minerals in the Bushveld complex of the North-West Province of South Africa. These minerals also carry the valuable platinum group metals (PGM). After separation of the metal sulphides from the gangue, these metal sulphides undergo a milling and magnetic separation stage in which the base metals are separated from the precious metals. The major base metal compounds are heazlewoodite (Ni_3S_2), djurleite ($Cu_{1.96}S$) with minor amounts of minor amounts of cobalt and iron sulphides. The base metals are then leached with acid at elevated temperatures under high pressure. Optimal leaching conditions have to be maintained to reduce losses of the base metals. Any improvement of the leaching process will result in substantial savings and may also contribute in reducing sulphur emission into the environment.

A thorough understanding of the basic chemistry of the leaching reactions is necessary to bring about any improvement of the leaching process.

1.2 AIMS

Chemically pure Ni_3S_2, heazlewoodite, was selected as model compound to elucidate the chemistry of acid leaching of nickel from the sulphide mineral. The following aims were set:

1. To collect, evaluate and summarise the available literature on the chemistry of sulphide mineral leaching.
2. Determination of the important process controlling factors of the acid leaching of Ni_3S_2 at ambient pressure.

3. Identify the oxidation processes that are active during the acid leaching of nickel sulphide.
4. Propose a chemical model for the leaching of nickel sulphide.

CHAPTER 2

LITERATURE:

LEACHING OF METAL SULPHIDES

In this chapter...

A survey of the available information on the chemical leaching of base metal sulphide minerals is given. Emphasis is placed on the leaching of nickel sulphide as applied in the nickel and platinum producing industry.

2.1 DEFINING THE TERM LEACHING

By making use of a hydrometallurgical process, that is chemical dissolution/leaching, metals can efficiently be extracted from sulphide concentrates or matte, leaving behind a residue of inert minerals originally present as well as insoluble decomposition products of the reacted minerals. This has become one of the most important means of recovery of base as well as precious metals from ores.

2.2 INTRODUCTION AND HISTORY OF LEACHING PROCESSES IN METALLURGY

An alloy of nickel was known in China over 2000 years ago. Miners were familiar with the reddish-coloured ore, which seemingly resembled Cu_2S. The miners named it "Kupfernickel" (Old Nick's copper), because they attributed their inability to extract copper from it to be the work of the devil.

A.F. Cronstedt isolated an impure metal from Swedish ores in 1751. He identified it with the metallic component of Kupfernickel and thus named the new metal "nickel".

It was only fifty-three years later in 1804 that J.B. Richter produced a much purer sample and was so able to determine its physical properties (*Greenwood and Earnshaw, 1997*).

The sources for platinum group metals (PGM's) have a composition that makes the production of base metals together with precious metals possible. The base metals consist of nickel together with copper, cobalt, and iron and are often referred to as BM's. These base metals usually occur in nature as an alloy of a combined mineralogical form, in combination with PGM's. Therefore it is necessary to separate the base metals from the platinum group metals in order to obtain high grade saleable metals (*Robinson, Course Notes, 2001*).

2.3 STRUCTURE AND PROPERTIES OF BASE METAL SULPHIDES

The base metals present in platinum group metals ore occur in the first row of the transition metals in Groups 7 – 12 of the periodic table of the elements. Nickel is the seventh most abundant transition metal and the twenty-second most abundant element in the earth's crust. The two commercially important ores of nickel are:

1. Laterites (oxide/silicate ores) mainly from New Caledonia, Cuba and Australia.
2. Sulphides (Ni associated with Cu, Co, PGM's and S) abundant in Canada, Russia and South Africa. (*Greenwood & Earnshaw, 1997*)

Sulphide ores are concentrated by flotation and magnetic separation processes. Silica is added to the nickel-copper concentrates, which are then subjected to roasting and smelting operations. This reduces the sulphide and iron contents by converting iron sulphide to oxide and then to the silicate, which is removed as a slag. The resulting "matte" of nickel and copper sulphides is subjected to a slow cooling process over a period of ± five days, which causes the formation of distinct phases, of which heazlewoodite (Ni_3S_2)

and chalcocite (Cu_2S) are two of the phases that form. Some atomic and physical properties of the elements concerned can be seen in Table 2.1.

Table 2.1 Atomic and physical properties of the elements iron, cobalt, nickel and copper (Greenwood and Earnshaw, 1997)

Properties	*Fe*	*Co*	*Ni*	*Cu*
Atomic number	26	27	28	29
Atomic weight (g/mol)	55.845	58.933	58.693	63.546
Electronegativity	1.8	1.8	1.8	1.9
Electronic configuration	$[Ar]3d^64s^2$	$[Ar]3d^74s^2$	$[Ar]3d^84s^2$	$[Ar]3d^{10}4s^1$
Density @ 20°C (g/cm^3)	7.874	8.90	8.908	8.95
Melting point (°C)	1535	1495	1455	1083
Boiling point (°C)	2750	3100	2920	2570
$\Delta H_{(fus)}$/kJ.mol^{-1}	13.8	16.3	17.2(±0.3)	13.0
$\Delta H_{(vap)}$/kJ.mol^{-1}	340(±13)	382	375(±17)	307(±6)

2.4 MODELS OF LEACHING PROCESSES

The mechanism of leaching may involve simple physical dissolution or dissolution made possible by chemical reaction. One, or a combination of, the following rates may be significant during leaching: the rate of transport of solvent into the material to be leached, migration of soluble fraction into the solvent and the diffusion of extract solution out of the insoluble material. The rate of a chemical reaction may also affect the rate of leaching. The dissolution reaction of metals into aqueous solutions is heterogeneous in nature. The overall reaction process usually consists of:

- Transport of reactants from bulk solution to the solid-liquid interface
- Adsorption of reactants to the solid surface
- Chemical reaction at the solid surface
- Desorption of soluble products of the reaction

- Transport of soluble products back to the bulk solution

(*Peters, 1992; Meng & Han, 1993*)

Provis et al. compiled a semi-empirical kinetic model for the acid-oxygen pressure leach of nickel-copper matte. Allowance was made for variations in acid concentration, O_2 partial pressure, and flow rate as well as particle size. It was assumed that the reaction rate determining process was either pore diffusion or the chemical reaction itself. Early in the leaching process some reactions that took place showed signs of the shrinking-core effect, where particles leach to highly porous states and subsequently expose the interior of these particles to reaction with species in solution. This was confirmed by scanning electron microscopy (SEM). The assumption that all the reactions followed first order kinetics was also made, meaning that there was a linear dependency between the reaction rate and the concentration of any reactants present as dissolved ions. This was also true for O_2 partial pressure if O_2 is reacting.

$$dN_A/dt = Vr_A \qquad 2.1$$

Where N_A = moles of A formed

t = time

V = total reaction volume (the actual volume changed due to sample taking, but this factor was removed from data by data smoothing to give results on a constant volume basis)

r_A = reaction rate (mol/m^3.s)

For initial reactions, provision was made for the shrinking-core effects, which took place at the solid-liquid interface, through incorporation of a $^2/_3$ power dependency term. Thus, the shrinking-core term was incorporated into the rate expression for the applicable reaction.

Due to the electrochemical nature of the system, the reaction mechanisms involve the transfer of electrons from one species to another, rather than the collision of multiple species at a liquid-solid interface (*Provis et al., 2003*).

The shrinking-particle model for spherical geometry can be expressed as equation 2.2 when assuming that the rate of dissolution is controlled by a surface reaction:

$$1-(1-X)^{1/3} = kt \qquad 2.2$$

Where k = constant (min^{-1})
t = reaction time elapsed (min)
X = conversion (fraction of nickel dissolved)

The equation changes if the reaction is controlled by a diffusion mechanism of reactants or products through a product layer, and becomes:

$$1-\tfrac{2}{3}X-(1-X)^{2/3} = kt \qquad 2.3$$

By plotting the above-mentioned equations on a graph for the specific reaction conditions used, *Bredenhann and van Vuuren* found that these models were exact fits for their leaching reactions and made the conclusion that, during the initial stages of leaching, the reaction rate was controlled by a surface chemical reaction and towards the end of the reaction, it changed into a diffusion controlled mechanism, probably due to the formation of a sulphur layer. This change between the two different control mechanisms seemed to be gradual and there existed a period of mixed control (*Bredenhann and van Vuuren, 1999*).

Hofirek stated in his study of the nickel-copper matte leaching, utilised at Rustenburg Base Metals Refinery that, according to a simplistic model of the leaching, the process could be proposed by the successive removal of metal atoms from the crystal lattice until part of, or the whole lattice rearranges to

form the next most energetically viable structure. This crystal structure rearrangement can be so rapid that only a very detailed and careful study can reveal the existence of all the intermediate structures. Specifically looking at the leaching of heazlewoodite (Ni_3S_2) through a metathesis reaction with copper(II) ions, he stated that the reactions may involve ionic species formed during the dissolution of the mineral crystal and reprecipitation of a new solid phase from solution as can be seen in the following sequence of reactions during the dissolution of heazlewoodite (*Hofirek, 1988)*:

$$2Ni_3S_2 + 4H^+ \rightarrow 4NiS + 2Ni^{2+} + 4H \qquad 2.4$$

$$4NiS + 2H^+ + \tfrac{1}{2}O_2 \rightarrow Ni_3S_4 + Ni^{2+} + H_2O \qquad 2.5$$

$$Ni_3S_4 + 2H \rightarrow 3NiS + H_2S \qquad 2.6$$

$$2Cu^{2+} + 2H \rightarrow 2Cu^+ + 2H^+ \qquad 2.7$$

$$2Cu^+ + H_2S \rightarrow Cu_2S + 2H^+ \qquad 2.8$$

The overall reaction can be seen as:

$$2Ni_3S_2 + 2Cu^{2+} + 2H^+ + \tfrac{1}{2}O_2 \rightarrow Cu_2S + 3NiS + 3Ni^{2+} + H_2O \qquad 2.9$$

Mulak stated that the dissolution of heazlewoodite in a nitric acid solution in the presence of copper(II) and iron(III) ions was controlled by a surface reaction mechanism (*Mulak, 1987*).

2.5 LEACHING OF SULPHIDE MINERALS

The extraction of metals by chemical dissolution, i.e., hydrometallurgy, has become one of the most important processes to recover metals from ores. By treating nickel-copper mattes by means of smelting, slag cleaning, and conversion techniques, sulphide concentrates are being produced. The sulphide concentrate matte is treated hydrometallurgically to separate the base metals from the precious metals and thus producing Ni, Cu and Co products.

A poor understanding of this leaching process kinetics exists, primarily due to the complex nature of the sulphide chemistry, as well as the fact that these sulphide concentrates usually consist of highly intergrown sulphide minerals (*Rademan et al., 1999*).

2.5.1 NICKEL SULPHIDES

Gerlach et al. looked at the dissolution of synthetic millerite (NiS) and heazlewoodite (Ni_3S_2) in sulphuric acid and found that during heazlewoodite leaching, millerite, and elemental sulphur formed as intermediate phases. They found that the dissolution rate of NiS was comparable with that of Ni_3S_2 (*Gerlach et al., 1970*).

Sinev et al. also confirmed the presence of millerite on the surface of heazlewoodite grains after leaching in either hydrochloric or sulphuric acid under normal pressure. Increase of the internal stresses of grains occurred by the gradual deposition of millerite, especially along pores and cracks, and this caused disintegration, which accelerated the dissolution process (*Sinev et al., 1975*).

Bredenhann and van Vuuren studied the leaching behaviour of a nickel sulphide concentrate at atmospheric pressure in an oxidative sulphuric acid solution. By using $NaNO_3$ and Fe(III) as oxidising agents at a pH of 1 and a temperature of 90°C, it was found that nitrate gave better leaching rates than iron(III).

By studying the leaching residues by means of X-ray diffraction, NiS and S were found to be the major components. It was found that the amount of sulphur formed during the reaction, increased as the $NaNO_3$ concentration increased. They stated that the following two reactions could possibly describe the leaching process:

$$3NiS + 2NO_3^- + 8H^+ \rightarrow 3Ni^{2+} + 3S + 2NO + 4H_2O \quad 2.10$$

or

$$NiS + 2NO_3^- + 4H^+ \rightarrow Ni^{2+} + 2NO_2 + S + 2H_2O \quad 2.11$$

A considerable disadvantage of sulphur formation is the decrease in the leaching rate caused by the sulphur layer formed on the concentrate particles. By plotting the percentage nickel extracted against time, it was obvious that the dissolution kinetics were fast at the beginning of the reaction and slowed down as the reaction proceeded, which supported a mechanism of surface reaction control followed by a diffusion-through-the-product-layer in the later stages of the reaction. By making use of rate constants, the Arrhenius activation energy was calculated and found to be 88 $kJ.mol^{-1}$ for the initial dissolution process, which suggested that a surface reaction was the rate determining step (*Bredenhann and van Vuuren, 1999*).

Arai et al. investigated the effect of non-stoichiometry on the oxidative leaching reaction of heazlewoodite in nitric acid and reported that the leaching rates were greatly influenced by the stoichiometries of the ores. The nickel rich heazlewoodite samples showed faster leaching kinetics than the nickel-deficient samples. The stoichiometry of the ores, however, did not influence the electric properties of Ni_3S_2. The conclusion was thus made that the heazlewoodite electric properties usually do not play a significant part in oxidative leaching reactions. It was also stated that heazlewoodite leaching under oxidative conditions proceeded through the formation of sulphate ions and elemental sulphur. A chemical reaction was found to be the rate controlling step (*Arai et al., 1982*).

During the kinetic study of the dissolution of synthetic heazlewoodite (Ni_3S_2) in nitric acid solution, performed by *Mulak*, a number of different parameters were investigated, such as nitric acid concentration, temperature, particle size, stirring intensity and addition of copper(II) and iron(III) ions. It was found that acid solution concentration had a significant effect on the leaching of Ni_3S_2. With a concentration of 2.0 $mol.dm^{-3}$ HNO_3, dissolution was completely

inhibited after 30 minutes of leaching and the rate of H_2S production was faster than its oxidation to S^0 and HSO_4^-. In 3.0 mol.dm^{-3} HNO_3, a rapid increase in the dissolution rate was noticed. This was explained by the significant oxidation of sulphide to sulphate ions at a higher HNO_3 concentration.

Temperature also played an important role. Below 50°C, even in 3.0 mol.dm^{-3} acid, the leaching rate was found to be very slow. *Mulak* ascribed this to the formation of H_2S gas, which covered the sulphide surface and caused saturation of the leaching solution. It was reported that, at temperatures below 50°C, hydrogen sulphide production occurred much faster than its oxidation to elemental sulphur or sulphate ions. At 50°C only 1.6% of sulphide was found to be oxidised to sulphate, while at 90°C this oxidized fraction was 91%.
The same was found to be true with NiS dissolution in acid dichromate solution (*Mulak, 1983*).

Under conditions where the reaction products are soluble, or leave the surface of reacting particles, the reaction of particulates can be formalised in terms of the fraction reacted (X in equation 2.2). By assuming that the area of the interface, which is decreasing with the dissolution process, controls the process rate, the function $1 - (1 - X)^{1/3}$ of equation 2.2 should be linear with time (t). By plotting $1 - (1 - X)^{1/3}$ against time, rate constants were calculated from the slopes of the straight lines. Between temperatures of 60 and 90°C in 3.0 mol.dm^{-3} HNO_3, dissolution followed a linear rate law. A value of 42.1 ± 0.8 kJ.mol^{-1} was calculated for the activation energy, which seemed to indicate that the chemical reaction on the surface was the slowest stage of dissolution of Ni_3S_2 and hence the rate determining step.

Particle size, together with the temperature, played an important role because retardation by H_2S gas became obvious in 2.0 mol.dm^{-3} acid solutions. While in a 3.0 mol.dm^{-3} acid solution, the H_2S gas was oxidized to elemental sulphur and sulphate. *Mulak* stated that, although the smaller fraction particles caused a higher nickel dissolution rate, it is important to combine this with the ideal

acid concentration and temperature to minimise the retardation effect of H_2S gas.

Stirring speed did not influence the leaching rate, which showed that the rate is chemically controlled and not influenced by transport processes of the solution. This is also in agreement with the calculated activation energy of 42.1 $\pm$ 0.8 kJ.mol^{-1}.

Mulak used the surface reaction model (see equation 2.2) to explain the dissolution reaction of Ni_3S_2.

The added copper(II) ions acted as catalyst for the dissolution reaction and enhanced the leaching rate, while bubbling air through the system also increased the dissolution rate. By means of scanning electron microscopy (SEM), it could be seen that the sulphur layer that formed on the particles could be influenced by the Cu^{2+} ions to become very porous and with easily recognizable separate sulphur crystallites.

Mulak found that the oxidation of H_2S to elemental S or SO_4^{2-} ions on the Ni_3S_2 surface seemed to be the rate determining step.

By making use of various analytical methods i.e. optical microscopy, X-ray diffraction, SEM, and chemical analysis, two intermediate phases were found which were millerite and elemental sulphur (*Mulak, 1985*).

In a later publication, *Mulak* reported on the catalytic action of copper(II) and iron(III) ions in nitric acid solutions. By looking at Ni_3S_2 particles before and after dissolution in HNO_3 that contained Cu^{2+} ions, he found that the leached grain was composed of two parts, one very porous, and the other very smooth. Microprobe analysis of the porous part showed copper and sulphur and the smooth part showed nickel and sulphur. Thus the conclusion could be made that copper(II) sulphide occurred only at selected surfaces on the grain. By calculating the activation energy from an Arrhenius plot for the dissolution of Ni_3S_2 in 2.0 mol.dm^{-3} HNO_3 in the presence of iron(III) ions, a value of 103.6 $\pm$ 4.2 kJ.mol^{-1} was obtained. This value showed that an electrochemical reaction on the surface was the slowest step of dissolution.

As mentioned above it was found that H_2S gas formation took place in 2.0 $mol.dm^{-3}$ HNO_3 solutions, since its generation was faster than its oxidation and this caused a completely inhibited reaction after 30 minutes of leaching (*Mulak, 1985*). It is known that Ni_3S_2 is unstable in acid oxidising solutions and that the formation of H_2S gas is a spontaneous reaction (*Okuwaki, 1984*). The addition of iron(III) or copper(II) ions caused an acceleration of the dissolution rate. This could be explained by the fact that these ions accept electrons from the evolved H_2S gas more rapidly than gaseous oxygen and form intermediate products that are oxidised by O_2 to reproduce the catalytic ions, as can be seen in the following series of reactions:

Acidic attack:

$$Ni_3S_2 + 2H^+ \rightarrow NiS + 2Ni^{2+} + H_2S + 2e^- \quad 2.12$$

$$NiS + 2H^+ \rightarrow Ni^{2+} + H_2S \quad 2.13$$

Formation of intermediate products:

$$Cu^{2+} + 2e^- \rightarrow Cu^0 \quad 2.14$$

$$2Cu^{2+} + 2\,H_2S \rightarrow Cu_2S + S^0 + 4H^+ \quad 2.15$$

$$Cu^{2+} + H_2S \rightarrow CuS + 2H^+ \quad 2.16$$

Oxidation of intermediate products:

$$3Cu^0 + 2NO_3^- + 8H^+ \rightarrow 3Cu^{2+} + 4H_2O + 2NO \quad 2.17$$

$$3Cu_2S + 2NO_3^- + 8H^+ \rightarrow 3CuS + 3Cu^{2+} + 4H_2O + 2NO \quad 2.18$$

$$3CuS + 2NO_3^- + 8H^+ \rightarrow 3Cu^{2+} + 3S^0 + 4H_2O + 2NO \quad 2.19$$

$$3CuS + 8NO_3^- + 8H^+ \rightarrow 3Cu^{2+} + 3SO_4^{2-} + 4H_2O + 8NO \quad 2.20$$

It was presumed by *Mulak* that similar reactions would take place in the presence of iron(III) ions with the formation of Fe^{2+}, FeS and FeS_2. FeS and FeS_2 formation was, however, not confirmed by the experiments. The colour of the heazlewoodite only changed to black after the leaching experiments (*Mulak, 1987*).

When looking at the leaching of nickel sulphide precipitates in hydrochloric acid, *Jha et al.* found that the leaching rate was more a function of chemical reaction control than transport control, since the elevation of the temperature from 70°C to boiling point caused a significant rise in the leaching rate.

When nickel metal or sulphur was added to the leaching solution, the effects suggested that the leaching reaction must be electrochemical in nature. If the leaching was controlled by ion transport, no increase in the dissolution rate should have been noticed, but the exact opposite of this occurred. By increasing the amount of nickel, an increase in the leaching rate was observed. Furthermore, addition of a small amount of sulphur will form only a very thin film on very fine particles, and if diffusion through this sulphur layer was rate controlling, there should not have been a drastic decrease in the leaching rate. There was, however, a big decrease in the leaching rate, which supported the conclusion that the leaching rate was a function of chemical reaction control (*Jha et al., 1983*).

It has been shown that, during the leaching of Ni-Cu matte, a series of quasi-intermediate sulphides with decreasing Ni to S and Cu to S ratios, i.e., Ni_3S_2-Ni_7S_6-NiS-Ni_3S_4 and Cu_2S-$Cu_{31}S_{16}$-$Cu_{1.8}S$-CuS, occurred. The metallic species are oxidised in order to release them into solution. The leaching of Ni alloy creates a porous structure in the matte particle that improves the leaching efficiency of the nickel and copper sulphides (*Rademan et al. 1999*).

Kanome et al. found significant diffusion effects in the acid leaching of heazlewoodite, with the leaching rate decreasing as the acid concentration increased due to a build-up of elemental sulphur (*Kanome et al., 1987*). When high positive redox potentials are present in the process, the elemental sulphur would not be noticed, and this was exactly what *Provis et al.* found.

Contradictory to previous studies, *Kanome et al.* found a constant leaching rate for the duration of the leaching reaction of Ni_3S_2, prepared by a wet process. Also contradictory to previous studies, he calculated a very low activation energy of 24.8 $kJ.mol^{-1}$, which showed that the diffusion process

was actually rate determining. The constant leaching rate was ascribed to an increase in the specific surface area of the sulphide particles because of formation of grooves on the Ni_3S_2 surface. A thin sulphur layer was observed on the sulphide mineral particles. It was concluded that the rate determining step seemed to be the diffusion of oxygen through this sulphur layer (*Kanome et al., 1987*).

Dyson and Scott found nickel sulphide concentrates difficult to leach with dilute acids, because of the sulphur surface coat that formed on the particles. Better leaching results were obtained with hydrochloric acid than with sulphuric acid (*Dyson and Scott, 1976*).

Dutrizac and Chen conducted a mineralogical study of the phases formed during the $CuSO_4$ - H_2SO_4 - O_2 leaching of nickel-copper matte that contained Ni_3S_2, Cu_2S and Ni alloy as major phases. By identifying the changes in the sulphide phases that occurred during leaching of the matte, it was possible to draw some conclusions.

It seemed like the Ni_3S_2 reacted with $CuSO_4$ and O_2 to form soluble nickel, polydymite (Ni_3S_4) and covellite (CuS). The originally present Cu_2S was converted to digenite ($Cu_{1.8}S$) and then to covellite. The covellite and polydymite were then oxidized to copper and nickel sulphate by the O_2 - H_2SO_4 system (*Dutrizac and Chen, 1987*).

$$2Ni_3S_2 + {}^3/_2O_2 + 3H_2SO_4 \rightarrow 3NiSO_4 + Ni_3S_4 + 3H_2O \qquad 2.21$$

$$3Ni_3S_2 + 2CuSO_4 + 2O_2 + 4H_2SO_4 \rightarrow 6NiSO_4 + Ni_3S_4 + 2CuS + 4H_2O \qquad 2.22$$

$$Cu_2S + 0.1O_2 + 0.2H_2SO_4 \rightarrow Cu_{1.8}S + 0.2CuSO_4 + 0.2H_2O \qquad 2.23$$

$$Cu_{1.8}S + 0.4O_2 + 0.8H_2SO_4 \rightarrow CuS + 0.8CuSO_4 + 0.8H_2O \qquad 2.24$$

$$CuS + 2O_2 \rightarrow CuSO_4 \qquad 2.25$$

$$Ni_3S_4 + H_2O + {}^{15}/_2O_2 \rightarrow 3NiSO_4 + H_2SO_4 \qquad 2.26$$

2.5.2 COPPER AND IRON SULPHIDES

Another metal that is part of the non-magnetic sulphide fraction of the matte, as discussed in Paragraph 2.5, is iron. Pyrrhotite ($Fe_{1-x}S$), with $x \leq 0.13$, pressure leaching in sulphuric acid solutions at temperatures below the melting point of sulphur (392K), showed a moderate dependence on temperature, while it was totally independent of sulphuric acid concentration. By leaching in 0.5 mol/l H_2SO_4, as much as 30% of the mineral was dissolved in the absence of oxygen.

A shrinking-core model with mixed control by half-order surface reaction and oxidant diffusion through a product layer fit the data well. Below temperatures of 393K, complete pyrrhotite oxidation was never achieved because of the formation of impervious sulphur product layers that covered the particles, arresting the reaction progress. By using a lignin sulphonate dispersant at temperatures above the melting point of sulphur, complete pyrrhotite oxidation was achieved. A high activation energy of 68.5 $\pm$ 11.2 $kJ.mol^{-1}$ implied a process controlled by surface chemical reactions (*Filippou et al., 1997*).

During the leaching of chalcopyrite ($CuFeS_2$), a passivating copper-rich surface layer was formed as a result of solid state changes that occurred in the mineral. This layer was thought to be a copper polysulphide, CuS_n, where n>2. A mixed diffusion/chemical reaction model could also explain the kinetics where the reaction rate is ultimately controlled by the rate at which the copper polysulphide leached (*Hackl et al., 1995*).

2.6 LEACHING PROCESSES IN THE PLATINUM GROUP METAL INDUSTRY

Platinum Group Metal (PGM) Companies, such as Anglo Platinum treat a nickel-copper converter matte (NCM) to selectively produce nickel, copper, a PGM concentrate, and by-products such as cobalt sulphate and sodium sulphate.

2.6.1 BASE METAL RECOVERY SCHEMES

Two main schemes exist for the industrial nickel recovery from a nickel-copper sulphide converter matte. These are the Sherrit-Gordon ammonia leach process (temperature of $\pm$ 140°C and total pressure of 550 kPa) and the Falconbridge process, in which nickel is selectively brought into solution under the action of strong hydrochloric acid (*Power, 1981*).

By using oxidative leaching, sulphide ions are oxidized, while non-oxidative leaching removes H_2S in order to bring the metal values contained in a sulphide mineral into aqueous solution.
The Sherrit-Gordon process is an oxidative leach, producing $[Ni(NH_3)_6]^{2+}$ and SO_4^{2-} ions in solution, while acid decomposition takes place in the Falconbridge process to produce $Ni^{2+}_{(aq)}$ and H_2S (*Power, 1981*).

2.6.2 ANGLO PLATINUM

At Rustenburg Base Metals Refinery (RBMR), which is part of a large integrated mining and metallurgical complex, Rustenburg Platinum Mines (the world's largest producer of PGM's), a converter matte that is obtained from the smelter, is treated. This converter matte undergoes magnetic separation in order to produce a metallic fraction, which contains the PGM's, and a sulphide fraction (nickel-copper matte) (Table 2.2), which holds the base metals. The metallic fraction undergoes enrichment in order to provide feed for the Precious Metals Refinery (PMR), and a three-stage leach process is utilised for the sulphide fraction (NCM) at the Base Metals Refinery.

Table 2.2 ***Example of the typical composition of nickel-copper matte. (Hofirek and Kerfoot, 1992)***

Element	*Typical (%)*	*Range (%)*
Ni	43	38 - 45
Cu	29	27 - 32
Co	0.5	0.3 – 0.7
Fe	1.5	1.0 – 2.0
S	22.5	21 - 24

2.6.2.1 LEACHING PROCEDURE

The process exists of three major treatment blocks: the leaching circuit, the nickel circuit, and the copper circuit as can be seen from Figure 2.1.

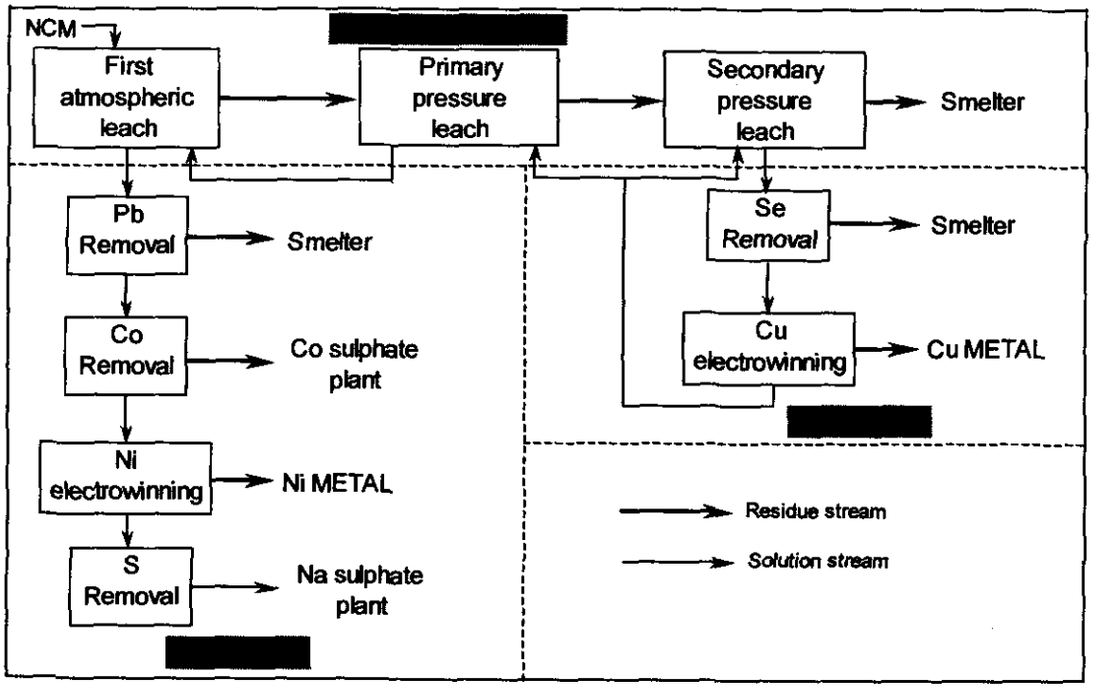

Figure 2.1 ***Simplified block diagram of the Rustenburg base metals refining process. (Hofirek and Nofal, 1995)***

- Leaching circuit

In order to assure selective dissolution of nickel, copper and cobalt from non-magnetic Ni-Cu matte (NCM), of which heazlewoodite (Ni_3S_2) and djurleite ($Cu_{1.96}S$) are the two major mineralogical species (more than 90% of the matte mass), the process consists of a three-stage leach. The first atmospheric leach stage simplifies the removal of copper and iron from the primary pressure leach solution by contact with fresh nickel-copper matte.

The second and third leach stages operate under pressure. Nickel is selectively leached by the primary pressure leach stage while the nickel circuit is being fed via the atmospheric leach with the nickel-rich solution.
The remaining base metals are dissolved in the secondary pressure leach and a copper-rich solution is fed to the copper circuit.

- Nickel circuit

Prior to the production of nickel metal through the process of electrowinning, the atmospheric leach stage solution has to undergo lead and cobalt removal. During the "sulphur removal" stage at the end of the nickel circuit, any sulphide oxidized during leaching is removed. During this stage, sodium hydroxide is used to fully neutralize part of the nickel spent electrolyte and thus leading to the formation of a sodium sulphate solution and a nickel hydroxide precipitate. By redissolving filtered nickel hydroxide in the remaining volume of spent electrolyte, the solution is recycled to the atmospheric leach stage. The sodium sulphate solution is then crystallised to produce saleable Na_2SO_4 crystals.

- Copper circuit

The second pressure leach stage provides the selenium removal stage with the solution that has to be purified. By making use of electrowinning cells, copper metal is then recovered. Recycling of copper spent electrolyte to the

primary as well as secondary pressure leach stages provides enough acid for the dissolution of the base metals.

2.6.2.2 LEACHING REACTIONS

It is necessary to process nickel copper matte (NCM), which originates from the original mined ore, in order to extract base and precious metals from the sulphide concentrates.

NCM leaching occurs through a series of metallic sulphide intermediates that are oxidized gradually over time to release the metal species into solution. Cementation of Cu sulphides takes place in the reaction of solid Ni sulphide species with aqueous Cu^{2+}. This takes place until the more reactive Ni species in the solid phase are depleted. Cementation then ceases where after the release of Cu into solution becomes evident. (*Provis et al., 2003*)

$$Ni_3S_2 + 2Cu^{2+} \rightarrow Cu_2S + NiS + 2Ni^{2+} \qquad 2.27$$

The reaction was confirmed by the presence of chalcocite (Cu_2S) and millerite (NiS) and only proceeded in the presence of hydrogen ions. It accelerated with increasing acid concentration. In an oxidising leach, chalcocite and millerite dissolution takes place to release copper and nickel into solution, as follows:

$$Cu_2S + 2H^+ + 0.5O_2 \rightarrow CuS + Cu^{2+} + H_2O \qquad 2.28$$

$$4NiS + 2H^+ + 0.5O_2 \rightarrow Ni_3S_4 + Ni^{2+} + H_2O \qquad 2.29$$

$$NiS + 2O_2 \rightarrow Ni^{2+} + SO_4^{2-} \qquad 2.30$$

Reactions 2.28 and 2.29 are supported by the presence of covellite (CuS) and polydymite (Ni_3S_4). These sulphide minerals undergo the following reactions:

$$Ni_3S_4 + 7.5O_2 + H_2O \rightarrow 3Ni^{2+} + 4SO_4^{2-} + 2H^+ \qquad 2.31$$

$$CuS + 2O_2 \rightarrow Cu^{2+} + SO_4^{2-} \qquad 2.32$$

$$CuS + 2H^+ + 0.5O_2 \rightarrow Cu^{2+} + S^0 + H_2O \quad 2.33$$

An excess of acid in the reaction system is consumed by the decomposition of heazlewoodite:

$$Ni_3S_2 + 2H^+ + 0.5O_2 \rightarrow 2NiS + Ni^{2+} + H_2O \quad 2.34$$

This decomposition of heazlewoodite (reaction 2.34) proceeds stepwise through the initial formation of godlevskite (Ni_7S_6):

$$3Ni_3S_2 + 4H^+ + O_2 \rightarrow Ni_7S_6 + 2Ni^{2+} + 2H_2O \quad 2.35$$

$$Ni_7S_6 + 2H^+ + 0.5O_2 \rightarrow 6NiS + Ni^{2+} + H_2O \quad 2.36$$

Another impurity besides copper in the matte is iron, which showed a significant effect on the leaching rate. During leaching of heazlewoodite, a substantial quantity of iron(II) ions was released into the solution. Any iron(III) present in the feed solution was rapidly reduced to the iron(II) state.
It is assumed that the dissolved iron acts as an electron carrier and enhances the leaching rate (*Hofirek and Kerfoot, 1992*):

$$Ni_3S_2 + 2Fe^{3+} \rightarrow 2Fe^{2+} + 2NiS + Ni^{2+} \quad 2.37$$

$$2Fe^{2+} + 2H^+ + 0.5O_2 \rightarrow 2Fe^{3+} + H_2O \quad 2.38$$

During the study of pressure oxidation of base metal monosulphides in the presence of iron, *Dobrokhotov* suggested the following mechanism (*Dobrokhotov, 1959*):

$$MeS \rightarrow Me^{2+} + S^{2-} \quad 2.39$$

$$S^{2-} + 2Fe^{3+} = S^0 + 2Fe^{2+} \quad 2.40$$

$$S^0 + 6Fe^{3+} + 4H_2O = SO_4^{2-} + 6Fe^{2+} + 8H^+ \quad 2.41$$

$$S^{2-} + 8Fe^{3+} + 4H_2O = SO_4^{2-} + 8Fe^{2+} + 8H^+ \quad 2.42$$

$$4Fe^{2+} + 4H^+ + O_2 = 4Fe^{3+} + 2H_2O \quad 2.43$$

It was apparent from thermodynamic analysis of the above given reactions that high acidity, low temperature and low oxygen partial pressure would favour reaction 2.40. The opposite of these reaction conditions will lead the reaction mechanism to follow direct oxidation of the sulphide ions to sulphate ions, as can be seen from reaction 2.42 (*Dobrokhotov, 1959*).

In the study of acid-oxygen pressure leaching of Ni-Cu matte by *Provis et al.*, the reaction conditions under investigation were: O_2 flow rate, O_2 pressure, initial particle size, pulp density, initial acid concentration and temperature.
The whole idea behind increasing the O_2 flow rate was to maintain a higher level of dissolved O_2 in solution, hereby increasing O_2 partial pressure and thus increasing the leaching rate. An empirical model describing a linear relationship between O_2 flow rate and effective partial pressure fitted almost all the experimental data satisfactorily.

If the O_2 flow rate was too high, the leaching rate was slowed down. This was ascribed to too many gas bubbles in the pulp, which reduces the available contact area between the solid and liquid interface. (*Provis et al., 2003*).

Rademan et al. studied the acid-oxygen pressure leaching of Ni-Cu matte. It was found that the leaching created a porous structure in the matte particle that improved the leaching efficiency of the nickel and copper sulphides. H_2S formation retarded the leaching process and lead to the formation of intermediate products like Ni_7S_6 and $Cu_{31}S_{16}$.

According to *Rademan et al.* the key to selective leaching of nickel from NCM is, the continuous precipitation reaction of copper ions as Cu_2S, that takes place during the leach. This is a substitution reaction, liberating nickel ions into solution (*Rademan et al., 1999*).

$$Ni_3S_2 + 2H^+ + \tfrac{1}{2}\,O_2 \rightarrow Ni^{2+} + 2NiS + H_2O \qquad 2.44$$

$$Ni + Ni_3S_2 + 4Cu^{2+} \rightarrow 4Ni^{2+} + 2Cu_2S \qquad 2.45$$

$$Ni_3S_2 + 2Cu^{2+} \rightarrow 2Ni^{2+} + NiS + Cu_2S \qquad 2.46$$

According to thermodynamic calculations, Ni_3S_2 is unstable in acid oxidising solutions and H_2S evolution takes place spontaneously (*Rademan et al., 1999*):

$$Ni_3S_2 + 2H^+ \rightarrow NiS + 2Ni^{2+} + H_2S + 2e^- \qquad 2.47$$

In the presence of copper(II) or iron(III) in nitric acid solutions, the H_2S gas is oxidized, which leads to an acceleration in the dissolution rate. Copper(II) or iron(III) ions accept electrons from the evolved H_2S more rapidly than gaseous oxygen. Intermediate products are formed which oxidise in the presence of oxygen, so that the catalytic ions are again produced (*Mulak, 1987*).

2.6.3 IMPALA PLATINUM

Impala Platinum treats a nickel-copper matte to dissolve the base metals in order to have the precious metals remain in the residue. The difference between Impala Platinum and Anglo Platinum is the fact that Impala Platinum doesn't magnetically separate the BM's from the PGM's before leaching of the NCM, as Anglo Platinum does. Whole matte leaching is utilised by Impala Platinum. As far as the nickel-copper matte leaching reactions and mechanisms go, there aren't major differences between the two platinum companies (*Plasket & Romanchuk, 1974; Rademan et al., 1999*).

2.7 CONCLUSIONS

Nickel-copper matte leaching, which contains heazlewoodite as one of the major constituents, occurred with the formation of a series of nickel and copper sulphide intermediates with decreasing nickel to sulphur and copper to sulphur ratios. This would be due to continuous oxidation of nickel and copper in order to release the metal species into solution.

A couple of leaching parameters critically important to control are temperature, acid concentration, catalytic ions [iron(III) & copper(II)] and

oxidative or non-oxidative environments. This will ensure fast leach kinetics and also reduce the chances of sulphur formation, which will retard the leaching process.

Iron(III) act as an electron carrier and enhances the leaching rate. Copper(II) ions are very important in the leaching of Ni_3S_2 during the cementation/metathesis reaction (reaction 2.9) where Cu_2S precipitates while Ni^{2+} goes into solution.

Oxygen and higher partial pressure enhanced the leaching kinetics. *Provis et al.* reported that if the O_2 flow rate becomes too high, the leaching is slowed down. They explained this to be due to the fact that too many gas bubbles may potentially reduce the available contact area between solid and liquid and thus slow down the leaching rate. This argument is, however, only valid for metal sulphides with hydrophobic surfaces. In the case of unmodified Ni_3S_2, the surface is hydrophilic as can be seen from the absence of flotation when gas is bubbled through an acidic suspension of Ni_3S_2.

Mulak (1983) reported that, at lower acid concentrations, dissolution was completely inhibited after 30 minutes of leaching due to H_2S production being faster than its oxidation. This explanation is doubtful as the leaching rate was found to be independent of the stirring rate, which supports the assumption that the leaching kinetics is not influenced by transport processes, but is rather chemically controlled.

In most cases a passivating layer was evident. Several compositions for the passivating layer are proposed. Some authors reported sulphur layers and others reported oxide layers. This may, however, be as a result of different leaching conditions and mediums used by the various investigators. It may also be due to the samples undergoing changes during preparation for surface analysis.

Kanome et al. reported results that were totally different from the other investigators. They found a constant leaching rate throughout, whereas other investigators found a fast initial leaching rate that slowed down over time.

Activation energies reported differed quite substantially, covering a range from as low as 24 $kJ.mol^{-1}$ to as high as 104 $kJ.mol^{-1}$.

Dyson and Scott found that better leaching results were obtained with hydrochloric acid than with sulphuric acid, which differs from the current kinetic study where it was found that sulphuric acid gave faster leaching rates than hydrochloric acid.

Leaching of nickel sulphides seems to undergo the shrinking-core effect where particles leach to highly porous states in order to expose the interior of the particles to the leaching solution. Evidence of initial surface chemical reaction control that changes to diffusion-through-the-product-layer was found. The change between the two different control mechanisms was reported to be gradual with a period of mixed control.
There are, however, differences in what the various investigators found. For example, *Bredenhann and van Vuuren* reported initial control through chemical surface reaction that changed into a diffusion controlled mechanism, while *Mulak* concluded that the leaching of heazlewoodite is controlled by a surface reaction mechanism. *Kanome et al.* reported a diffusion controlled mechanism.

Copper and iron sulphides showed similar leaching characterisations as nickel sulphides. A shrinking-core model with mixed control by half-order surface reaction and diffusion through a passivating layer seemed evident with iron sulphides, which was also the case with nickel sulphides.

CHAPTER 3

EXPERIMENTAL:

LEACHING OF SYNTHETIC HEAZLEWOODITE

In this chapter...

The experimental approach and technique that have been utilised during this leaching study are discussed in Paragraphs 3.1 and 3.2. In Paragraph 3.3 the analytical method and apparatus are described and this is followed by the description of the data processing in the last paragraph.

3.1 EXPERIMENTAL APPROACH

By performing leaching experiments on a single surface of solid Ni_3S_2, the industrial leaching process could be simulated in a controlled manner.
The kinetic approach of this study can be defined as the study of the reaction rate as a function of process controlling factors (*Atkins, 1998*). In the case of acid leaching of Ni_3S_2, these factors are most probably the type of acid, additional leaching agents, leaching inhibitors, reagent concentration, and temperature.

By making use of the monovariance method, i.e. by changing one of the above-mentioned factors in a regular manner, the continued change of reagents and/or product concentration over time can provide information regarding rate equations, reaction order, as well as the reaction mechanism.

3.2 EXPERIMENTAL TECHNIQUE

3.2.1 REAGENTS

Millipore milli-Q deionised water was used during preparation of the leaching acids, as well as for the standard solutions for the atomic absorption

spectrophotometric analysis. The following chemicals were used during the investigation: sulphuric acid (H_2SO_4), nitric acid (HNO_3), hydrochloric acid (HCl), perchloric acid ($HClO_4$), iron(III) sulphate ($Fe_2(SO_4)_3.9H_2O$), iron(II) sulphate ($FeSO_4.7H_2O$), copper(II) sulphate ($CuSO_4.5H_2O$) and nickel nitrate ($Ni(NO_3)_2.6H_2O$). Analytical grade reagents from MERCK were used without further purification. A synthetically prepared heazlewoodite nugget was used for the leaching and electrochemistry runs.

3.2.2 MANUFACTURE OF Ni_3S_2 SAMPLES

For the leaching experiments of this study, synthetic heazlewoodite (Ni_3S_2) was used. The Ni_3S_2 was prepared at Anglo Platinum Research Centre (ARC). Stoichiometric amounts of nickel metal (~45µm powder) and elemental sulphur were calculated and mixed to render a 100g Ni_3S_2 nugget. This mixture was heated in a laboratory furnace to a temperature of 1150°C for one hour, to form molten Ni_3S_2. The reagents were protected from the atmosphere by a layer of Borax. The furnace was switched off and the crucible was removed after 24 hours. After the cooling process, a Ni_3S_2 nugget was obtained. By cutting disks from this Ni_3S_2 nugget with a water-cooled diamond saw, smaller polycrystalline Ni_3S_2 pellets were fabricated (See Figure 3.1). These pellets were then imbedded in Araldite resin.

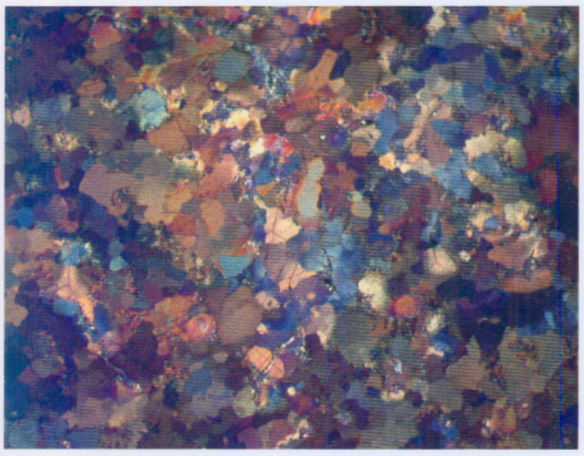

Figure 3.1 Light microscope photo of etched Ni_3S_2 pellet taken under polarized light

A polished section of Ni_3S_2 was etched in 0.5 mol.dm^{-3} H_2SO_4 for 24 hours after which a polarized photo was taken. A Nikon ECLIPSE ME600 Light Microscope equipped with a Fujix Digital Camera (HC-300Zi) was used to

take Figure 3.1. A 5× Nikon CF PLAN objective lens was used to obtain the 3mm section shown.

Heazlewoodite is the stable form of Ni_3S_2 at ambient conditions. Scanning Electron Microscopy analyses done at ARC showed that the nickel sulphide had the proper composition.

SEM micrographs showed that the initial nickel sulphide surface was non-porous. It was also shown that the surface became rougher in an uncontrollable manner. The geometric surface areas of these irregular pellets were determined by a method used in the early days of gas chromatography to measure the area of the chromatogram peaks. A photocopy of the exposed surface of the pellet was made next to a metal disk of known diameter. After enlarging the images to a suitable size, both images were then cut out carefully and weighed. Reliable values for the heazlewoodite surfaces could be calculated. Typical values are shown in Table 3.1.

Table 3.1 Geometric surface areas of Ni_3S_2 pellets

Pellet number	*Surface area (mm^2)*
1	142.3
2	135.6
3	136.7
4	159.4
5	116.1
6	128.1
7	143.5
8	120.0
9	99. 5
10	83.7
11	127.6
12	67.9

Each pellet surface area was brought into consideration during the kinetic calculations of the leaching experiments.

The exposed Ni_3S_2 surfaces of the pellets were treated on emery paper (320 – 1000 mesh) and polished with a soapy suspension of 0.3 μm Alumina powder and a 0.25 μm diamond suspension. There was a thread attached to each pellet to immerse it into solution during the experiment.

3.2.3 LEACHING PROCEDURE

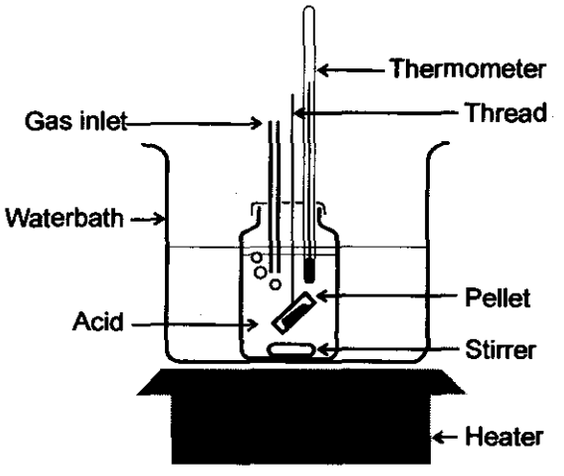

Figure 3.2 Schematic diagram of the leaching experimental set up

A 50 mL beaker, which contained 40 mL of the leaching acid, was immersed in a water bath, on top of a heater. The water bath sufficiently regulated the temperature of the solution. Gas, whether it was nitrogen or oxygen, was purged through the solution during experiments, by means of a gas inlet.

A magnetic stirrer in the solution brought about agitation. It was experimentally found that stirring did not influence the leaching rate. The purpose of stirring was to physically remove gas bubbles on the surface of the metal sulphide. The Ni_3S_2 pellet was hung in the leaching acid after the required temperature was reached. By hanging the pellet in the solution against an angle, interference of the leaching process by gas bubbles was prevented. After the leaching period, the acid was made up to 50,00 mL with

deionised water. The nickel content of the samples was measured by means of atomic absorption spectroscopy.

The leaching procedure was continued with fresh acid without repolishing the nickel sulphide surface. This process was repeated until the total leaching time of 301 minutes was obtained.
Acids were chosen in order to cover different kind of aspects:

- Nitric acid - Oxidation acid
- Sulphuric acid - Industrial reference
- Hydrochloric acid - Complexing acid
- Perchloric acid - Non-oxidising, non complexing acid
  (Perchloric acid is non-oxidising at the concentration used in this study)

3.3 ANALYTICAL METHODS AND APPARATUS

3.3.1 EXPERIMENTAL ERRORS

Each experiment was repeated at least once of which average values are reported. The standard deviation was calculated by the STDEV function in EXCEL.

3.3.2 ATOMIC ABSORPTION SPECTROPHOTOMETRY

The nickel content of the samples was analysed by a Varian SpektrAA 250 Plus Atomic Absorption Spectrophotometer. Atomic absorption standard solutions were made up over the range that covers the expected nickel concentrations found in the samples. This was done in the same acid as used during the experiments, to provide a reliable calibration curve for the atomic absorption analysis. In those cases where the metal concentration was too high, the leach solutions were diluted with the appropriate acid solutions, in which case the adjustment was brought into consideration during the calculations.

3.3.3 ELECTRON MICROSCOPY

Energy dispersive spectrometry-scanning electron microscopy (EDS-SEM) was utilized to obtain information about the physical nature of the surfaces of the Ni_3S_2 pellets. By using this technique, surface information can be obtained at a considerably higher resolution than by optical microscopy, which is limited by diffraction effects. It was not necessary to treat the sample upfront by coating the surface with metallic film, since the metal sulphides are conductors of electricity. It is thus safe to assume that the surface was not altered substantially and that the results were true of the original surface.

An FEI Quanta 200 ESEM microscope system was utilised. To standardise the spectra peaks the Oxford Inca Quant optimisation method for nickel and copper was used.

3.4 DATA PROCESSING

Reaction rate is defined as the change of the amount of a reactant or product per unit time. The reaction rates were calculated by fitting a linear trendline through the experimental data points in a graph of the accumulated amount of dissolved nickel against the corresponding total leaching time. The rate constant is reported as milligram nickel leached per square meter geometric surface area per second. A rate equation was derived as follows:

Per definition the following is true:

$$-\frac{dr}{dt} = k \qquad 3.1$$

Where r = distance in meter

t = time in seconds

k = rate constant in $m.s^{-1}$

For a spherical particle without a diffusion layer:

$$\frac{dc}{dt} = \frac{-d_{vol}}{dt} = \frac{-d}{dt}(\tfrac{4}{3}\pi r^3) = 4\pi r^2 \frac{-dr}{dt} \qquad 3.2$$

Where c = concentration in solution

r = radius of sphere

$\frac{dr}{dt}$ = dissolution rate in $m.s^{-1}$

For a single flat surface:

$$\frac{dc}{dt} = surface \times \frac{-dr}{dt} \qquad 3.3$$

Where r = thickness of pellet

The reason why it was decided to work mainly with a flat surface can be seen from equations 3.2 and 3.3. If the shrinking-core principles, as used by *Bredenhann & van Vuuren (1999)*, are applied to the flat geometry of the pellets used in this study, the kinetics for a flat surface simplifies to a pseudo zero order reaction with regards to the surface. The principles used by *Bredenhann & van Vuuren* are applicable on spherical particles only. Therefore, the rate equation used during this study, has the following form:

$$\frac{dc}{dt} = surface \times k \qquad 3.4$$

CHAPTER 4

RESULTS:

LEACHING OF SYNTHETIC HEAZLEWOODITE

In this chapter...

The leaching reactions were investigated by studying the following process parameters: different acids and temperatures, the influence of nitrogen and oxygen as well as the influence of ions, such as copper(II) and iron(III) ions on the leaching rate. The activation energies for the specific temperature range were calculated. Some scanning electron microscopy (SEM) images studied are presented.

4.1 CHARACTERISTICS OF THE LEACHING SYSTEM

By making use of the monovariance method, different process parameters were studied. Since the acid concentration of the different leaching solutions was held at 0.5 mol.dm^{-3}, pH was not regarded as an appropriate parameter. The calculated pH values for the different acids are reported in Table 4.1.

4.1.1 REPRODUCIBILITY

Figures 4.1 and 4.2 were obtained from different pellets but under the same conditions.

During the leaching experiments it was noticed that the reproducibility using the same pellet was fair, but the results obtained from different pellets differed very much.

The mean slopes for the duplicate determinations for pellet 1 differed by about 14%. A similar result was obtained for pellet 2. However, the slopes for pellet 2 are about double of that for pellet 1, as can be seen in Figures 4.1 and 4.2.

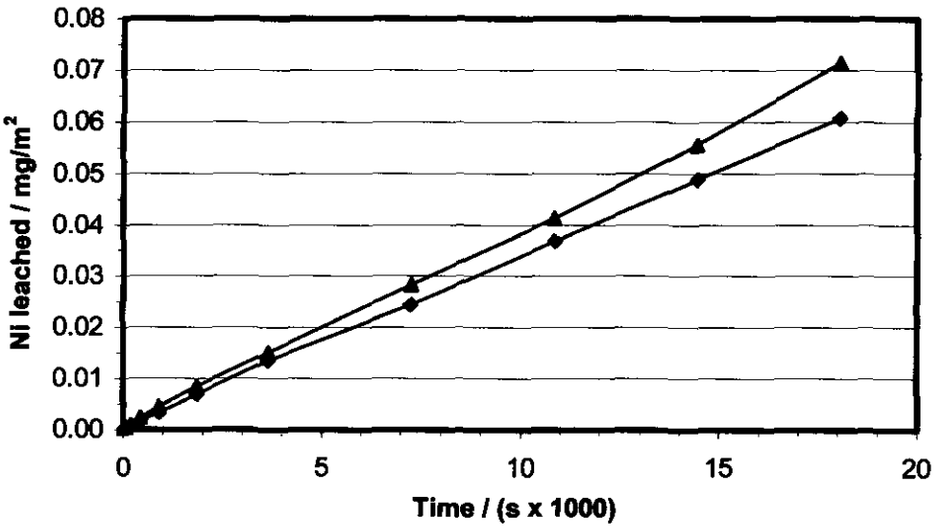

Figure 4.1 Pellet 1: Duplicate leaching experiments
[H_2SO_4] = 0.5 mol.dm^{-3}, Temperature = 75°C, O_2 atmosphere

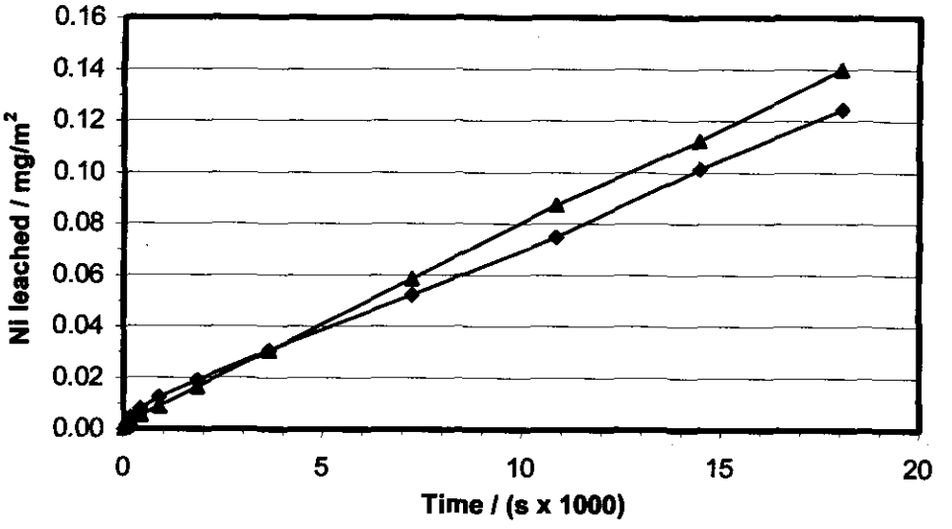

Figure 4.2 Pellet 2: Duplicate leaching experiments
[H_2SO_4] = 0.5 mol.dm^{-3}, Temperature = 75°C, O_2 atmosphere

Apparently there is a difference in both pellets, although both are from the same original Ni_3S_2 nugget.

4.2 STUDY OF THE Ni_3S_2 SURFACE BY SCANNING ELECTRON MICRSOSCOPY IMAGES

For the leaching experiments the pellets were prepared by treatment on three different emery papers with grits between 320 and 1000 mesh. There after it was polished on a cloth with 0.3 μm Alumina powder suspended in a soap solution as well as with a 0.25 μm diamond suspension.

Exactly the same was done with platelets that were cut from the original nugget (Paragraph 4.2.1). One platelet was used as a reference, while the other one was used for studying the surface after etching in sulphuric acid.

4.2.1 Ni_3S_2 PLATELET STUDIES

Figure 4.3 is a scanning electron micrograph of a polished Ni_3S_2 platelet.

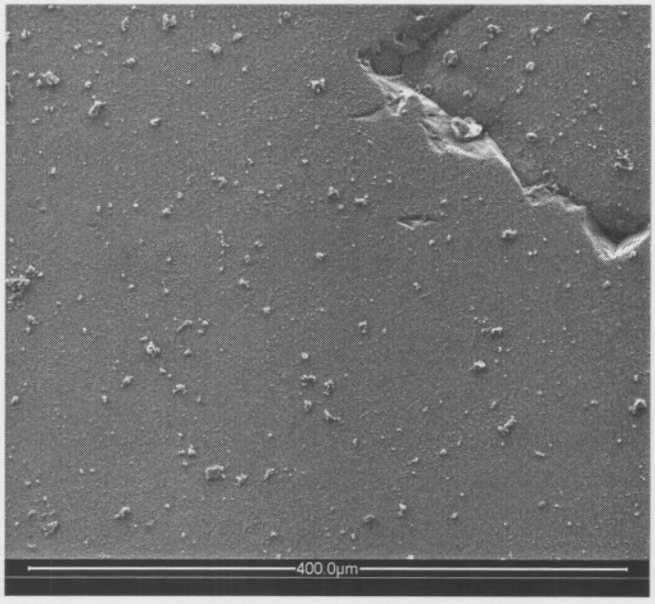

Figure 4.3 SEM micrograph of polished side of Ni_3S_2 platelet (reference)

This platelet was then put in a 0.5 mol.dm^{-3} sulphuric acid solution at ambient temperature for approximately 7 days to etch, where after some SEM micrographs were taken of the etched surface as shown in Figure 4.4.

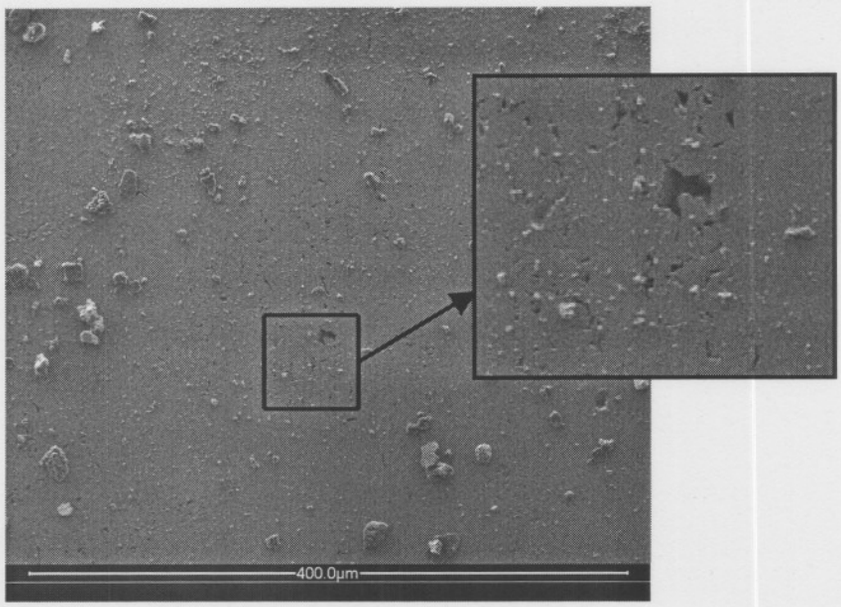

Figure 4.4 SEM micrograph of polished side of Ni_3S_2 platelet after etching in 0.5 mol.dm^{-3} H_2SO_4 for 7 days

When comparing Figures 4.3 and 4.4, some corrosion cracks are noticeable. The enlargement shows these corrosion cracks more clearly. Both figures show debris on the surface.

4.2.2 CROSS SECTION STUDIES

Two additional platelets were cut from the original nugget to be used for cross section studies. They were prepared in exactly the same way as the platelets for the surface studies (see Paragraph 4.2) in order to obtain one reference platelet. The second platelet was put in a beaker that contained 0.5 mol.dm^{-3} sulphuric acid for a period of 7 days at ambient temperature. After the 7 days it was broken in half and SEM images were taken of the fracture, which can be seen in the following figures:

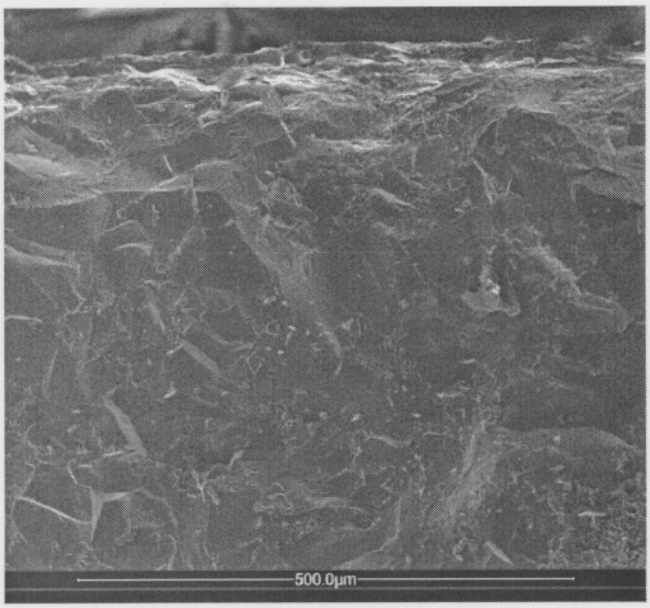

Figure 4.5 SEM micrograph of fracture of Ni_3S_2 platelet before leaching (reference)

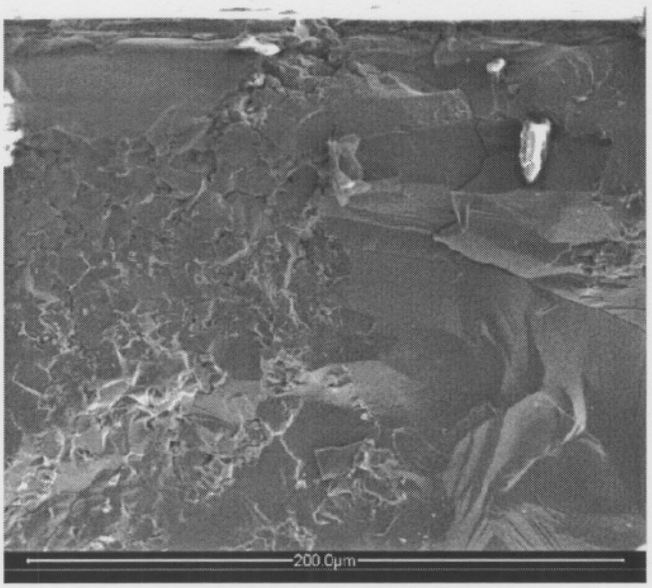

Figure 4.6 SEM micrograph of fracture of Ni_3S_2 platelet after etching in 0.5 mol.dm^{-3} sulphuric acid at room temperature for 7 days

When comparing Figure 4.5 with Figure 4.6 some leaching channels are clearly visible on the left side of the Figure. This shows that penetration of the leaching acid and thus disintegration of the platelet occurred at this specific

area. On the right hand side it seems like the platelet structure is still intact and no penetration occurred there. No similar structures were found in the non-leached platelets. No crystal structure is discernible on the fracture.

4.3 THE INFLUENCE OF DIFFERENT ACIDS ON THE DISSOLUTION RATE

To study the influence of different acids on the leaching rate of synthetic Ni_3S_2, leaching experiments with different acids at a concentration of 0.5 $mol.dm^{-3}$ were performed at least in duplicate, as were all the other kinetic experiments. Average values are reported.

pH values for the acids were calculated using *OLIAnalyser, Version 1.2, 2002, OLI Systems ,Inc.* The values are reported in Table 4.1.

Table 4.1 Calculated pH values for the acids used at a concentration of 0.5 $mol.dm^{-3}$

Leach acid (0.5 $mol.dm^{-3}$)	*Calculated pH values*
HNO_3	0.45
H_2SO_4	0.37
$HClO_4$	0.39
HCl	0.42

The acids at the reported pH values are comparable, since sulphuric acid acts as a mono-protic acid.

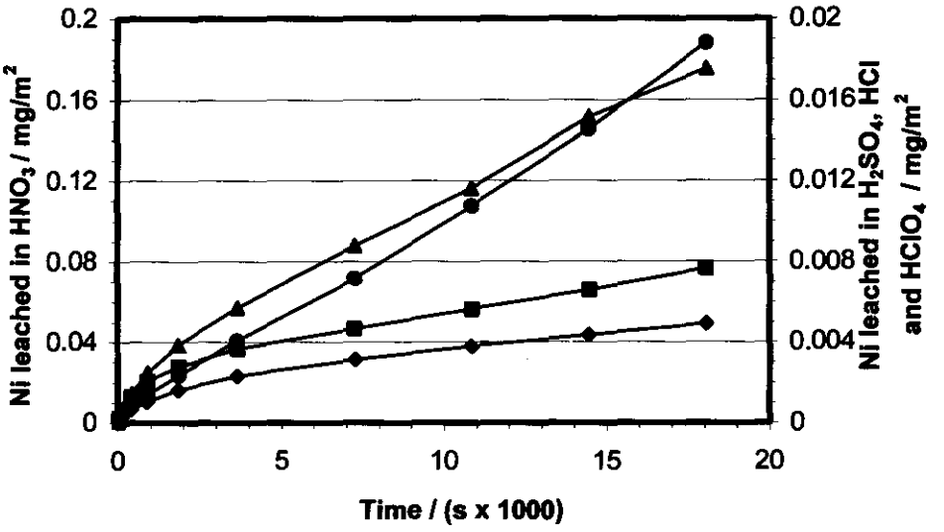

Figure 4.7 The influence of different acids on the leaching rate
[Acid] = 0.5 mol.dm^{-3}, T = 75°C, N_2 atmosphere
● HNO_3, ▲ H_2SO_4, ■ $HClO_4$, ● HCl

The graphs are plots of the amount of nickel dissolved against the reaction time. From the slopes of the graphs a specific dissolution rate in mg.m^{-2}.s^{-1} could be calculated.

As can be seen from Figure 4.7, nitric acid gave the highest leaching rate i.e. 9.97 mg.m^{-2}.s^{-1}. The dissolution rate decreased in the following order: HNO_3 > H_2SO_4 > $HClO_4$ > HCl as reported in Table 4.2. Although the leaching rate at the beginning is much faster than later, after about one hour the leaching rate started to level off.

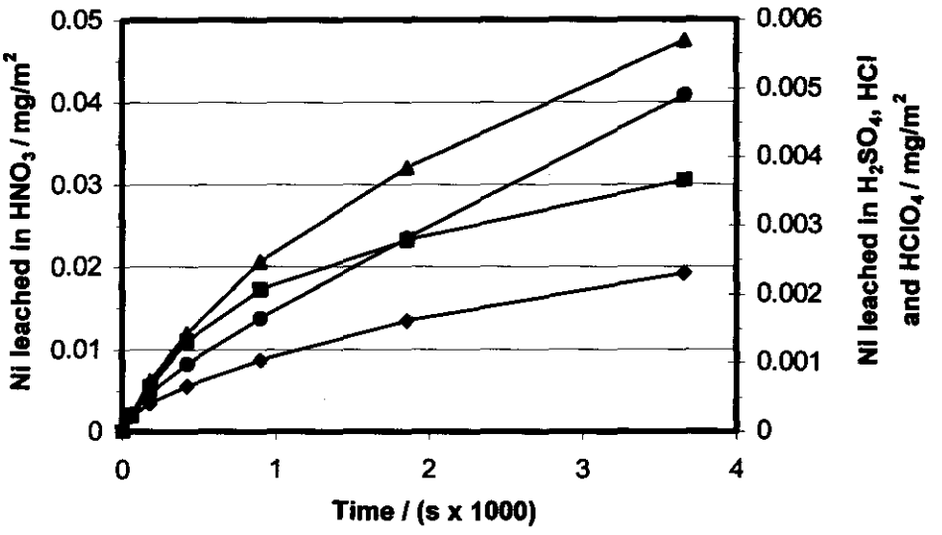

Figure 4.8 ***The first hour of the leaching reaction***
[Acid] = 0.5 mol.dm^{-3}, T = 75°C, N_2 atmosphere
● HNO_3, ▲ H_2SO_4, ■ $HClO_4$, ● HCl

A fast leaching rate in the first part of the reaction is evident from Figure 4.8. In the cases of HCl and $HClO_4$, the leaching rate started to level off after the first hour and stayed constant for the remaining time of the reaction. With H_2SO_4 the levelling off is less, while HNO_3 maintained a slightly higher dissolution rate.

Table 4.2 ***Comparison of the different steady leaching rates of the various acids used***
[Acid] = 0.5 mol.dm^{-3}, T = 75°C, N_2 atmosphere

Leach acid (0.5 mol.dm^{-3})	*Ni leaching rate / mg.m^{-2}.s^{-1}*
HNO_3	9.97 ± 0.23
H_2SO_4	0.87 ± 0.02
$HClO_4$	0.31 ± 0.02
HCl	0.22 ± 0.02

4.4 THE INFLUENCE OF DIFFERENT TEMPERATURES ON THE DISSOLUTION RATE

The influence of temperature on the leaching reactions was studied between the range of 22 and 75°C. This was achieved by leaching the synthetic Ni_3S_2 in 0.5 mol.dm^{-3} H_2SO_4 at different temperatures and keeping the temperature constant (±1°C) at the required value. The results are given in Figure 4.9.

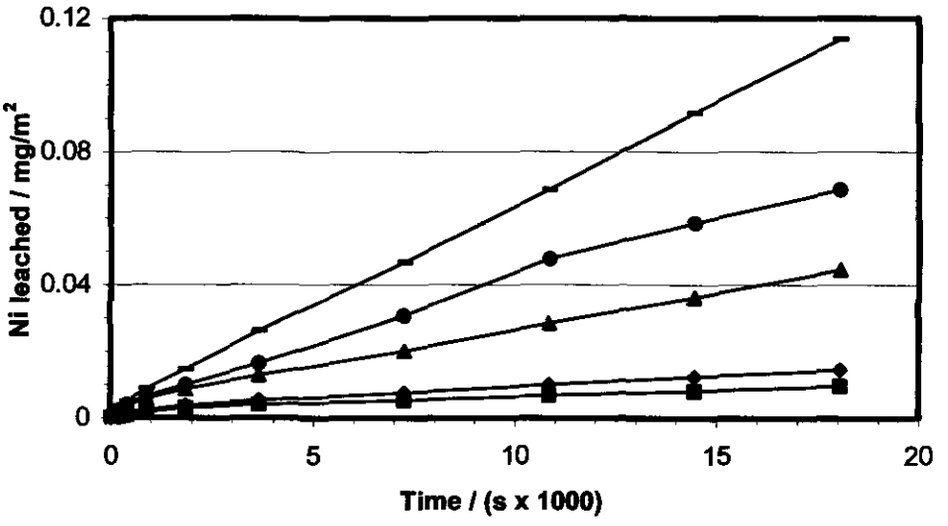

Figure 4.9 ***The influence of different temperatures on the leaching rate [H_2SO_4] = 0.5 mol.dm^{-3}, N_2 atmosphere***

■22°C, ●35°C, ▲ 50°C, ● 60°C, - 75°C

From Figure 4.9, leaching dissolution rates were calculated and reported in Table 4.3. The conclusion was made that temperature plays an important role in this leaching reaction, as could be expected. The dissolution rate increased as the temperature increased. From the best fit trendline through the data points at different temperatures, the gradients of these lines were used to calculate the Arrhenius activation energy, which is shown in Paragraph 4.5.

Table 4.3 Comparison of the initial and steady nickel leaching rates at different reaction temperatures
[H_2SO_4] = 0.5 mol.dm^{-3}, N_2 atmosphere

Leaching temperature / °C	*Leaching temperature / K*	*Initial dissolution rate / mg.m^{-2}.s^{-1}*	*Steady dissolution rate / mg.m^{-2}.s^{-1}*
22	295	2.28 ± 0.07	0.43 ± 0.03
35	308	3.64 ± 0.34	0.69 ± 0.02
50	323	8.33 ± 0.10	2.23 ± 0.02
60	333	9.47 ± 0.92	3.74 ± 0.13
75	348	12.00 ± 1.1	6.10 ± 0.04

4.5 ACTIVATION ENERGY

Some reaction rates are found to be dependent on the temperature in such a way that the rate increases as the temperature is increased. This phenomenon can be expressed by the Arrhenius-equation (*Atkins, 1998*). This equation is written as:

$$k = Ae^{-E_a/RT} \qquad 4.1$$

Equation 4.1 can be handled graphically when it is rewritten as:

$$\ln k = \ln A - E_a/RT \qquad 4.2$$

This temperature dependence is expressed by the Arrhenius parameters i.e. A and E_a, which are the pre-exponential factor (mg.m^{-2}.s^{-1}) and the activation energy (kJ.mol^{-1}) respectively. k is the rate constant, R is the gas constant (8.314 J.K^{-1}.mol^{-1}) and T is the temperature in Kelvin.

Using equation 4.2 and plotting ln k against $1/T$, A can be calculated from the intercept and E_a from the slope of the line. The Arrhenius equation can be used to predict rate constants at specific temperatures.

The temperature dependence of the leaching reaction was studied at 22, 35, 50, 60, and 75°C in 0.5 mol.dm^{-3} H_2SO_4 under N_2 atmosphere. From Figure 4.9, rate constants were calculated for the initial part of the leach as well as for the steady part of the leach. From these calculated rate constants two Arrhenius plots (Figures 4.10 and 4.11) were drawn to obtain the Arrhenius parameters, which are reported in Table 4.4.

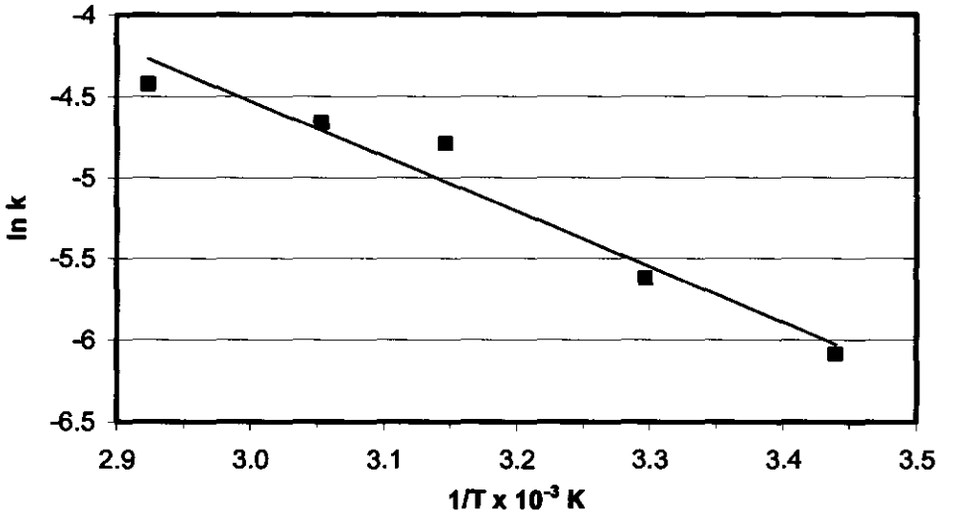

Figure 4.10 Graph of ln k against 1/T for the initial leaching rate [H_2SO_4] = 0.5 mol.dm^{-3}, N_2 atmosphere

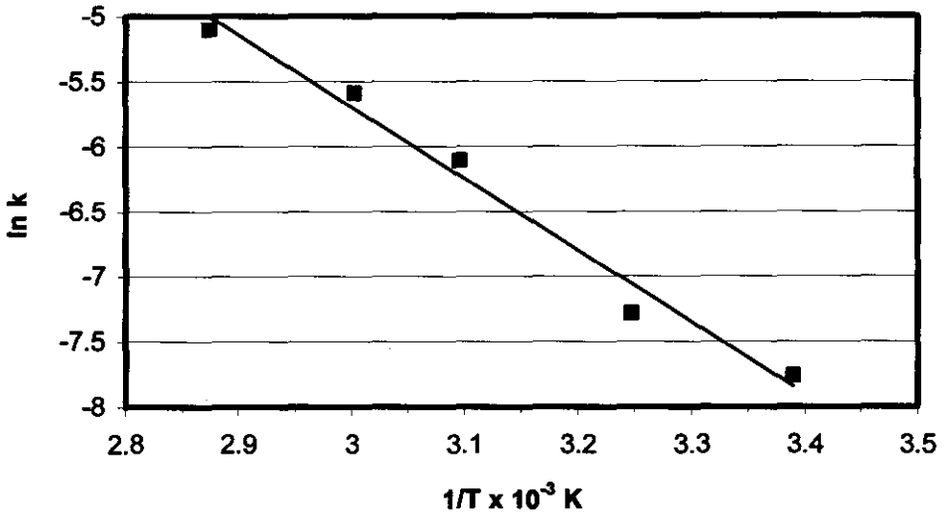

Figure 4.11 Graph of ln k against 1/T for at the steady leaching rate $[H_2SO_4]$ = 0.5 mol.dm^{-3}, N_2 atmosphere

Table 4.4 Calculated Arrhenius parameters for the acid leaching of heazlewoodite $[H_2SO_4]$ = 0.5 mol.dm^{-3}, N_2 & O_2 atmosphere

Arrhenius parameters	*Initial leaching rate*	*Steady leaching rate*
Gradient (m)	-3.40 ± 0.43	-5.50 ± 0.45
Activation energy (E_A/kJ.mol^{-1})	28.22	45.75
y-intercept (c)	5.48 ± 1.36	10.81 ± 1.41
Pre-exponential factor (A/mg.m^{-2}.s^{-1})	240.81	49513.47

For the first part of the reaction an activation energy of 28.22 kJ.mol^{-1} was calculated, while for the last part of the reaction the calculated activation energy was found to be 45.75 kJ.mol^{-1}. This issue will be discussed in further detail in Chapter 8.

4.6 THE INFLUENCE OF NITROGEN AND OXYGEN ON THE DISSOLUTION RATE

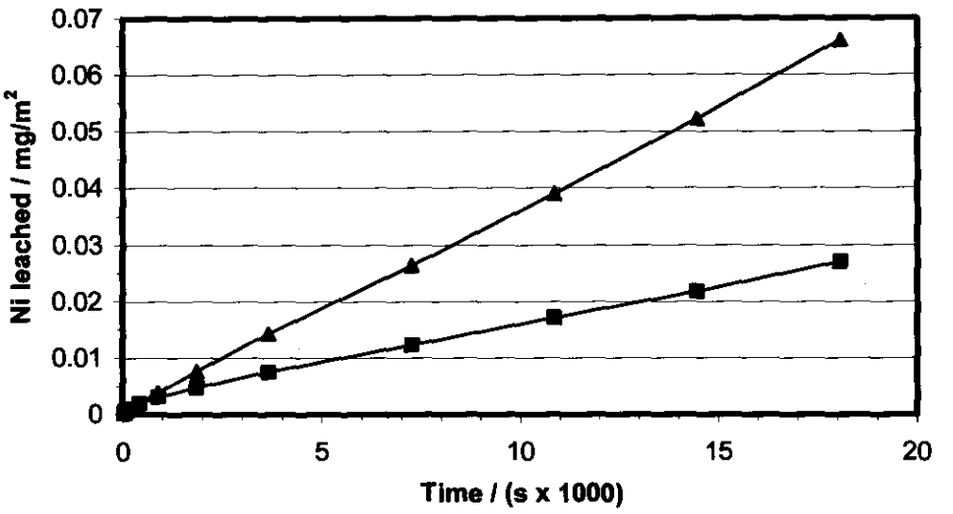

Figure 4.12 The influence of nitrogen and oxygen atmosphere on the leaching rate
$[H_2SO_4] = 0.5\ mol.dm^{-3}$, T = 75°C
■ N_2, ▲ O_2

From Figure 4.12 it can be seen that oxygen gas enhances the leaching rate of heazlewoodite in sulphuric acid. The enhancing effect of O_2 on the leaching rate was found to be present for all sample pellets tested, but varied much from pellet to pellet.

Table 4.5 Comparison of the different leaching rates influenced by nitrogen and oxygen
$[H_2SO_4] = 0.5\ mol.dm^{-3}$, T = 75°C

Leach atmosphere	*Ni dissolution rate / $mg.m^{-2}.s^{-1}$*
N_2	1.45 ± 0.04
O_2	3.61 ± 0.02

As can be seen from Table 4.5 the dissolution rate of nickel in the presence of oxygen is more than double of that in the presence of nitrogen.

4.7 THE INFLUENCE OF IRON(III) AND COPPER(II) ON THE ACID LEACHING

4.7.1 IRON(III) IONS

Three different concentrations of iron(III) ions in H_2SO_4 solution were used during the experiments, i.e. 0.1 mol.dm^{-3}, 0.01 mol.dm^{-3} and 0.001 mol.dm^{-3}. The influence of nitrogen and oxygen was tested in combination with the different concentrations of interfering ions.

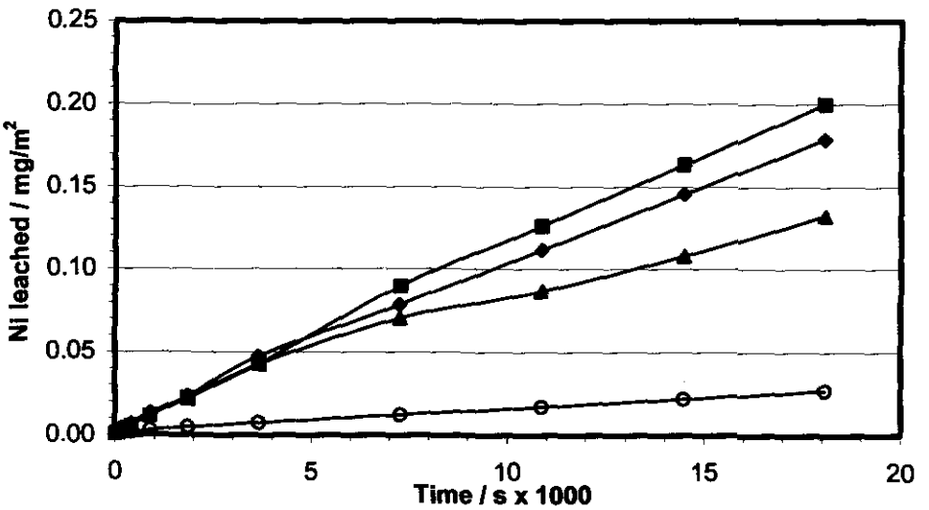

Figure 4.13 The difference in leaching rate in the presence of iron(III) ions
[H_2SO_4] = 0.5 mol.dm^{-3}, T = 75°C, N_2 atmosphere
■ [Fe(III)] = 0.1 mol.dm^{-3}, ◆ [Fe(III)] = 0.01 mol.dm^{-3},
▲ [Fe(III)] = 0.001 mol.dm^{-3}, ○ [Fe(III)] = 0 mol.dm^{-3}

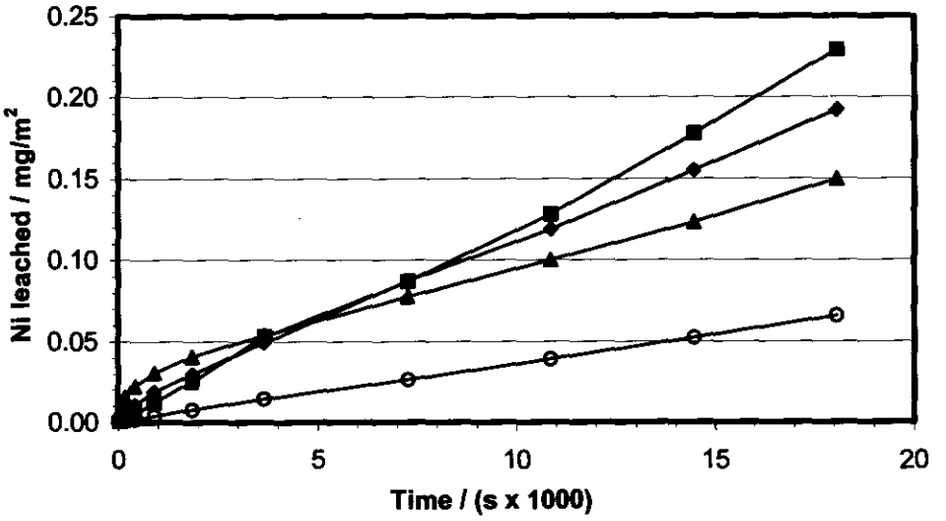

Figure 4.14 The difference in leaching rate in the presence of iron(III) ions

[H_2SO_4] = 0.5 mol.dm^{-3}, T = 75°C, O_2 atmosphere

■ [Fe(III)] = 0.1 mol.dm^{-3}, ● [Fe(III)] = 0.01 mol.dm^{-3},

▲ [Fe(III)] = 0.001 mol.dm^{-3}, ○ [Fe(III)] = 0 mol.dm^{-3}

By looking at Figures 4.13 and 4.14, it is clear that even in the lowest iron(III) concentration, the leaching rate was still increased. The dissolution rates for leaching in the presence of iron(III) ions are summarized in Table 4.6.

Table 4.6 Comparison of the different leaching rates in the presence of iron(III) ions

[H_2SO_4] = 0.5 mol.dm^{-3}, T = 75°C, N_2 & O_2

N_2		O_2	
[Fe(III)] (mol.dm^{-3})	*Ni dissolution rate / mg.m^{-2}.s^{-1}*	*[Fe(III)] (mol.dm^{-3})*	*Ni dissolution rate . mg.m^{-2}.s^{-1}*
0.1	11.2 ± 0.14	0.1	12.4 ± 0.20
0.01	9.83 ± 0.17	0.01	10.4 ± 0.20
0.001	7.29 ± 0.31	0.001	7.56 ± 0.42
0	1.45 ± 0.04	0	3.61 ± 0.02

Iron(III) had an overall enhancing effect, but there is no substantial difference between leaching in the presence of iron(III) or in a combination of iron(III) and oxygen. Only when no iron(III) ions are present the effect of an O_2 atmosphere is substantial.

A pellet was taken and treated on three different emery papers with grits between 320 and 1000 mesh. It was polished on a cloth with 0.3μm Alumina powder and then with a 0.25μm diamond suspension. The Alumina was dispersed in a very diluted solution of dishwashing liquid. The pellet was then etched in a 0.5 $mol.dm^{-3}$ sulphuric acid solution that contained 0.1 $mol.dm^{-3}$ Fe(III) ions. The SEM micrograph of this pellet is given below as Figure 4.15.

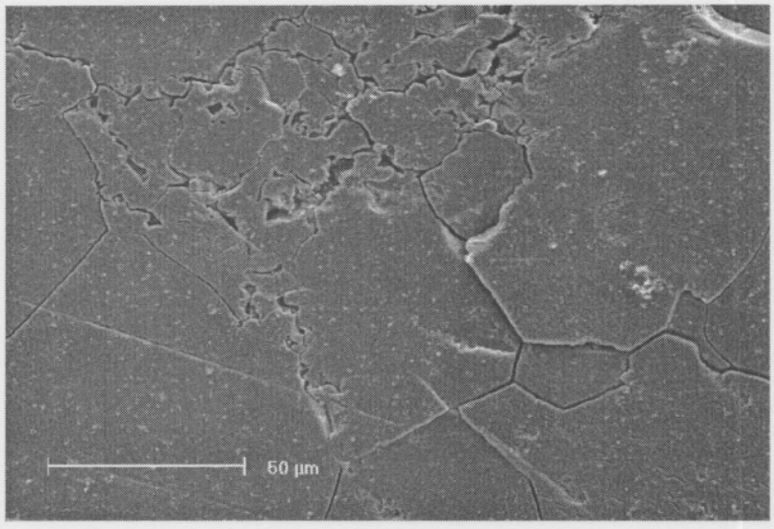

Figure 4.15 SEM micrograph of Ni_3S_2 pellet etched in 0.5 $mol.dm^{-3}$ H_2SO_4 solution that contained 0.1 $mol.dm^{-3}$ Fe(III) ions

The iron(III) ions caused crack formation of the pellet surface as can be seen in Figure 4.15.

According to the results it seems like the iron(III) is chemically involved in the heterogeneous oxidation of the nickel sulphide. With an excess of iron(III) ions in solution, oxygen is of less importance.

4.7.2 COPPER(II) IONS

The experiments conducted in the presence of copper(II) ions were done with three different concentrations, i.e. 0.1 mol.dm^{-3}, 0.01 mol.dm^{-3} and 0.001 mol.dm^{-3}.

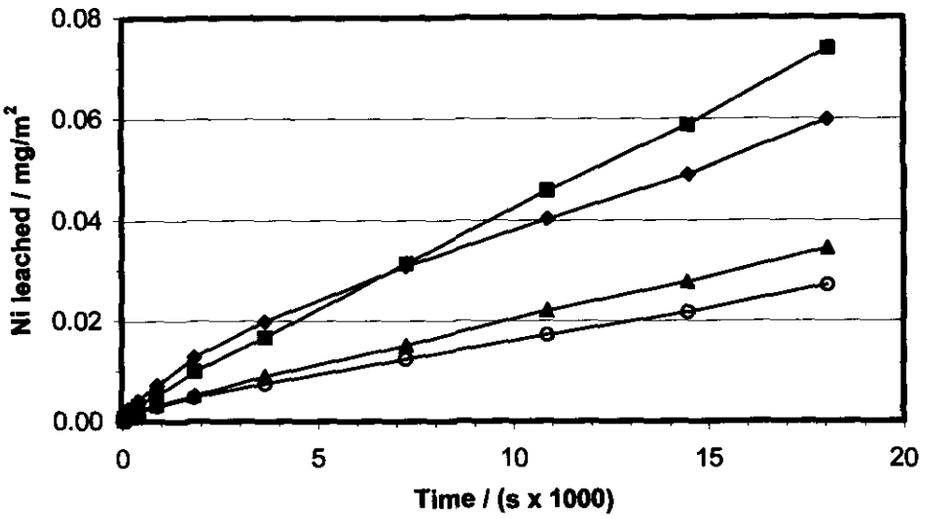

Figure 4.16 The difference in leaching rate in the presence of copper(II) ions
[H_2SO_4] = 0.5 mol.dm^{-3}, T = 75°C, N_2 atmosphere
■ [Cu(II)] = 0.1 mol.dm^{-3}, ◆ [Cu(II)] = 0.01 mol.dm^{-3},
▲ [Cu(II)] = 0.001 mol.dm^{-3}, ○ [Cu(II)] = 0 mol.dm^{-3}

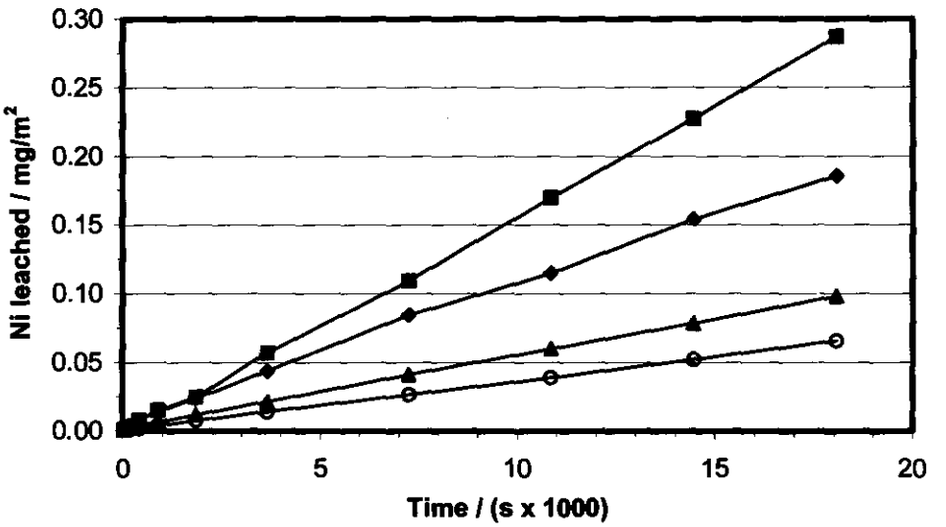

Figure 4.17 The difference in leaching rate in the presence of copper(II) ions

[H_2SO_4] = 0.5 mol.dm^{-3}, T = 75°C, O_2 atmosphere

■ [Cu(II)] = 0.1 mol.dm^{-3}, ◆ [Cu(II)] = 0.01 mol.dm^{-3},

▲ [Cu(II)] = 0.001 mol.dm^{-3}, ○ [Cu(II)] = 0 mol.dm^{-3}

Once again as can be seen from Figures 4.16 and 4.17, copper(II) ions enhanced the leaching rate of Ni_3S_2. In the absence of O_2 the effect of copper(II) is lower than that of iron(III), but for oxygenated solutions the influence of both ions is similar. Calculated leaching rates are reported in Table 4.7.

Table 4.7 Comparison of the different leaching rates in the presence of copper(II) ions
[H_2SO_4] = 0.5 mol.dm^{-3}, T = 75°C, N_2 & O_2

N_2		O_2	
[Cu(II)] (mol.dm^{-3})	*Ni dissolution rate / mg.m^{-2}.s^{-1}*	*[Cu(II)] (mol.dm^{-3})*	*Ni dissolution rate / mg.m^{-2}.s^{-1}*
0.1	4.03 ± 0.04	0.1	15.8 ± 0.13
0.01	3.24 ± 0.14	0.01	10.3 ± 0.15
0.001	1.86 ± 0.03	0.001	5.35 ± 0.03
0	1.45 ± 0.04	0	3.61 ± 0.02

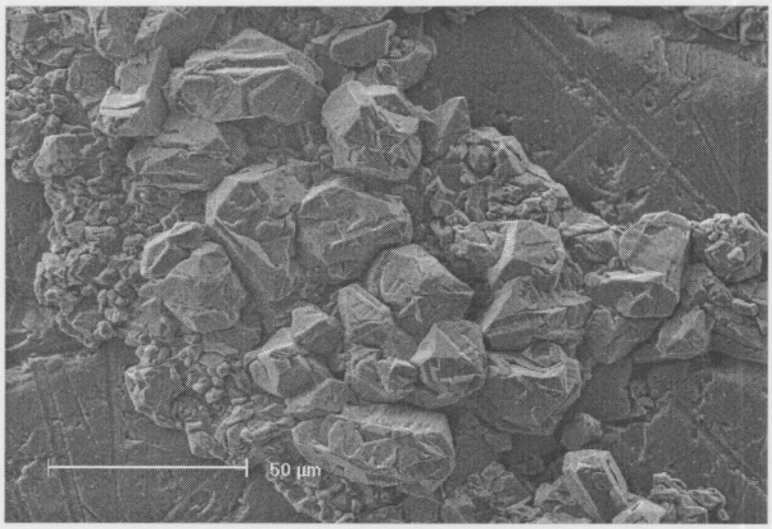

Figure 4.18 SEM micrograph of Ni_3S_2 pellet etched in 0.5 mol.dm^{-3} H_2SO_4 solution that contained 0.1 mol.dm^{-3} Cu(II) ions

The crystals seen in Figure 4.18 were identified as metallic copper crystals by EDS-SEM. Oxygen now plays a bigger role than with iron(III). No free sulphur was detected by scanning electron microscopy. More detail on the effect of iron(III) and copper(II) ions on the leaching rate is discussed in Chapter 8.

4.8 CONCLUSIONS

As far as reproducibility goes, it was found that it was fair in one pellet, but differed quite substantially from one pellet to another.

From scanning electron microscopy images, it seemed evident that leaching was not an evenly distributed process that occurred over the whole surface of the pellet. It rather seemed that leaching occurred predominantly at cracks or 'weak parts' on the surface. This was especially clear on the cross-section studies, which showed leaching channels at specific locations on the pellet surface.

The results obtained from different acids differed from what *Dyson and Scott* found. They reported that hydrochloric acid gave a higher leaching rate than sulphuric acid, while the current study showed that sulphuric acid gave a lower leach rate than nitric acid, but still performed better than hydrochloric acid.

When studying the influence of copper(II) and iron(III) ions, it seemed like copper formed a precipitate on the surface, while the iron enhanced the disintegration process of the surface.

It was obvious that higher temperatures enhanced leaching and by calculating the activation energies, two distinctive areas were identified. The values obtained were 28.233 and 45.75 $kJ.mol^{-1}$ respectively.

Enhancing the oxidative leaching conditions by the application of oxygen caused an increase in leaching rate.

CHAPTER 5

LITERATURE:

ELECTROCHEMISTRY OF METAL SULPHIDES

In this chapter...

Corrosion theory of metal sulphides is discussed, together with the available literature on the electrochemistry of base metal sulphides that is related to metal sulphide leaching.

5.1 ELECTROCHEMICAL CORROSION OF METAL SURFACES

Stoichiometrically the dissolution of Ni_3S_2 must be described as a simultaneous oxidation-reduction and acid-base reaction (see reactions 2.4 to 2.6). The oxidation-reduction can be described and investigated with the theory and experimental tools that were developed by electrochemists. The aim of the electrochemistry was to support the understanding of the leaching process.

5.1.1 THEORY OF CORROSION

Corrosion can generally be described as the destruction of a metal or alloy by chemical or electrochemical change or physical dissolution into an aqueous solution. The conversion of surface portions of a metal to oxide as a result of air or oxygen can be described as oxidation, which can be seen as a type of corrosion.

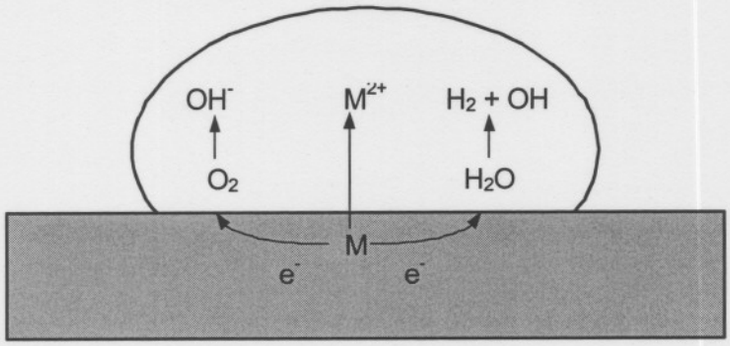

Figure 5.1 Schematic version of corrosion between a drop of water, which is O_2 enriched at its boundary with air.

If the water droplet is slightly acidic and oxygen-enriched at the boundary with air (see Figure 5.1), corrosion will take place at the metal-solution interface. Electrons donated by the metal reduce the oxygen at the edges of the drop, where the O_2 concentration is higher. Those electrons are replaced by others released elsewhere as $M \rightarrow M^{2+} + 2e^-$ (*Atkins, 1998*).

Non-oxidative dissolution of a solid takes place when the formal oxidation states of the solute species are identical in solution and in the solid state. When any of the solute species exist in different oxidation states in solid and solution phases, oxidative (or reductive) dissolution takes place. For this type of dissolution it is necessary for electrons to be transferred across the solid/solution interphase (*Scott & Nicol, 1976*).

The oxidative dissolution of sulphide minerals in the presence of oxidants such as ferric ions is a well-known example. In a typical mixed-potential electrochemical process the simultaneous anodic oxidation of the mineral and the cathodic reduction of the oxidant result in these reactions (*Nicol, 1983*).

For a naturally corroding metal there is electrochemical process occurring on its surface at a measurable rate. These include at least one anodic and one cathodic process. These processes can each be described by Tafel equations. The partial currents are algebraically additive. By elucidating the

current and potential values in the Tafel equation, a general rate equation for the corroding metal can be derived (*Wagner and Traud, 1938*).

5.1.2 THE DOUBLE LAYER

When electrons leave an electrode, this leads to a decrease in the local cation concentration, and the electrode becomes positively charged relative to the solution nearby. The Stern model can describe the interface between the electrode and solution. This model is a combination of the Helmholtz and Gouy-Chapman models.

According to the Helmholtz model, a double layer exists with solvated ions arranged along the electrode surface (See Figure 5.2). These ions are restricted from the electrode by their hydration spheres. An outer Helmholtz plane (OHP) exists, which is the plane running through the solvated ions, present next to the electrode surface. Ions that have discarded their solvating molecules and are now attached to the electrode surface by chemical bonds are regarded as the inner Helmholtz plane (IHP).

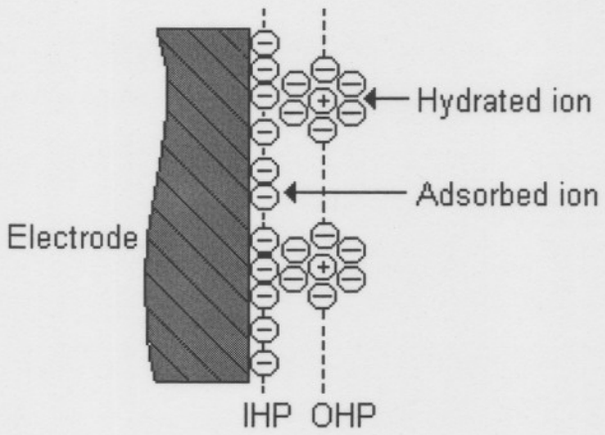

Figure 5.2 The Helmholtz double layer model (Atkins, 1998)

The Gouy-Chapman model (see Figure 5.3) claims that the local concentrations of cations and anions differ from the bulk concentration, with

ions of opposite charge clustering close to the electrode and ions of the same charge being repelled from the electrode.

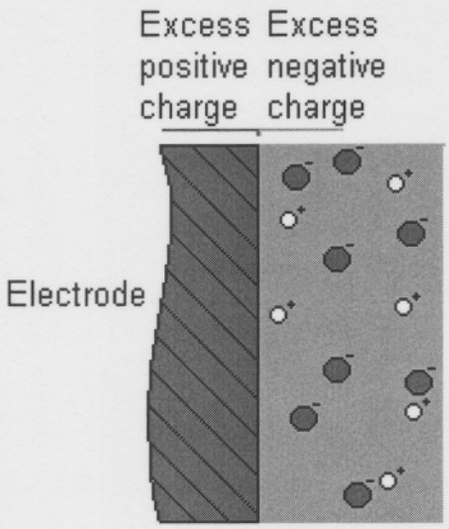

Figure 5.3 The Gouy-Chapman double layer model (Atkins, 1998)

Because the Helmholtz model overemphasizes the rigidity of the local solution at the electrode and the Gouy-Chapman model underemphasizes the double layer structure, the Stern model (Figure 5.4), which is a combination of these two models, states that the ions closest to the electrode are constrained into a rigid Helmholtz plane while outside that plane the ions are dispersed as in the Gouy-Chapman model (*Atkins, 1998*).

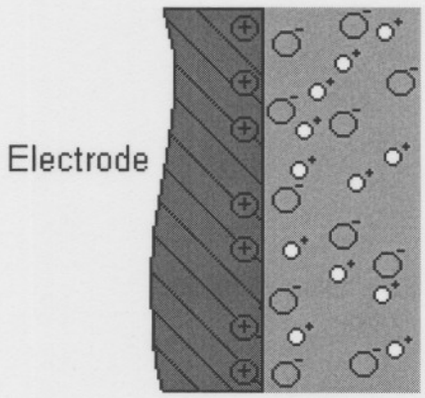

Figure 5.4 The Stern model (Rieger, 1994)

5.1.3 STANDARD POTENTIALS

The potential of an electrochemical cell is related to the activities of the reactants and products of the cell reaction and indirectly to their molar concentrations.

Hydrogen's potential is used as the standard potential to measure the probability of corrosion. Metals with potentials greater than that of hydrogen (0.0 V) and less than that of oxygen (1.23 V) will not corrode with the formation of hydrogen gas. These metals can, however, be corroded by solutions containing dissolved oxygen (*Lorenzen, 1991*). The Nernst equation is generally used to calculate potential at non-standard concentrations (*Skoog, Holler and Nieman, 1998*). At equilibrium:

$$E = E^0 - RT/nF \ln K \qquad 5.1$$

Where E = total change in potential
E^0 = standard cell potential
R = gas constant
T = temperature in Kelvin
n = number of electrons involved in the half reaction
F = Faraday's constant
K = equilibrium constant

E^0 is a constant that is called the standard electrode potential, where the activities of reagents and products are unity:

$$E^0 = RT/nF \ln K \qquad 5.2$$

5.1.4 ELECTROCHEMICAL CELLS

Some chemical reactions can be driven by an applied potential in an electrochemical cell. Electrochemical cells in which a chemical reaction is forced by added electric energy are called electrolytic cells. Electron

producing or consuming ionic reactions take place on the surface of electrodes. A requirement of these electrodes is that they have to be electronic conductors. The electrodes are connected to an external voltage source in order to generate electric charge transfer via electrons between the electrodes. For internal charge transfer through ionic conduction, electrolytes are used (*Perry & Green, 1984*).

5.1.5 CYCLIC VOLTAMMETRY AND CHRONOPOTENTIOMETRY

In voltammetry, the kinetics of electrode processes can be studied by recording the current as function of potential and potential sweep rate. More specifically, cyclic voltammetry can be applied to monitor the oxidation and reduction of species on the electrode surface and in solution, respectively.

Information on the kinetics of the electrode process can be obtained from the shape of the IV (current-potential) curve, while the change in shape as the rate operating conditions are altered, provides additional information on the processes involved.

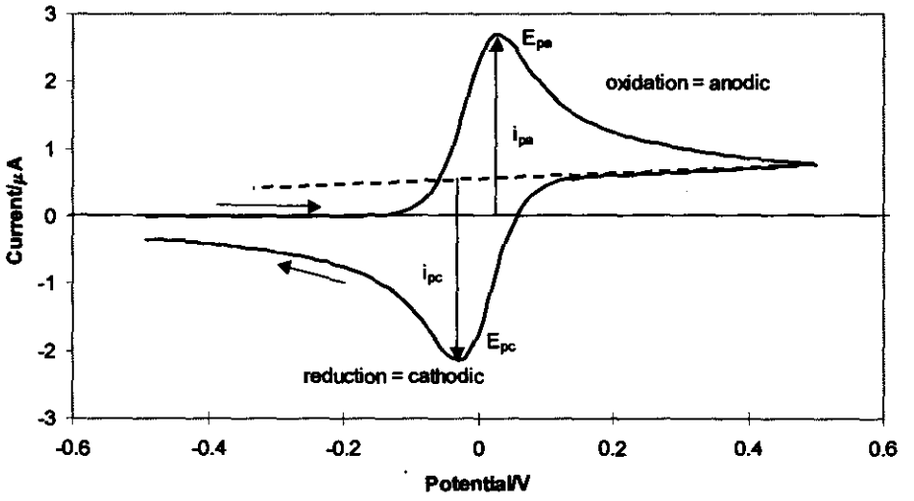

Figure 5.5 Typical diffusion controlled cyclic voltammogram for a reversible redox couple

E_{pa} and E_{pc} are the maximum anodic and cathodic potential values respectively, and i_{pa} and i_{pc} are the accompanying anodic and cathodic current values.

The sweep rate influences the appearance of the curve in such a way that if it is too fast or too slow, some processes might not have the time to occur or new reactions may even appear. In most cases it can be expected that the position of the current peaks stay unchanged, but the current height might change.

When the matching peak on the reverse phase of cyclic voltammetry is absent, it indicates that the oxidation or reduction is irreversible.
Therefore, it is important to obtain the most appropriate reaction conditions for the working electrode before experimental data can be collected.

Chronopotentiometry is another electrochemical method to study the kinetics of electrode processes, where the potential is monitored over time (*Atkins, 1998*).

By the use of these two methods, i.e. cyclic voltammetry and chronopotentiometry (by means of a rotating electrode for the chronopotentiometry), an electrochemical study was conducted.

In classical chronopotentiometry the current is controlled. In the present investigation the potential was used to monitor the changes on the Ni_3S_2 surface during acid leaching without forcing the reaction by an applied potential. This implies chronopotentiometry at zero current - essentially an open circuit.

Mathematically rigorous descriptions of potential-current-time relations have been developed (*Bard and Faulkner, 1980*). In the case where the reaction at the surface of the electrode is a combination of reduction-oxidation reactions and thermic reactions that alter the electrode surface as well as the

composition of the solution, these mathematical relations break down. A quantitative description becomes less reliable and a more empirical approach is appropriate.

5.2 ELECTROCHEMISTRY OF METAL SULPHIDES

The usual hydrometallurgical route for the extraction of metals from their ores requires the oxidation of the sulphide to either elemental sulphur or sulphate. The dissolved metal can then be separated from the residue and treated further. An alternative method for the dissolution of the more soluble metal sulphides (NiS, FeS and ZnS) is non-oxidative treatment with acid, with the subsequent liberation of hydrogen sulphide (*Filmer and Nicol, 1980*):

$$MS + 2H^+ \rightarrow M^{2+} + H_2S \qquad 5.3$$

5.2.1 ELECTROCHEMICAL DISSOLUTION PROCESSES OF METAL SULPHIDES

Similarly to a metal, a sulphide mineral can be used as an electrode because it is an electronic conductor. Sulphide conductivity is sometimes as high as metal conductivity. In general the specific conductivities of sulphide minerals are in the order of 10^3 to 10^{-3} $\Omega^{-1}.cm^{-1}$. (*Peters, 1977).*

A sulphide mineral can decompose in four kinds of solutions, which are:

- Oxidising solutions with consequent elemental sulphur or sulphate ions in solution, dependant on pH and oxidising potential.
- Reducing solutions with formation of H_2S or sulphide ion and lower valence sulphide or metal phase.
- Strong acid solutions, consequentially forming H_2S and metal dissolution into solution.
- Strong alkali solutions with sulphide ions in solution, as well as metal oxides or lower valence sulphides (*Peters, 1976*).

A Pourbaix (E_h-pH) diagram of sulphide minerals in contact with aqueous solutions of selected composition, gives information on the stability/instability of the species. The potential-pH equilibrium diagrams have the essential purpose of supplying a thermodynamic framework for electrochemical reactions involving an aqueous solution. The corrosion resistance of nickel should depend on the pH and the presence of oxidising agents. Nickel should be uncorrodible in neutral or alkaline solutions free from oxidising agents, slightly corrodible in acid solutions free from oxidising agents, and very corrodible in acid or very alkaline solutions containing oxidising agents. Neutral or alkaline oxidising solutions should cover the nickel surface with a layer of oxide (*Pourbaix, 1966*).

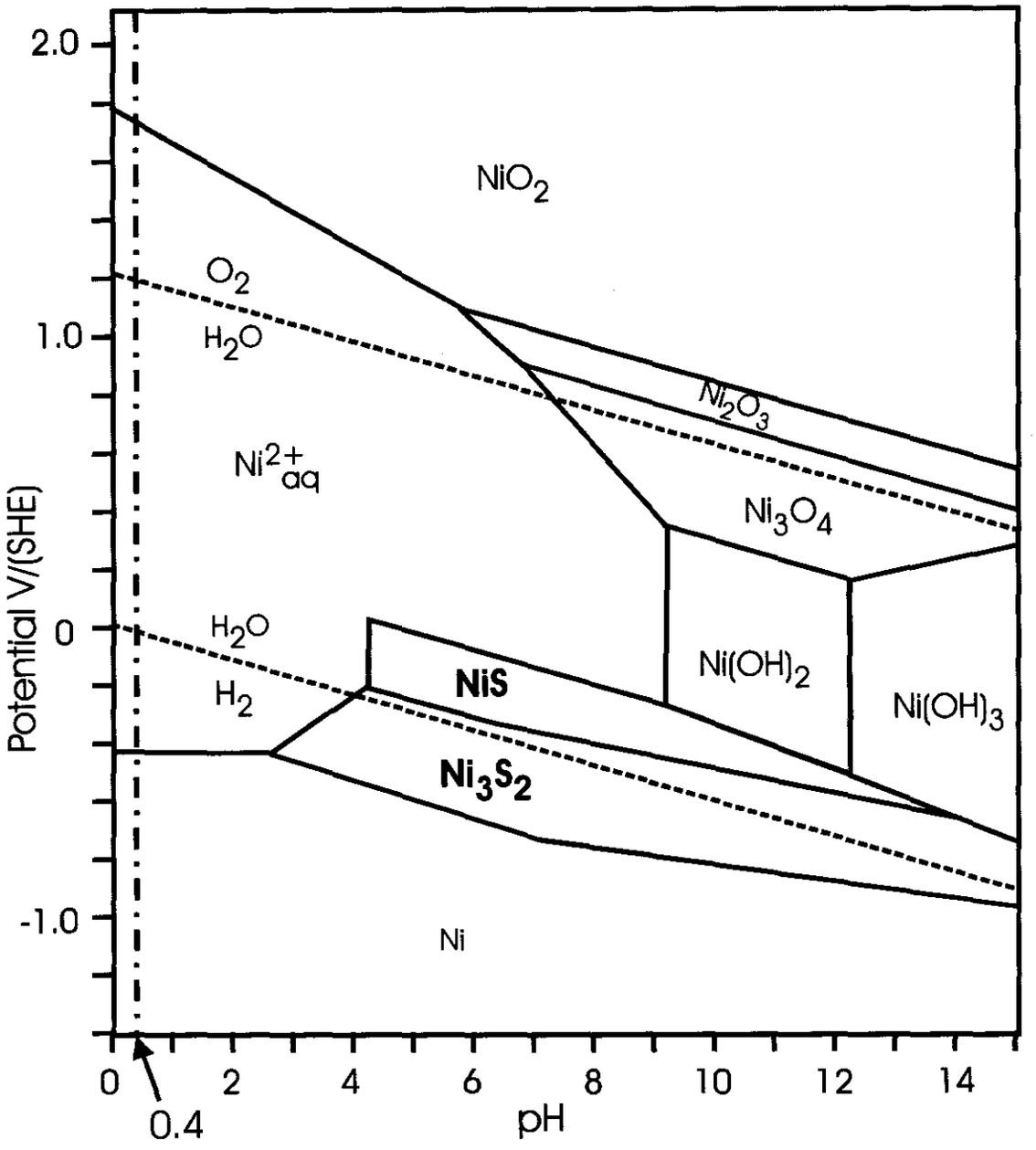

Figure 5.6 A combined Eh-pH diagram for the Ni-H_2O-O_2-S system at 25°C and 1 atmosphere. (Garrels & Christ, 1965; Marcus & Protopopoff, 1997)

At a pH of 0.4, which is the pH where this leaching and electrochemistry study was conducted, it can be seen from Figure 5.6 that Ni_3S_2 and NiS are not stable. Below a potential of –0.4 V nickel metal should start to precipitate and H_2 gas formation will accommodate this plating reaction. Above 1.8 V NiO_2 will start to form together with O_2 gas formation.

With an increase in pH up to 2.8, Ni_3S_2 starts becoming stable, but only at a specific voltage of –0.42 V. NiS is stable between pH 4.2 and 14.

According to *Peters*, nickel sulphide decomposition could possibly occur via four reaction paths, where Ox is the oxidation agent and Ox^- is the reduced form of the oxidative agent:

- Alkali oxidation

$$NiS + 5H_2O + 8Ox \rightarrow NiO + SO_4^{2-} + 10H^+ + 8Ox^- \quad 5.4$$

- Acid oxidation

$$NiS + 2Ox \rightarrow Ni^{2+} + S^0 + 2Ox^- \quad 5.5$$

- Acid decomposition

$$NiS + 2H^+ \rightarrow Ni^{2+} + H_2S \quad 5.6$$

$$Ni_3S_2 + 6H^+ \rightarrow 3Ni^{2+} + 2H_2S + H_2 \quad 5.7$$

- Reduction

$$Ni_3S_2 + 4H^+ + 4R \rightarrow 3Ni^0 + 2H_2S + 4R^+ \quad 5.8$$

The alkali oxidation reaction (reaction 5.4) is utilised in the Sherritt Gordon ammonia leach process and the acid decomposition reactions (reactions 5.6 and 5.7) are utilised in the Falconbridge matte leach process. The reduction reaction (reaction 5.8) has not been reported and may be unobservable because nickel has a high hydrogen overvoltage that won't permit reaction 5.8 to continue after the first traces of nickel are formed (*Peters, 1976).*

5.2.2 NICKEL SULPHIDES

Dissolution processes of nickel-copper sulphides involve mixed potential leaching reactions and can thus be described in terms of an electrochemical model. The electrochemistry of nickel sulphides is of interest in determining the mechanisms of leaching reactions. Leaching of metals in a sulphide mineral into solution can be either oxidising or reducing to form sulphide ions or H_2S respectively. Ni sulphide leaching is a complicated process due to the series of sulphides that form as the leaching process proceeds (*Power, 1982*).

In the electrochemical study of cyclic voltammetry with a rotating disc and ring-disc electrodes of nickel sulphides (NiS), conducted by *Power*, a passive layer was found to consist of a metal deficient nickel sulphide layer and sulphur. Due to the fact that rotating electrodes were used, all peaks observed were due to surface processes, as diffusion processes are suppressed.

For these electrochemical studies, the temperature varied between 22 and 25°C for the different runs, with a scan rate of 200 $mV.s^{-1}$ at a rotating disc speed of 2000 r.p.m. All potentials were reported with respect to the saturated calomel electrode. Two different electrolytes at a concentration of 1 $mol.dm^{-3}$ were used namely: $HClO_4$ and HCl containing 10^{-3} $mol.dm^{-3}$ $K_4[Fe(CN)_6]$.
The main features of the cyclic voltammetry were a passive region from –0.1 to +0.6 V, anodic formation of insoluble species between +0.8 and +1 V, transpassive dissolution above +1 V, reduction of anodically formed species below –0.1 V, a cathodic process that may be hydrogen evolution below –0.4 V and oxidation at –0.3 V of species formed during the aforementioned cathodic reaction.

During ring-disc studies, with a NiS disc surrounded by a glassy carbon ring, ferrocyanide ions were used as an indicator of electrochemical activity of the disc surface. The oxidation of ferrocyanide and the consequent reduction current due to the ferricyanide reduction at the ring was clearly evident. By

making use of electroplated copper on the carbon disc, it was shown that the anodically formed products contained sulphur:

$$2Cu + H_2S - 2e^- \rightarrow Cu_2S + 2H^+ \qquad 5.9$$

The conclusion was thus drawn that these compounds formed on the surface of NiS by anodic oxidation in acid solution, contained excess sulphur and was thus either sulphur rich nickel sulphides or elemental sulphur.

By washing with CS_2, after the electrode was cycled at anodic potentials and held at a potential at which the current was zero on the return sweep, the cathodic sweep was then completed. The cathodic peak showed a decrease in height, which only returned to its original height after several cycles. If the cathodic peak was due to a layer of pure sulphur, the reduction peak should have been totally eliminated after washing with CS_2, as was shown by the equivalent experiment on galena (PbS) where the passive layer is only sulphur. Even though this layer is an electronic conductor, it nonetheless passivates the surface by blocking the transport of nickel ions from the bulk NiS to the solution. The following reactions were reported to be potentially responsible for the formation of a passive layer on NiS in the potential region from 0 to 0.8 V (*Power, 1981*):

$$2NiS - 2e^- \rightarrow NiS_2 + Ni^{2+} \qquad E^0 = -0.34\ V \qquad 5.10$$

$$NiS - 2e^- \rightarrow S + Ni^{2+} \qquad E^0 = +0.09\ V \qquad 5.11$$

Above 0.57V the possibility for Ni_2S_3 formation exists:

$$3NiS - 2e^- \rightarrow Ni_2S_3 + Ni^{2+} \qquad E^0 = +0.58\ V \qquad 5.12$$

Possible reduction reactions were restricted to:

$$S + 2e^- + 2H^+ \rightarrow H_2S \qquad E^0 = -0.1\ V \qquad 5.13$$

$$Ni_2S_3 + 2e^- + 2H^+ \rightarrow 2NiS + H_2S \qquad E^0 = +0.39\ V \qquad 5.14$$

$$NiS_2 + 2e^- + 2H^+ \rightarrow NiS + H_2S \qquad E_0 = -0.33\ V \qquad 5.15$$

In a second study conducted by *Power* on the electrochemistry of Ni_3S_2, the anodic and cathodic behaviour in 1 mol.dm^{-3} perchloric acid solutions was examined. Synthetic single phase heazlewoodite rotating disc and ring-disc electrodes were utilized. A sulphur rich sulphide layer, which passivates the electrode surface, was found. The formation of H_2S and hydrogen was observed at cathodic potentials.

Similarly with NiS, the anodic limit seemed to play an important role in determining the composition of the anodically formed passive layer. As the anodic limit shifted to more positive values, the cathodic reduction peak became more negative. This means that the oxidation products that were formed became more difficult to reduce.
A rotating ring-disc electrode with a Ni_3S_2 disc surrounded by a silver ring was used to detect the presence of dissolved H_2S by the following reaction:

$$2Ag\ (s) + H_2S\ (aq) - 2e^- \rightarrow Ag_2S\ (s) + 2H^+\ (aq) \qquad 5.16$$

As a result of a slow potential sweep at the disc, H_2S formation was detected at the ring. A peak in the ring current corresponded to a peak in the region of –0.1 V due to cathodic reduction of anodic products on the disc, which indicated that the passive layer on the Ni_3S_2 disc consisted of either sulphur or a sulphur-rich nickel sulphide. This was in agreement with the behaviour of millerite (NiS) (*Power, 1981*), as well as chalcopyrite ($CuFeS_2$) (*Parker et al., 1981*).

By looking at cyclic voltammetry of the Ni_3S_2 rotating disc electrode in $HClO_4$ at 60°C, different regions were obtained. For example: a region of passivation and transpassive dissolution on the anodic side, with the reduction of anodically formed surface products on the cathodic side. H_2 evolution was also evident on the cathodic side. These observations were much the same as the reactions for NiS as found in Power's previous study, conducted in 1981 (*Power, 1982*).

Transpassive dissolution is a complicated process including electron and ion transport through a surface film, multistep electrochemical reactions at the film/solution interface and transport of reaction products in the bulk solution (*Bojinov et al., 2000; Betova et al., 2002*).

By washing experiments with CS_2 it could be proved or disproved that the anodically formed layer is sulphur. The electrode was removed from solution on the cathodic-going sweep, after formation of anodic products has occurred and before any cathodic reduction has taken place. CS_2, acetone, and water were then used to wash the electrode, where after it was returned to the solution. The cathodic-going sweep was resumed, and any changes in the reduction behaviour of the sample were noted.

In the case of galena, PbS, the only surface product is S and CS_2 washing will lead to total elimination of the cathodic peak. As described previously for NiS, the reduction peak became only a little smaller after a CS_2 wash. The conclusion was thus made that the passive layer was a sulphur rich sulphide phase containing little or no elemental sulphur. In the case of Ni_3S_2 the CS_2 wash at +0.6 V lead to slight decreases in the height of the reduction peak. Higher anodic limits lead to greater decreases. Thus, below +0.6 V, little sulphur is formed and the passive layer on the Ni_3S_2 surface is a sulphur-rich sulphide phase. Above +0.6 V more sulphur is formed.

By examining potentiostatic transients, *Power* looked at the growth of the passive layer. The electrode was kept at a potential where the passive film does not exist and then stepped to a potential where the passive layer formed. The resulting current-time transient was recorded and current was plotted against time. A linear dependence was found between the current and $(time)^{1/2}$. This implied a rate-limiting diffusion step. *Power* found that the anodically formed film was unstable and dissolved chemically in the solution.

Through microscopic studies it was shown that the surface had become roughened by differential corrosion and that solid products such as S, NiS or $NiSO_4$ may also add to the porous nature of the surface.

Some experiments in 1.0 mol.dm^{-3} HCl solution showed the possibility of a passive oxide film. Indications of two or more parallel mechanisms with complex behaviour existed (*Power, 1982*).

Ghali et al. studied the dissolution behaviour of compact Ni_3S_2 electrodes made by fusing the pure synthesized nickel sulphide powder at high temperatures. In acidic iron(III) chloride solutions at 25 ± 0.5°C, they looked at different influencing factors, i.e., suspension density, particle size of powder and applied potential. By increasing the suspension density, decreasing the particle size (increased surface area) and rising the applied potential, the nickel sulphide dissolution rate could be increased.

By plotting dissolution against time, a flattening of the curve was observed. This is characteristic of reactions controlled by diffusion rate. This decrease of dissolution rate with time is a common observation (as was seen in this leaching study and its accompanying literature), and it is believed that this was caused by the formation of β-NiS (millerite), which was detected during the course of the reaction. Increases in dissolved nickel from the suspension with an increase in imposed potential could be explained by the following sequence of reactions taking place:

$$Ni_3S_2 + 6Fe^{3+} \rightarrow 3Ni^{2+} + 2S^0 + 6Fe^{2+} \qquad 5.17$$

$$Fe^{3+} + e^- \rightarrow Fe^{2+} \text{ (cathodic compartment)} \qquad 5.18$$

$$Fe^{2+} \rightarrow Fe^{3+} + e^- \text{ (anodic compartment)} \qquad 5.19$$

Higher anodic currents increase the Fe^{3+} concentration, which accelerates the dissolution rate of nickel sulphide.

A decrease in the rate of dissolution and detection of β-NiS in the product correlates with the following reaction:

$$Ni_3S_2 \rightarrow 2\beta\ NiS + Ni^{2+} + 2e^- \qquad 5.20$$

This confirms the formation of millerite as a possible intermediate phase (*Ghali et al., 1979*).

Filmer and Nicol, in their study of non-oxidative dissolution of nickel sulphides with a rotating ring-disc, found that a chemical or an electrochemical reaction at the electrode surface controlled the dissolution rate. Activation energies between 50 and 65 $kJ.mol^{-1}$ were calculated for the reaction and were indicative of a chemically controlled reaction.

By making use of rotating ring-disc electrodes with different nickel sulphide stoichiometric compositions (see Table 5.1) and a silver ring, *Filmer and Nicol* found that the rate of dissolution was dependant on the potential of the sulphide and the nickel-to-sulphur stoichiometric ratio.

Table 5.1 Some of the synthetic disc materials used which contained heazlewoodite (Filmer and Nicol, 1980)

Sample number	*Stoichiometry*	*Dominant phase*	*Minor phase*
1	$Ni_{1.54}S$	Ni_3S_2	Ni metal
2	$Ni_{1.45}S$	Ni_3S_2	α-Ni_7S_6
3	$Ni_{1.20}S$	α-Ni_7S_6	Ni_3S_2

The rate of the non-oxidative dissolution of these nickel sulphides followed a similar dependence as Nicol and Scott found for the non-oxidative dissolution of iron sulphides. The maximum dissolution rate was around –0.3 V, which decreased slightly with anodic or cathodic potential shifts.

At more anodic potentials (greater than –0.1 V), these samples were oxidized. The following reactions, which are feasible at a potential of –0.1 V, can be ascribed to the oxidation reactions:

$$Ni_3S_2 \rightarrow 2NiS + Ni^{2+} + 2e^- \qquad 5.21$$

$$2NiS \rightarrow NiS_2 + Ni^{2+} + 2e^- \qquad 5.22$$

It was found that the speed at which the ring-disc electrodes were rotated had no significant effect on the dissolution rate. Thus the conclusion was made that the rate determining reaction in the non-oxidative dissolution of nickel sulphides was not the diffusion of the reactants or products through the solution. This assumption was also supported by the calculated activation energies.

The dissolution of nickel rich heazlewoodite samples (Table 5.1, sample no.1) was dependent on the concentration of the acid used. This could be explained by the fact that the rate of dissolution of nickel from nickel sulphides containing metal is limited by the rate of dissolution of the nickel metal, which is dissolved relatively slowly by a mixed-potential mechanism.

When looking at the dependence of dissolution on acid concentration, sample numbers 2 and 3 in Table 5.1 showed a dependence on the transfer of either ionic or electron charges. This dependence of the rate of nickel dissolution on the concentration of hydrochloric acid exhibited by samples 2 and 3 is similar to that of iron sulphides under similar conditions (*Filmer and Nicol, 1980*).

Kato and Oki studied the anodic reaction of heazlewoodite in sulphuric acid solution and stated that the dissolution of Ni_3S_2 depended on two successive processes:

$$Ni_3S_2 \rightarrow 2NiS + Ni^{2+} + 2e^- \qquad 5.23$$

$$NiS \rightarrow Ni^{2+} + S^0 + 2e^- \qquad 5.24$$

$$NiS + 4H_2O \rightarrow Ni^{2+} + SO_4^{2-} + 8H^+ + 8e^- \qquad 5.25$$

Reactions 5.24 and 5.25 proceeded simultaneously (*Kato & Oki, 1973*).

5.2.3 COPPER SULPHIDES

During chalcopyrite ($CuFeS_2$) oxidation, a surface film, which seemed to be a metal deficient polysulphide, much like the nickel sulphides (*Power 1981, 1982*) was formed. This film was thermally unstable and slowed transport of Cu(I) and Fe(II) ions and electron transfer to or from electro active species in solution. Three electrochemical processes can cause currents during the corrosion of chalcopyrite (*Parker et al., 1981*):

- Oxidation of chalcopyrite: $CuFeS_2 \rightarrow Cu^{2+} + Fe^{2+} + 2S + 4e^-$ 5.26
- Reduction of Fe(III) or Cu(II) at the corroding surface.
- Oxidation of iron (II) or copper (I) salts on the corroding chalcopyrite.

In the study conducted by *Hillrichs and Bertram* on the anodic dissolution of copper sulphides in sulphuric acid solution, they examined $Cu_{2-x}S$ ($x<1$) and CuS.

During the anodic dissolution of CuS in sulphuric acid, the formation of metastable non-stoichiometric copper oxide or hydroxide was noticed. Only after the dissolution of these layers, total decomposition of CuS started (*Hillrichs and Bertram, 1983*).

The results obtained by $Cu_{2-x}S$ dissolution in sulphuric acid solution were interpreted by a combination of several concurrent reactions: solid state reaction and diffusion through an anodically formed CuS product layer, diffusion in the pores of the product layer and resistance polarization in the pores of the $CuSO_4$ precipitation. Thin metastable oxide films were noticed (*Hillrichs and Bertram, 1983*).

5.2.4 IRON SULPHIDES

Non-oxidative dissolution of a solid occurs when the formal oxidation states of the solute species are identical both in the solution and in the solid states. When one or more of the solute species exist in different oxidation states in the solid and solution phases, oxidative dissolution takes place (*Nicol and Scott, 1979*). By using three types of iron sulphides, *Nicol and Scott* studied the kinetics of non-oxidative dissolution in acids.

$$Fe_9S_{10} + 2H^+ + 2e^- \rightarrow 9FeS + H_2S \qquad 5.27$$

$$H_2S \rightarrow S^0 + 2H^+ + 2e^- \qquad 5.28$$

$$9FeS + 18H^+ \rightarrow 9Fe^{2+} + 9H_2S \qquad 5.29$$

They made rotating-disc electrodes from FeS, Fe-FeS and Fe_9S_{10}. The rate of dissolution of all three sulphides was found to increase only slowly with the concentration of chloride ions between 10^{-3} mol.dm^{-3} and 1 mol.dm^{-3}, when the rate as a function of chloride concentration was studied. With concentrations above 1 mol.dm^{-3}, a more rapid increase occurred.
When studying the rate as a function of potential, it was found that the rate increases with decreasing potential to a maximum at about –0.3 V, below which it decreases slowly with decreasing potential.

In the cyclic voltammetry studies with the various iron sulphide electrodes in dilute acid solutions over the potential ranges in which dissolution occurs, well-defined anodic and cathodic processes occurred. For FeS a cathodic peak at – 0.28 V with a corresponding anodic peak at – 0.06 V were found. For Fe_9S_{10} and Fe-FeS an anodic peak and a shoulder occurred at 0 V and – 0.5 V respectively. No cathodic peaks were evident for these two sulphides.

For Fe_9S_{10} and FeS cyclic voltammograms in solutions of varying acidity were drawn. FeS showed that the cathodic peak becomes smaller and shifts to more cathodic potentials with increasing pH, while the anodic peak showed little change in position. The cathodic behaviour for Fe_9S_{10} was similar to that

of FeS, but the anodic peak became more intense and well defined in solutions with high acidity.

It was found that the transfer of the reactant species across the electrochemical potential barrier at the solid-solution phase boundary, i.e., a process of ionic charge transfer, were rate limiting. It is important to notice that only an FeS compound that is exactly stoichiometric dissolves in accordance with the accepted theory of ionic charge transfer. Any non-stoichiometric iron-deficient iron sulphides must be reduced to exactly stoichiometric FeS before spontaneous non-oxidative dissolution can occur. The effects of potential on the rates of non-oxidative dissolution of the iron sulphides are not unique. Nickel, lead, and zinc sulphides show similar characteristics during non-oxidative dissolution (*Nicol and Scott, 1979*).

5.2.5 SINGLE CRYSTAL STUDIES

Scherer et al. reported on the study of Ni(111) single crystals surfaces in air and in H_2SO_4 solution (*Scherer et al., 2003*). The major results were:

- After exposure to air at room temperature, the surface was covered by a three to four layer thick (111)-oriented NiO film, which consisted of parallel and anti-parallel oriented oxide grains.

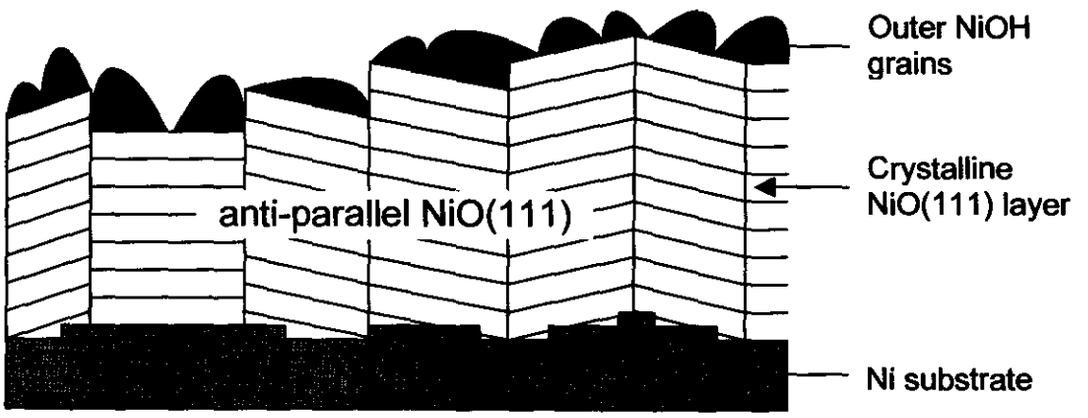

Figure 5.7 Structural model of the passive film formed on Ni (111) in H_2SO_4 solution. (Scherer et al., 2003)

- When the electrode was immersed into a 0.05 mol.dm^{-3} H_2SO_4 solution, the air-formed oxide was reduced. This resulted in atomically smooth, oxide-free Ni electrode surfaces. Experiments indicated the presence of an O/OH or anion species, which induced an outward relaxation of the Ni surface atoms. Monolayer deep pits on the reduced Ni surface are proposed to result from mass transport processes during air oxidation and the subsequent electrochemical reduction.

- Between potentials of –0.25 and –0.20 V, dissolution of the oxide-free Ni surface in 0.05 mol.dm^{-3} H_2SO_4 took place via a step flow mechanism. At more positive potentials, Ni dissolved with higher rates and the Ni surface roughness increased substantially during dissolution.

- Step-flow etching of Ni(111) in H_2SO_4 proceeded isotropically with no preference of certain step orientations, but not uniformly, i.e. it exhibited pronounced differences in the local dissolution rate.

- Through a two-step process an initial hydroxide/hydrated oxide phase was converted into NiO, which lead to passive film formation.

- Structural studies of the passive film supported the duplex model, which suggested a dense, crystalline inner layer, consisting of an anti-parallel oriented NiO (111) film and a more porous outer layer of Ni hydroxide (*Scherer et al., 2003*).

5.3 CONCLUSIONS

Dissolution of metal sulphides involves mixed potential reactions and therefore electrochemical processes can be utilized to study these reactions. Specifically cyclic voltammetry and chronopotentiometry are two electrochemical methods that can be used for studying electrode kinetics, especially for the study of oxidation-reduction reactions.

During the corrosion of nickel sulphide electrodes, it has been reported by numerous investigators that a passive layer, mostly consisting of a metal deficient nickel sulphide layer as well as sulphur, formed during the dissolution process. Once again, similar to the leaching literature, different passivating layers were reported. *Power* reported a sulphur rich sulphide layer when leaching with perchloric acid, while an oxide layer seemed to be present when hydrochloric acid was used as leaching agent.

Ghali et al. stated that the leach reactions were controlled by diffusion rate, while *Filmer and Nicol* found calculated activation energies that support chemically controlled reactions. However, *Ghali et al.* used a still standing electrode, while *Filmer and Nicol* utilised a rotating ring-disc electrode.

Different regions were identified on cyclic voltammograms of Ni_3S_2, under which passivation, oxidation, reduction, and gas evolution were reported. In a couple of cases it was reported that heazlewoodite dissolved electrochemically via the formation of millerite, NiS. This is in agreement with the leaching literature reviewed in Chapter 2.

In some aspects it seems as if the electrochemistry supports the leaching reactions of metal sulphide systems, but still the different authors reported different observations and results.

CHAPTER 6

EXPERIMENTAL:

ELECTROCHEMISTRY OF SYNTHETIC HEAZLEWOODITE

In this chapter...

The experimental approach, sample preparation, and technique that has been utilised during this electrochemical study of Ni_3S_2 are discussed in Paragraphs 6.1 to 6.3. The data processing is described in the last paragraph.

6.1 EXPERIMENTAL APPROACH

The chemical potentials and activities of electrolyte solutions and the thermodynamic properties of non-electrolyte solutions can be studied in much the same way. The difference, however, is that electrolyte solutions have two distinctive features.

Firstly, the strong interactions between ions in solution, thus leading to non-ideal conditions even in dilute systems.

Secondly, electron transfer that takes place in ion reactions, which allows us to study these reactions in an electrochemical cell.

An external source of current can drive non-spontaneous reactions, which provides additional information for the elucidation of the mechanism of the redox-reaction. (*Atkins, 1998*). This is achieved by recording the current, potential and time relationships.

6.2 SAMPLE PREPARATION

During this study the same synthetic heazlewoodite (Ni_3S_2) nugget was used as in the kinetic study. Small disks were cut from the nugget with a diamond saw. Electrical contact was achieved by soldering a short copper wire on to the disk which was connected by a coaxidal wire to the potensiostat. This was then imbedded in Epofix resin, produced by Struers© A/S, Denmark. The

exposed electrode surfaces were measured by the same method as described in Paragraph 3.2.2. The measured surface areas can be seen in Table 6.1.

Table 6.1 The surface areas of the fabricated Ni_3S_2 electrodes

Electrode number	*Surface area (mm^2)*
1	28.86
2	13.56
3	28.83
4	30.33
5	9.43
6	19.61

6.2.1 CYCLIC VOLTAMMETRY

The exposed Ni_3S_2 electrode surfaces were treated on 2000 grit emery paper, after which it was polished on 0.3 μm Alumina powder as well as with a 0.25 μm diamond suspension from Struers©. The electrode was put in an ultrasonic bath with deionised water for 5 minutes to remove all loose impurities from the surface. After the five-minute period in the ultrasonic bath, the electrode was immediately put in the electrolyte and the experiment was started. All data were recorded versus a 1 $mol.dm^{-3}$ KCl normal calomel electrode.

6.2.2 CHRONOPOTENTIOMETRY

To obtain a new surface, the electrode was polished on 2000 grit emery *in situ* for 30 seconds while it was rotating at 600 r.p.m. (Figure 6.2). All data were recorded versus a 1 $mol.dm^{-3}$ KCl normal calomel electrode.
Rotating the electrode prevented the growth of a thick diffusion layer that would influence the potential.

6.3 ELECTROCHEMICAL TECHNIQUE

6.3.1 REAGENTS

Millipore milli-Q deionised water was used to make up all electrolyte solutions. The following chemicals were used during the investigation: sulphuric acid (H_2SO_4), nitric acid (HNO_3), hydrochloric acid (HCl), perchloric acid ($HClO_4$), iron(III) sulphate ($Fe_2(SO_4)_3.9H_2O$), iron(II) sulphate ($FeSO_4.7H_2O$), copper(II) sulphate ($CuSO_4.5H_2O$) and Epofix resin. Analytical grade reagents from MERCK were used without further purification. Ni_3S_2 electrodes, prepared from the original synthetically prepared Ni_3S_2 nugget, were used during the electrochemical study.

6.3.2 ELECTROCHEMICAL APPARATUS

6.3.2.1 CYCLIC VOLTAMMETRY

As mentioned earlier, two methods were used, each with its own experimental set up. The cyclic voltammetry was conducted with a conventional three-electrode cell as can be seen in Figure 6.1.

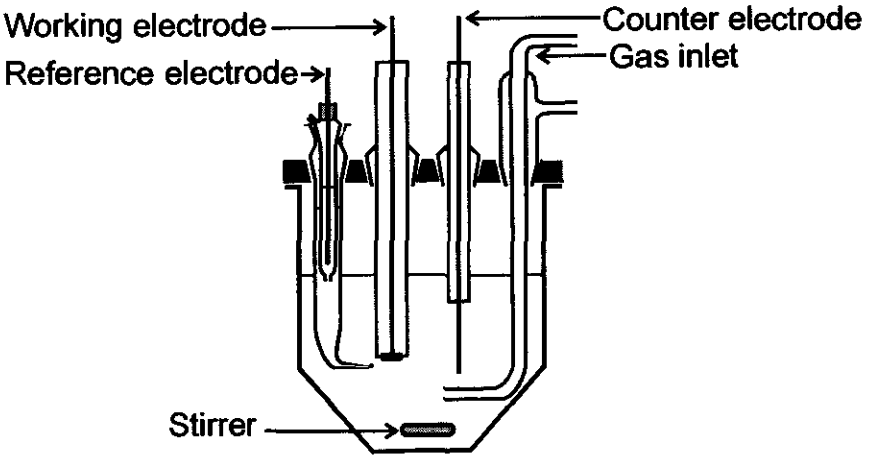

Figure 6.1 A schematic drawing of a conventional three-electrode cell

The cell contained the electrolyte, a stirrer, the three electrodes, as well as a gas inlet. The electrolyte was changed accordingly to the type of experiment, since different electrolytes were investigated. A magnetic stirrer brought about agitation in order to remove any gas bubble formation on the electrode surface. The stirrer was also used to mix the solution in between runs in order to ensure a well mixed electrolyte. The stirrer was switched off during the voltammetric scans. The working electrode consisted of synthetic heazlewoodite as discussed in Paragraph 6.2. A normal calomel electrode was used as reference electrode while a platinum wire was used as counter electrode. During scans the system was purged with nitrogen or oxygen through a gas inlet, depending on the experimental requirements. The solution was undisturbed for 30 seconds before the measurements started. This set up was connected to a potentiostat (Autolab PG STAT 20) in order to record the data.

The Autolab PG STAT 20 is a digital instrument and the cyclic voltammograms are strictly speaking staircase voltammograms. For slow scan rates, as were used in this study, the difference between normal sweep voltammetry and staircase voltammetry is insignificant (*User Manual for General Purpose Electrochemical Systems*).

6.3.2.2 CHRONOPOTENTIOMETRY

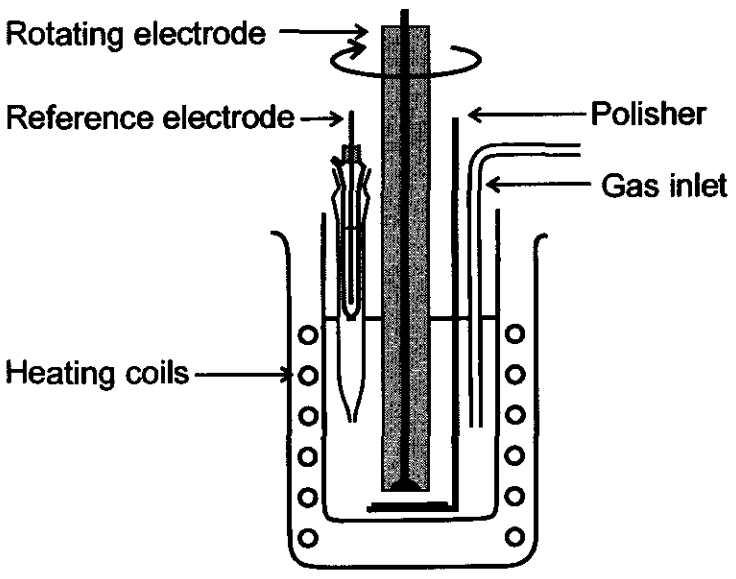

Figure 6.2 A schematic drawing of the rotating electrode cell

Figure 6.2 shows the set up for the chronopotentiometric experiments. It is important to note that only the Ni_3S_2 working electrode and normal calomel electrode were used for these experiments. The system was purged with nitrogen or oxygen through a gas inlet. Heating coils with circulating water controlled the temperature during experiments. The electrode rotated at 600 r.p.m. The polisher remained in the solution during the experiments.

6.4 DATA PROCESSING

The measured potential values, obtained from the cyclic voltammetry, were corrected to confirm with the standard hydrogen convention. This was achieved by adding +0.2801V to the measured potential values to compensate for the potential of the 1 $mol.dm^{-3}$ KCl normal calomel electrode.

Peak potential values and peak current values were obtained by standard methods (*Atkins, 1998*). The built in functions of the potentiostat software, General Purpose Electrochemical System (GPES) for Windows, Version 4.2, Eco Chemie B.V., Utrecht The Netherlands, 1995, were generally used.

The reproducibility in one electrode was found to be reasonable, but once again the reproducibility seemed to be poor from one electrode to another. The decision was thus made to conduct as many runs as possible on one electrode to ensure maximum reproducibility.

CHAPTER 7

RESULTS:

ELECTROCHEMISTRY OF SYNTHETIC HEAZLEWOODITE

In this chapter...

By looking at cyclic voltammetry and chronopotentiometry of synthetic heazlewoodite electrodes, an electrochemical study was conducted to look at the oxidation – reduction reactions taking place. Similar to the leaching experiments, different parameters were studied after the ideal potential limits were determined. Results of this study are presented in the following paragraphs.

7.1 ELECTROCHEMICAL METHODS

By making use of cyclic voltammetry and chronopotentiometry the electrochemical reactions and characteristics of synthetic heazlewoodite electrodes were studied. The first method that was investigated was cyclic voltammetry, where current is monitored as the potential is changed at a constant rate.

7.2 CYCLIC VOLTAMMETRY

7.2.1 DETERMINING THE RUNNING CONDITIONS

It is important to determine the appropriate potential limits for the cyclic voltammetry runs before different parameters can be studied. For these runs, the same electrode was used in 0.5 mol.dm^{-3} H_2SO_4 under N_2 atmosphere at room temperature. During these preliminary runs it was decided to scan in two windows. The wider window's (see Figure 7.1) cathodic potential (<0 V) depended on the reduction of the electrolyte. The anodic limit (>0 V) was determined by the run-away oxidation rate above 1.2 V v. SHE. It seemed like

no oxidation peaks were visible at anodic potentials greater than 0.6 V. The narrow window's (see Figure 7.2) potential limits were thus decided to be around 0 V v. SHE for the cathodic limit and about 1.05 V v. SHE for the anodic limit. Figures 7.1 and 7.2 show these two windows with the associated peaks. The same electrode was used for this exercise for the sake of reproducibility.

During all the runs the starting position of the Figures (indicated by a cross) was selected to give a low electrode current in order to prevent any large scale alteration of the surface by an applied potential before the voltage scan was started.

There were three scan cycles that can be seen as:

- FIRST CYCLE
- SECOND CYCLE
- THIRD CYCLE

The aim of the arrows in the cyclic voltammograms is to aid in the understanding of the scan direction and to show more clearly which peaks formed on the forward scan (from start potential to first vertex potential) and which formed on the backward scan (from first vertex to second vertex potential). The cyclic voltammograms on which arrows were not used should be regarded the same as the last indicative one with arrows.

For the cyclic voltammetry the exposed Ni_3S_2 electrode surfaces were treated on 2000 grit emery paper, after which it was polished on 0.3 μm Alumina powder as well as a 0.25 μm diamond suspension from Struers©. The electrode was put in an ultrasonic bath with deionised water to remove all loose impurities from the surface. After five minutes in the ultrasonic bath, the electrode was immediately put in the electrolyte and the experiment was started.

All the data was measured with regards to a 1 $mol.dm^{-3}$ KCl normal calomel electrode and the potentials were corrected by adding +0.2801 V to the

original potential values. The reported potentials are consequently against the normal hydrogen electrode. This correction was done on all the cyclic voltammograms.

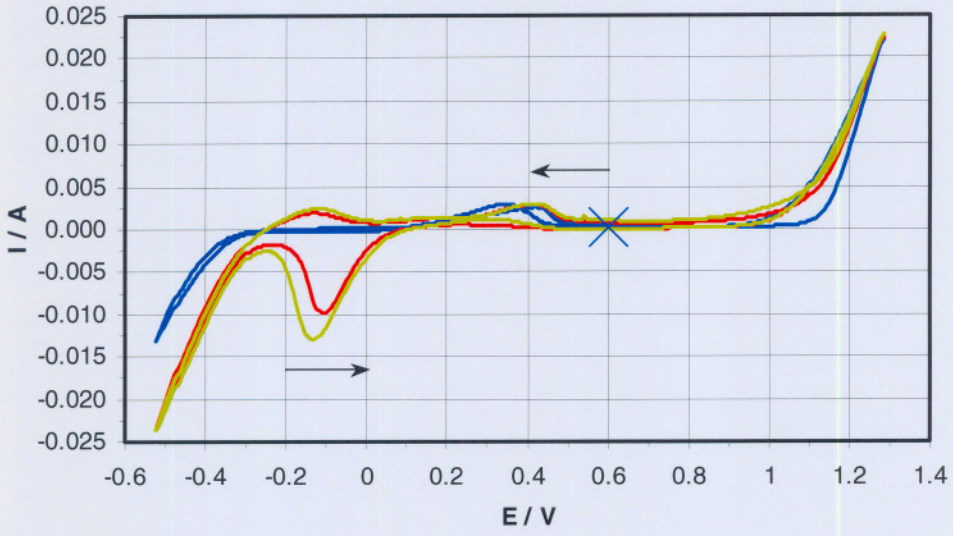

Figure 7.1: Wide window

Start Potential = 0.63 V, First Vertex Potential = -0.49 V, Second Vertex Potential = 1.31 V, Step potential = 0.0048 V, Scan Rate = 0.2 V/s, $[H_2SO_4]$ = 0.5 mol.dm^{-3}, N_2

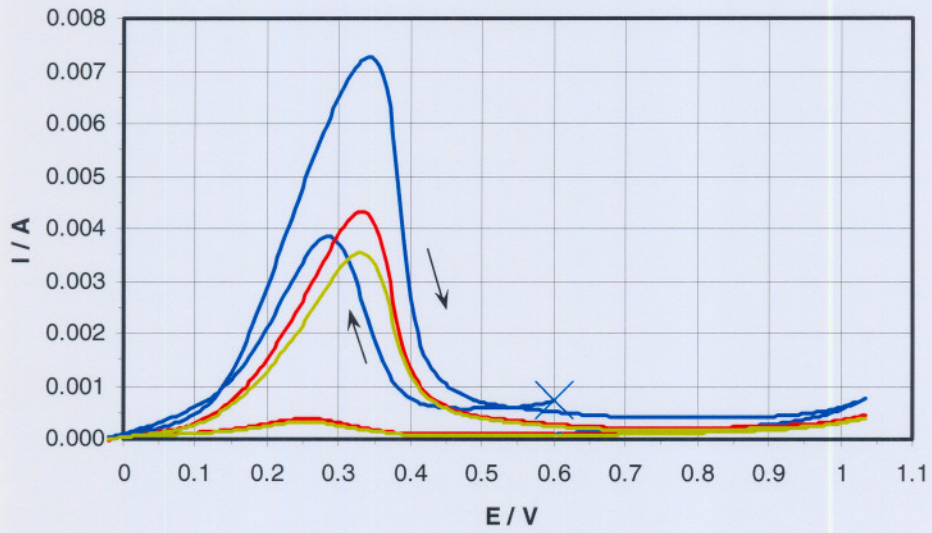

Figure 7.2: Narrow window:

Start Potential = 0.63 V, First Vertex Potential = 0.01 V, Second Vertex Potential = 1.06 V, Step potential = 0.0048 V, Scan Rate = 0.2 V/s, $[H_2SO_4]$ = 0.5 mol.dm^{-3}, N_2

The reduction peaks observed at –0.1 V (see Figure 7.1), were found to be dependent on the anodic limit, more specifically the area above 1 V. This peak at –0.1 V could possibly be regarded as a result of gas release, the decomposition of the mineral at negative potentials or the reduction of the oxidation products formed between 0.2 and 0.6 V. This is well in conjunction with what *Power (1982)* reported in his study of the electrochemistry of Ni_3S_2. Therefore it was decided to concentrate on the deactivation peak formed between 0.2 and 0.6 V where no gas formation took place.

In contrast with *Kato and Oki (1973)*, who worked up to a voltage of 2.5 V, the current study was only able to work below 1 V because of the heavy gas formation that started to take place around 1.1 V. It would have been impossible to interpret the experimental results properly at higher potentials. *Kato and Oki (1973)* reacted nickel foil and sulphur to obtain Ni_3S_2 below the melting point of Ni_3S_2. This might explain the difference with the results obtained in this study.

The solution was stirred to determine whether or not the peaks arouse as a result of diffusion or as a result of chemical reaction on the electrode surface. This run was also conducted on electrode 1 in 0.5 $mol.dm^{-3}$ H_2SO_4 at room temperature under N_2. In this case the solution was stirred by means of a magnetic stirrer.

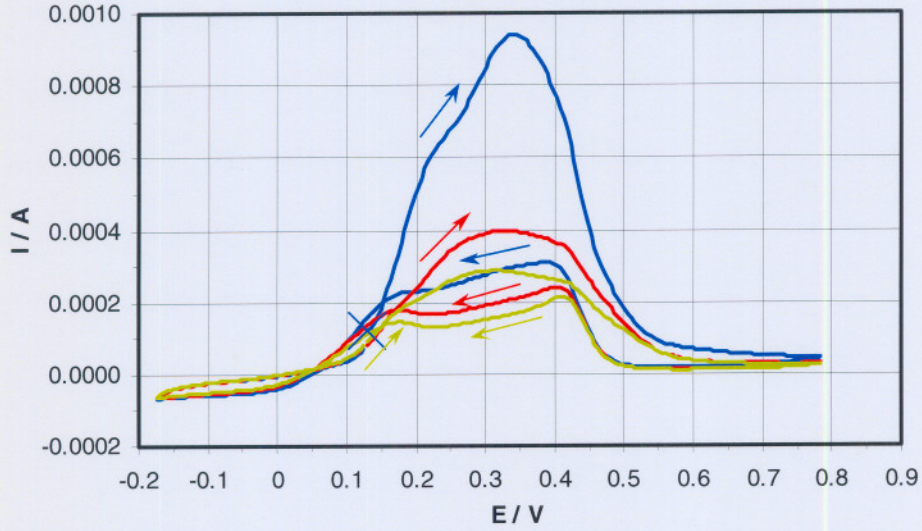

Figure 7.3: Scan rate = 10 mV/s
Start Potential = 0.16 V, First Vertex Potential = 0.81 V,
Second Vertex Potential = -0.14 V, Step potential = 0.0048 V,
[H_2SO_4] = 0.5 mol.dm^{-3}, N_2

It was found that stirring the solution did not cause the peaks to disappear as is evident from Figure 7.3 when compared to Figure 7.14, which was obtained under similar conditions. This confirmed that the peaks were not as a result of diffusion, but rather due to surface changes.

7.2.2 REPRODUCIBILITY RESULTS

Because of the experience with the leaching experiments, it was decided to test the reproducibility of the cyclic voltammetric measurements. Figures 7.4 and 7.5 were obtained from electrode 3, while Figures 7.6 and 7.7 were obtained from electrode 1 in 0.5 mol.dm^{-3} H_2SO_4 at room temperature under nitrogen atmosphere.

The results from electrode 3 showed that the peak position and height stayed almost unchanged, and the same for the results obtained from electrode 1. Thus the reproducibility was once again, similar to the leach experiments, found to be fair in one electrode, but from one electrode to another the results seemed to differ.

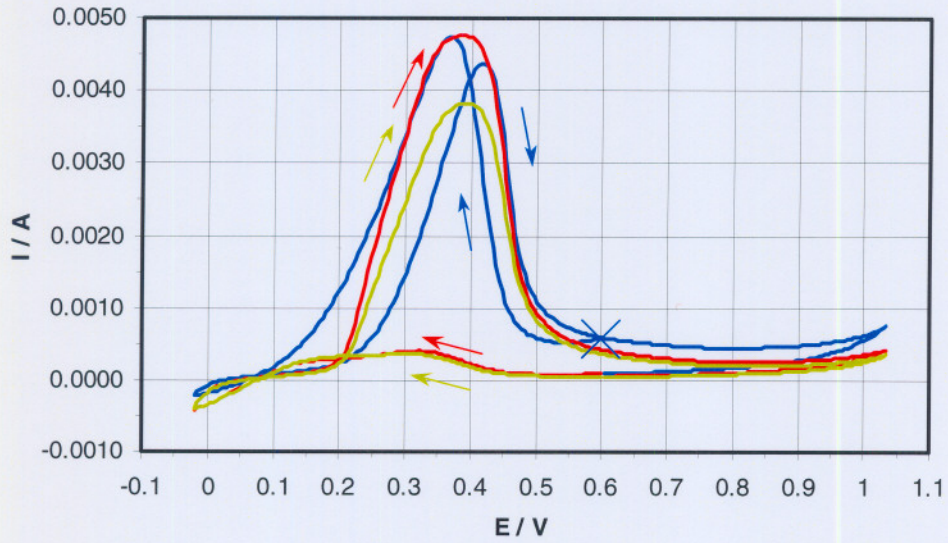

Figure 7.4: Electrode 3 in 0.5 mol.dm^{-3} H_2SO_4 at room temperature under N_2:

Start Potential = 0.63 V, First Vertex Potential = 0.01 V, Second Vertex Potential = 1.06 V, Step potential = 0.0048 V, Scan Rate = 0.2 V/s

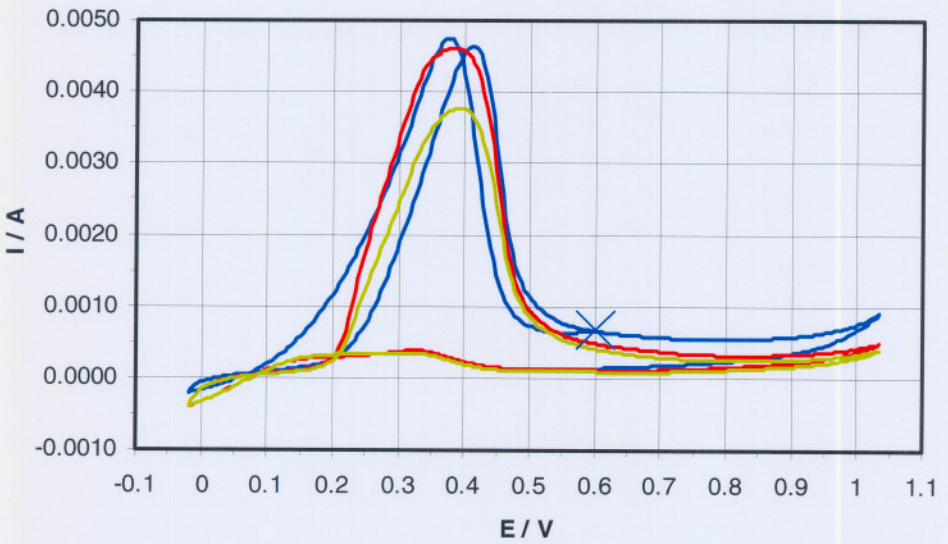

Figure 7.5: Duplicate: electrode 3 in 0.5 mol.dm^{-3} H_2SO_4 at room temperature under N_2:

Start Potential = 0.63 V, First Vertex Potential = 0.01 V, Second Vertex Potential = 1.06 V, Step potential = 0.0048 V, Scan Rate = 0.2 V/s (Arrows as in Figure 7.4)

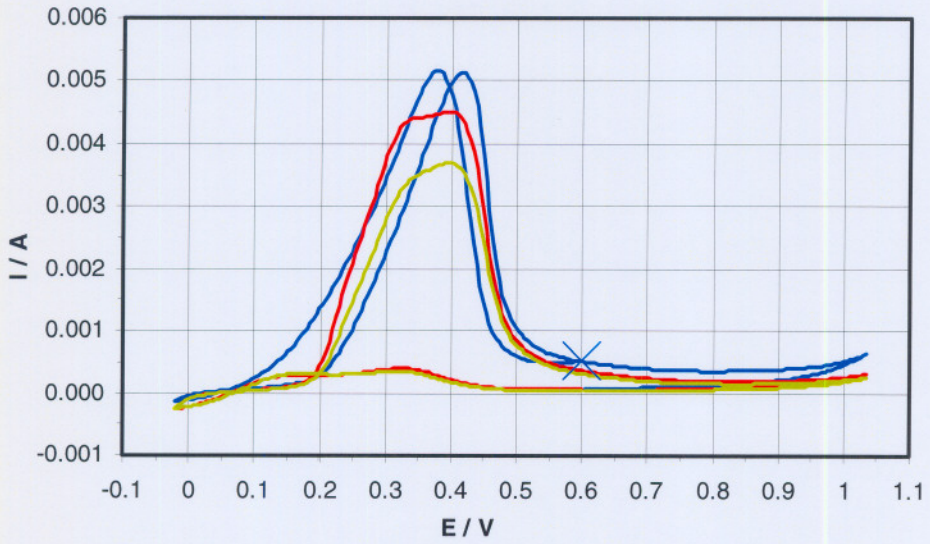

Figure 7.6: Electrode 1 in 0.5 mol.dm^{-3} H_2SO_4 at room temperature under N_2:

Start Potential = 0.63 V, First Vertex Potential = 0.01 V, Second Vertex Potential = 1.06 V, Step potential = 0.0048 V, Scan Rate = 0.2 V/s (Arrows as in Figure 7.4)

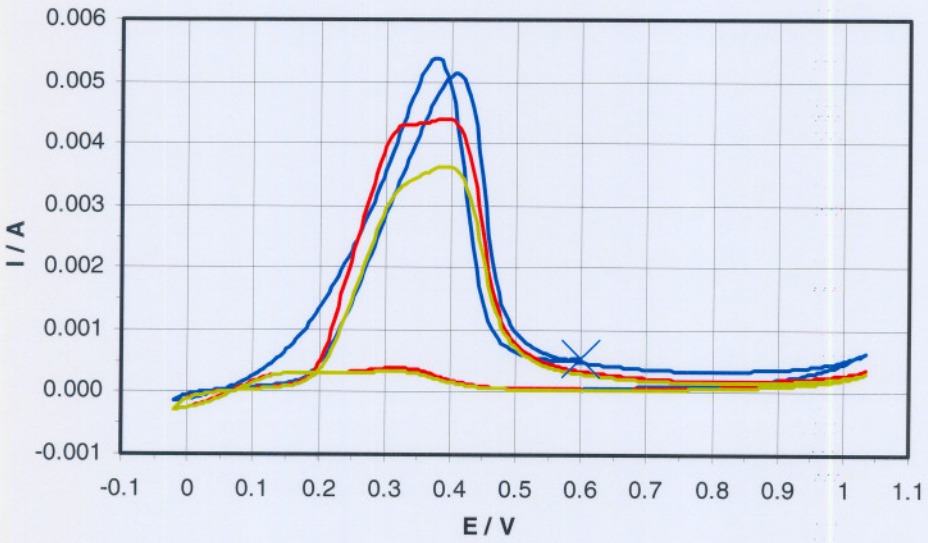

Figure 7.7: Duplicate: electrode 1 in 0.5 mol.dm^{-3} H_2SO_4 at room temperature under N_2:

Start Potential = 0.63 V, First Vertex Potential = 0.01 V, Second Vertex Potential = 1.06 V, Step potential = 0.0048 V, Scan Rate = 0.2 V/s (Arrows as in Figure 7.4)

7.2.3 CURRENT DENSITIES

A number of electrodes were fabricated of which the current densities were calculated. The current densities were obtained by dividing the maximum current value for the forward scan by the geometric surface area of the electrode. The same was done for the backward scan. The runs were conducted on the six different electrodes in 0.5 mol.dm^{-3} H_2SO_4 at room temperature under N_2 atmosphere.

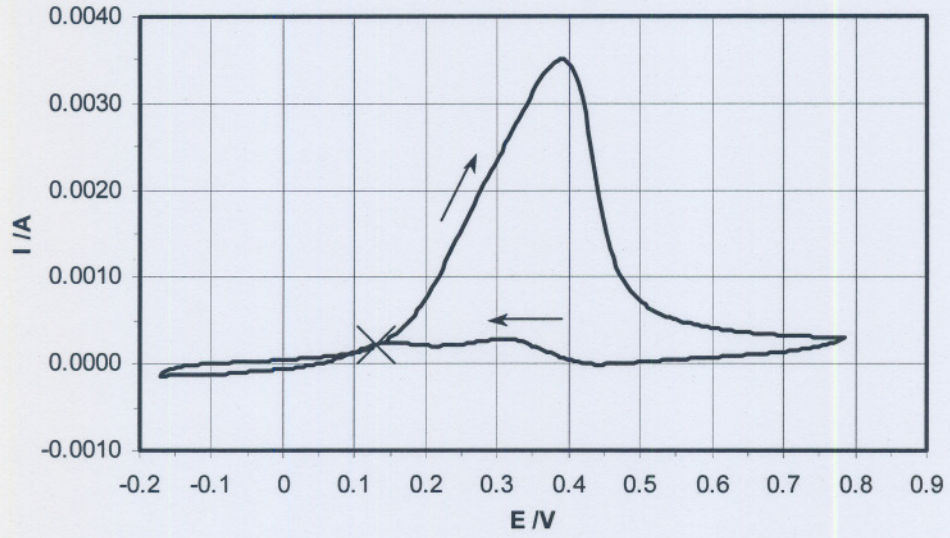

Figure 7.8: Electrode 1

Start Potential = 0.16 V, First Vertex Potential = 0.81 V, Second Vertex Potential = -0.14 V, Step potential = 0.0048 V, Scan Rate = 0.1 V/s, [H_2SO_4] = 0.5 mol.dm^{-3}, N_2

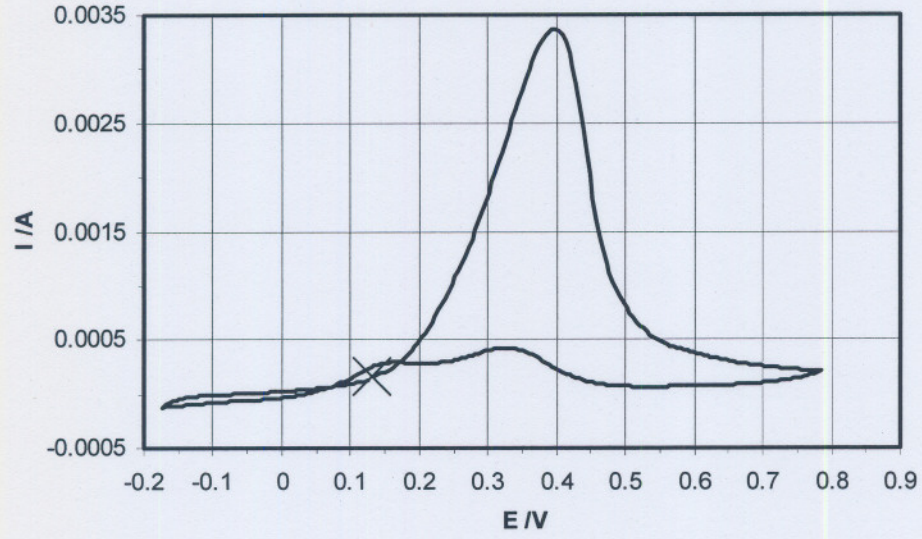

Figure 7.9: Electrode 2

Start Potential = 0.16 V, First Vertex Potential = 0.81 V, Second Vertex Potential = -0.14 V, Step potential = 0.0048 V, Scan Rate = 0.1 V/s, $[H_2SO_4]$ = 0.5 mol.dm^{-3}, N_2 (Arrows as in Figure 7.8)

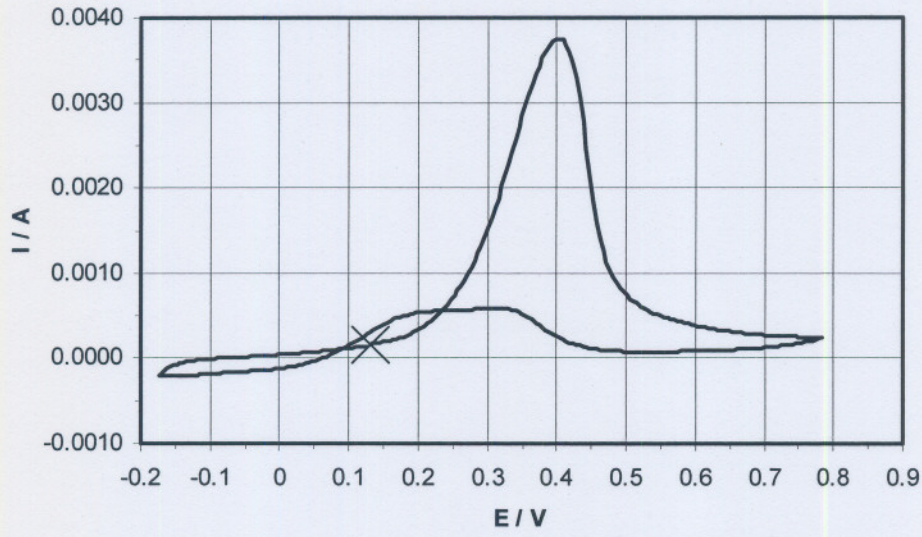

Figure 7.10: Electrode 3

Start Potential = 0.16 V, First Vertex Potential = 0.81 V, Second Vertex Potential = -0.14 V, Step potential = 0.0048 V, Scan Rate = 0.1 V/s, $[H_2SO_4]$ = 0.5 mol.dm^{-3}, N_2 (Arrows as in Figure 7.8)

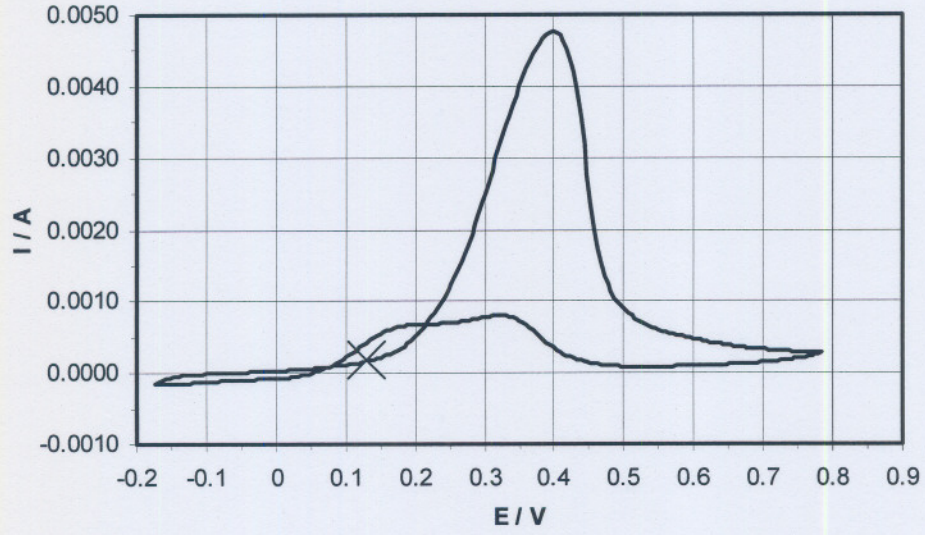

Figure 7.11: Electrode 4

Start Potential = 0.16 V, First Vertex Potential = 0.81 V, Second Vertex Potential = -0.14 V, Step potential = 0.0048 V, Scan Rate = 0.1 V/s, $[H_2SO_4]$ = 0.5 mol.dm^{-3}, N_2 (Arrows as in Figure 7.8)

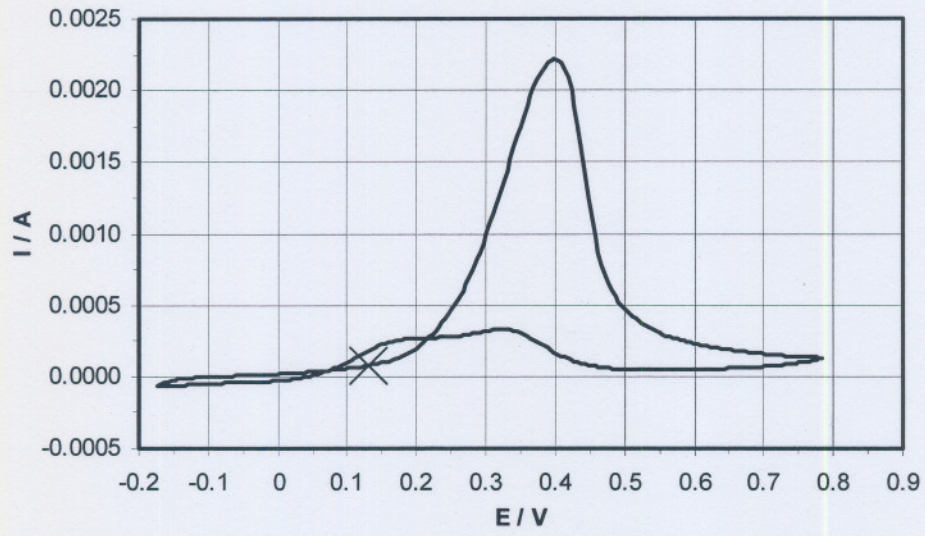

Figure 7.12: Electrode 5

Start Potential = 0.16 V, First Vertex Potential = 0.81 V, Second Vertex Potential = -0.14 V, Step potential = 0.0048 V, Scan Rate = 0.1 V/s, $[H_2SO_4]$ = 0.5 mol.dm^{-3}, N_2 (Arrows as in Figure 7.8)

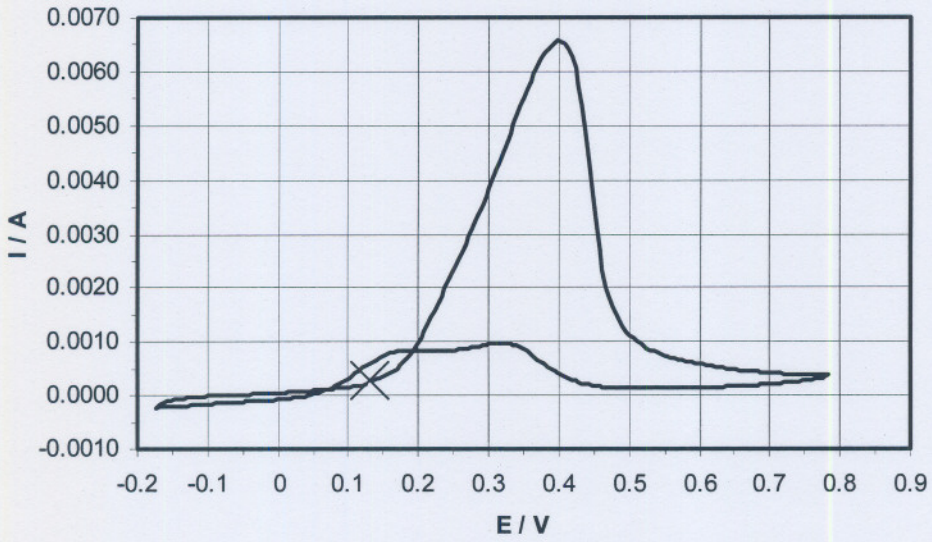

Figure 7.13: Electrode 6

Start Potential = 0.16 V, First Vertex Potential = 0.81 V, Second Vertex Potential = -0.14 V, Step potential = 0.0048 V, Scan Rate = 0.1 V/s, [H_2SO_4] = 0.5 mol.dm^{-3}, N_2 (Arrows as in Figure 7.8)

The measured currents obtained from Figures 7.8 to 7.13 and the calculated electrode current densities are reported in Table 7.1. Current densities are calculated according to geometric surface areas to accentuate the difference between the pellets.

Table 7.1 Surface areas, maximum current and current densities of the electrodes

Electrode #	*Geometric surface area/mm^2*	*Forward scan / mA*	*Current density/ A/m^2*	*Backward scan/ mA*	*Current density/ A/m^2*
1	19.61	3.51	179.08	0.29	14.79
2	9.43	3.46	366.91	0.43	45.60
3	30.33	3.75	123.64	0.60	19.78
4	28.83	4.76	165.11	0.80	27.75
5	13.56	2.22	163.72	0.33	24.34
6	28.86	6.57	227.65	0.97	33.61

Although the current densities for different electrodes show large variations, the general shape of the cyclic voltammograms did not change much. This is indicative that the composition of the surface does not differ much between the pellets. The variation in current densities, support the findings in the kinetic study where it was shown that the reproducibility from one pellet to another was poor. If this was not true, the current densities should not have differed as much as it does.

7.2.4 DETERMINING THE INFLUENCE OF DIFFERENT SCAN RATES

The shape of a cyclic voltammetric curve is largely determined by the reaction rate of the chemical species that are involved in the electrochemical reactions. Short-lived species can be observed only when the scan rate is high enough. At slow scan rates, species might be observed that are formed in slow reactions.

The following series of cyclic voltammograms show the effect of different scan rates.

All the runs were conducted on electrode 1 in 0.5 mol.dm^{-3} sulphuric acid at room temperature under N_2.

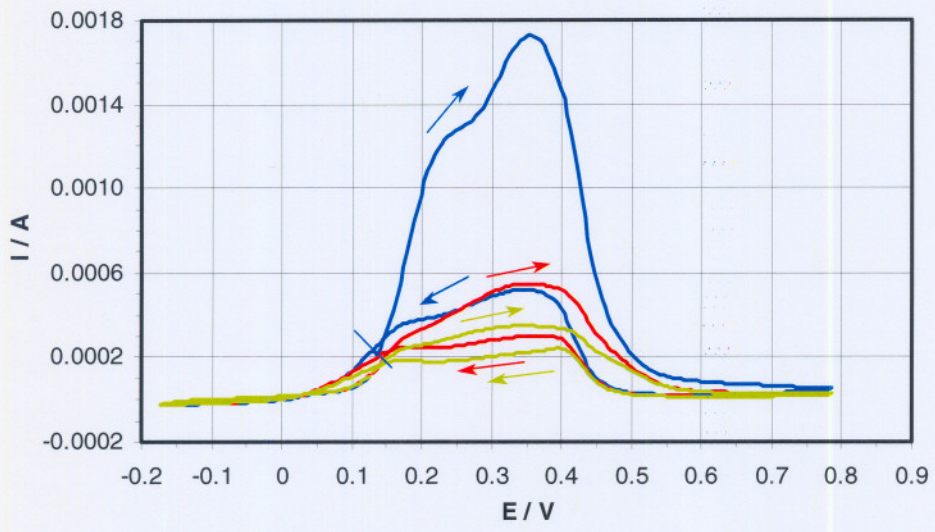

Figure 7.14: Scan rate = 10 mV/s
Start Potential = 0.16 V, First Vertex Potential = 0.81 V,
Second Vertex Potential = -0.14 V, Step potential = 0.0048 V,
[H_2SO_4] = 0.5 mol.dm^{-3}, N_2

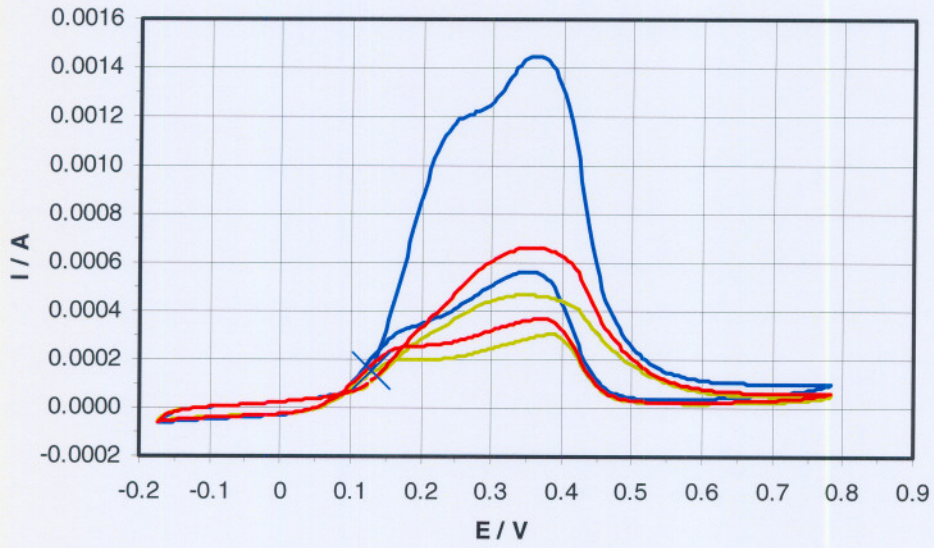

Figure 7.15: Scan rate = 20 mV/s
Start Potential = 0.16 V, First Vertex Potential = 0.81 V,
Second Vertex Potential = -0.14 V, Step potential = 0.0048 V,
[H_2SO_4] = 0.5 mol.dm^{-3}, N_2 (Arrows as in Figure 7.14)

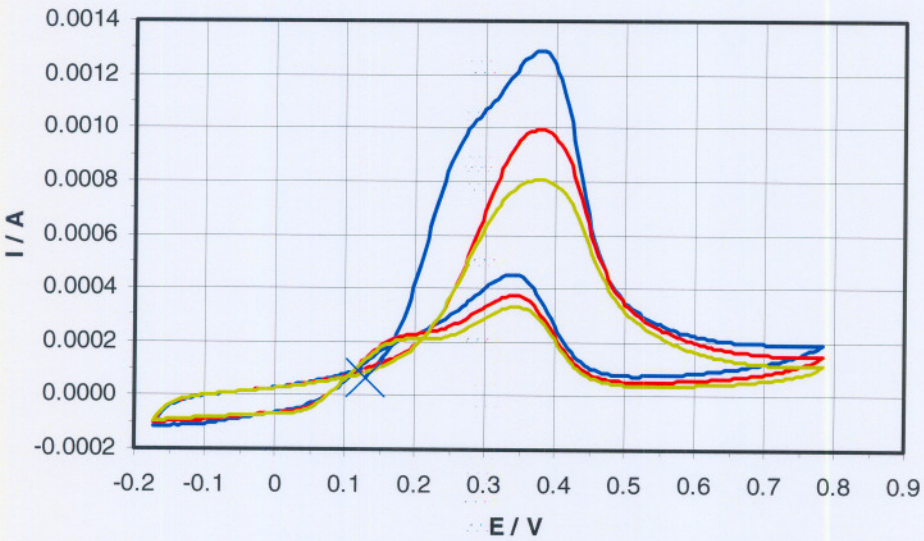

Figure 7.16: Scan rate = 50 mV/s
Start Potential = 0.16 V, First Vertex Potential = 0.81 V,
Second Vertex Potential = -0.14 V, Step potential = 0.0048 V,
[H_2SO_4] = 0.5 mol.dm^{-3}, N_2 (Arrows as in Figure 7.14)

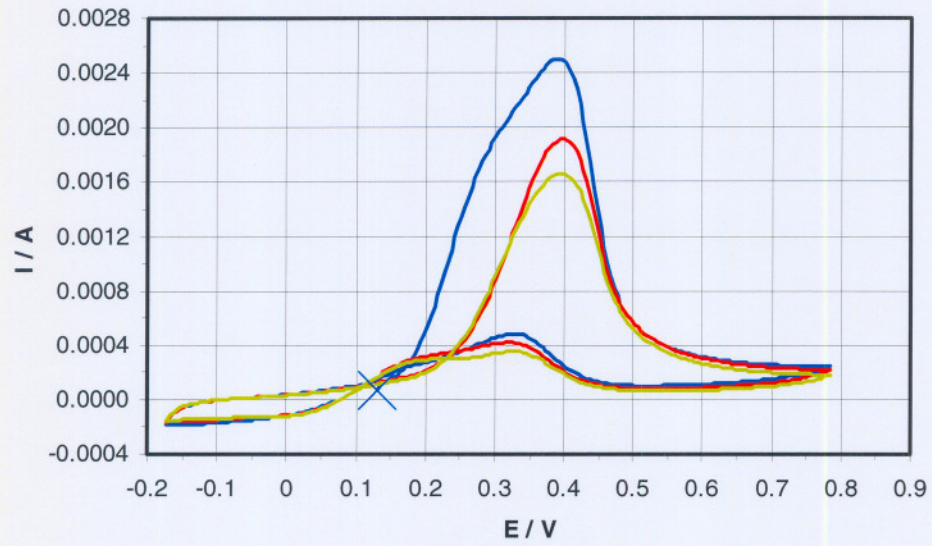

Figure 7.17: Scan rate = 100 mV/s
Start Potential = 0.16 V, First Vertex Potential = 0.81 V,
Second Vertex Potential = -0.14 V, Step potential = 0.0048 V,
[H_2SO_4] = 0.5 mol.dm^{-3}, N_2 (Arrows as in Figure 7.14)

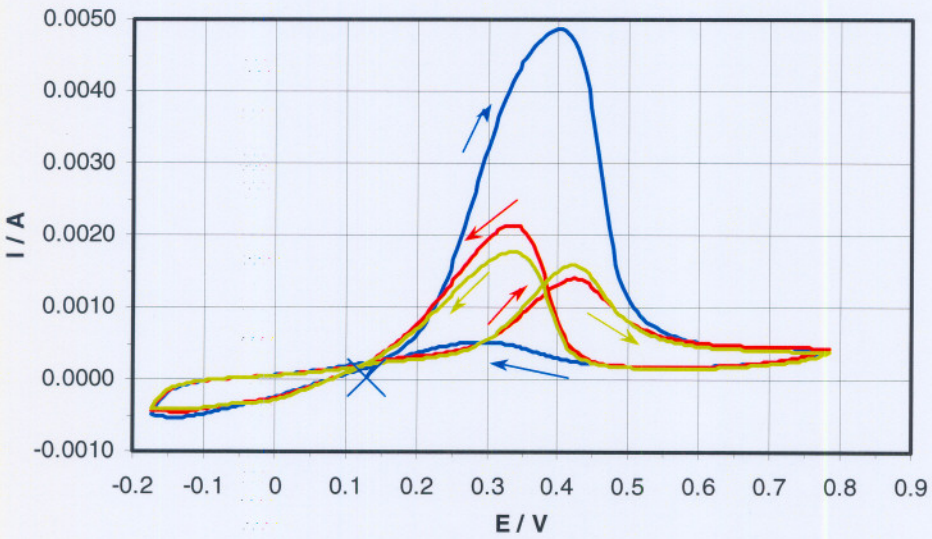

Figure 7.18: Scan rate = 300 mV/s
Start Potential = 0.16 V, First Vertex Potential = 0.81 V,
Second Vertex Potential = -0.14 V, Step potential = 0.0048 V,
[H_2SO_4] = 0.5 mol.dm^{-3}, N_2 (Arrows as in Figure 7.14)

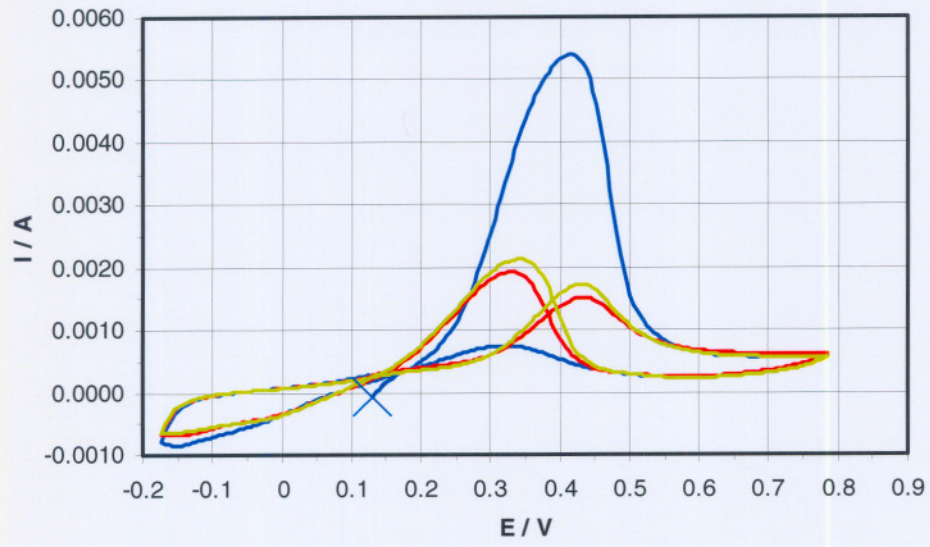

Figure 7.19: Scan rate = 600 mV/s
Start Potential = 0.16 V, First Vertex Potential = 0.81 V,
Second Vertex Potential = -0.14 V, Step potential = 0.0048 V,
[H_2SO_4] = 0.5 mol.dm^{-3}, N_2 (Arrows as in Figure 7.14)

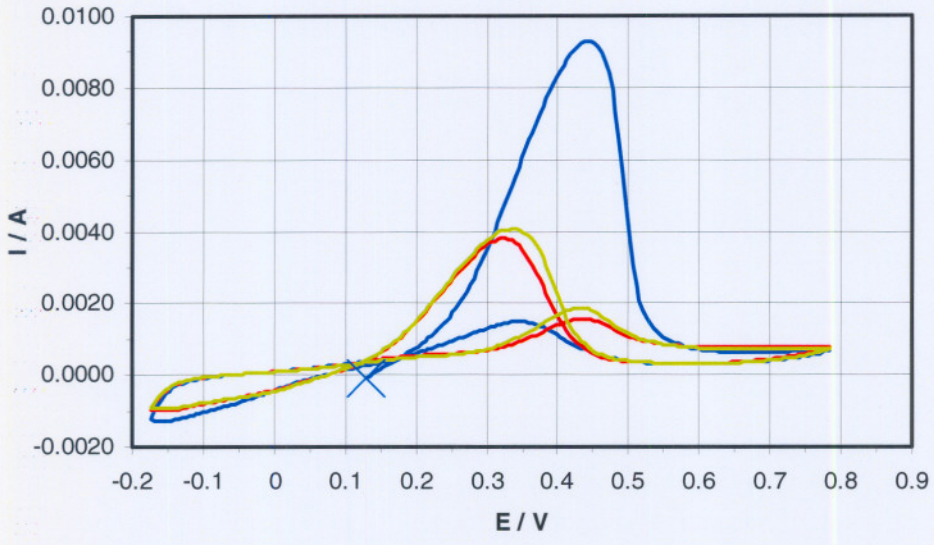

Figure 7.20: Scan rate = 1000 mV/s
Start Potential = 0.16 V, First Vertex Potential = 0.81 V,
Second Vertex Potential = -0.14 V, Step potential = 0.0048 V,
[H_2SO_4] = 0.5 mol.dm^{-3}, N_2 (Arrows as in Figure 7.14)

Tables 7.2 and 7.3 show the different scan rates with the associated potential and maximum current values for the three scan cycles.

Table 7.2 ***The potential-current values of the maximum points on the forward scan (start to first vertex potential) at different scan rates***

Scan rate	*E / V*	*I / mA*
10 mV/s		
First cycle	0.356	1.73
Second cycle	0.345	0.550
Third cycle	0.335	0.350
20 mV/s		
First cycle	0.355	1.45
Second cycle	0.355	0.663
Third cycle	0.340	0.468
50 mV/s		
First cycle	0.374	1.29
Second cycle	0.374	0.994
Third cycle	0.374	0.805
100 mV/s		
First cycle	0.384	2.50
Second cycle	0.394	1.92
Third cycle	0.389	1.66
300 mV/s		
First cycle	0.399	4.86
Second cycle	0.423	1.40
Third cycle	0.423	1.59
600 mV/s		
First cycle	0.413	5.39
Second cycle	0.428	1.51
Third cycle	0.428	1.73
1000 mV/s		
First cycle	0.443	9.29
Second cycle	0.428	1.57
Third cycle	1.428	1.87

Table 7.3 ***The potential-current values of the maximum points on the backward scan (first to second vertex potential) at different scan rates***

Scan rate	*E / V*	*I / mA*
10 mV/s		
First cycle	0.340	0.519
Second cycle	0.364	0.303
Third cycle	0.394	0.243
20 mV/s		
First cycle	0.350	0.565
Second cycle	0.364	0.369
Third cycle	0.384	0.306
50 mV/s		
First cycle	0.340	0.453
Second cycle	0.340	0.372
Third cycle	0.345	0.331
100 mV/s		
First cycle	0.325	0.482
Second cycle	0.320	0.419
Third cycle	0.325	0.353
300 mV/s		
First cycle	0.296	0.524
Second cycle	0.330	2.14
Third cycle	0.330	1.76
600 mV/s		
First cycle	0.320	0.750
Second cycle	0.325	1.93
Third cycle	0.340	2.13
1000 mV/s		
First cycle	0.345	1.49
Second cycle	0.320	3.80
Third cycle	0.340	4.06

By inspecting the cyclic voltammograms it can be seen that the double peak of the first cycle that is visible at low scan rates (see Figures 7.14 to 7.16) fuses into a single peak at the higher scan rates (see Figures 7.17 to 7.20). At high scan rates, equilibrium on the electrode surface is not reached. The peaks from the second and third cycles drifted apart at higher scan rates.

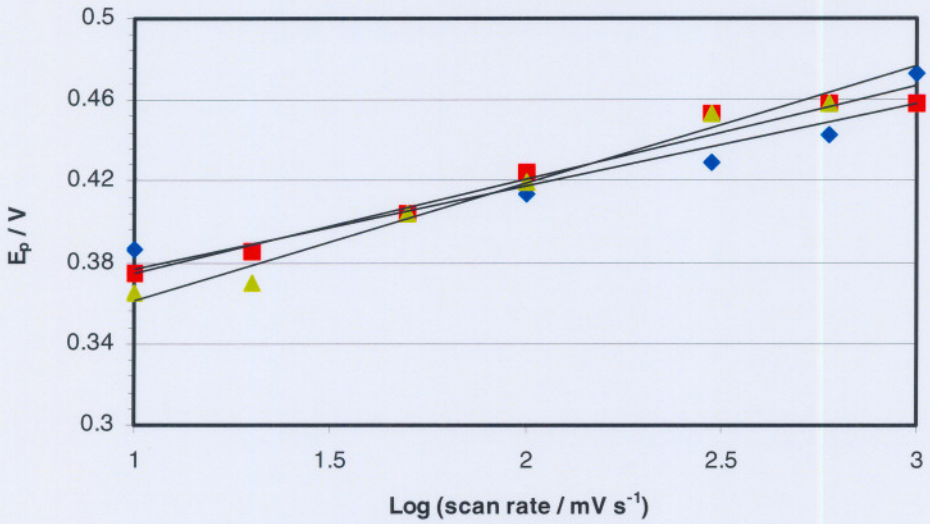

Figure 7.21 Peak potential (E_p) against log of forward scan rates
◆ First forward cycle, ■ Second forward cycle,
▲ Third forward cycle

According to *Bard and Faulkner (1980)*, for totally irreversible systems E_p is a function of scan rate and will shift in a negative direction by an amount of $1.15RT/\propto n_a$ (or $30/\propto n_a$) mV at 25°C for each tenfold increase in ν.

Where	R	=	gas constant
	T	=	temperature in Kelvin
	$\propto$	=	transfer coefficient
	n_a	=	number of electrons transferred per molecule

The gradients for the three lines were determined by means of linear regression and are reported in Table 7.4.

Table 7.4 Calculated gradient values from Figure 7.20

Cycle	*Gradient*
First	0.041 ± 0.005
Second	0.046 ± 0.004
Third	0.058 ± 0.004

For n_a = 1 and α = 0.5 the expected value for the slope is 0.060. For reversible systems a zero slope is expected. The obtained slopes are in accordance with a quasi-reversible oxidation at the surface. This interpretation might be too simplistic because of the formation of an inert layer.

For the backward scan the above-mentioned model cannot describe the data, since the reaction occurring is not the reduction of the oxidation species.

7.2.5 STUDYING THE INFLUENCE OF THE SCAN DIRECTION

Changing the scan direction may well have an effect on the oxidation-reduction peaks that form. Instead of cycling to oxidative (positive potentials) conditions before cycling to reducing (negative potentials), the scan direction was changed to reducing-oxidising. Runs were conducted on electrode 1 in 0.5 mol.dm^{-3} H_2SO_4 at room temperature under N_2. The results are presented in Figures 7.22 and 7.23.

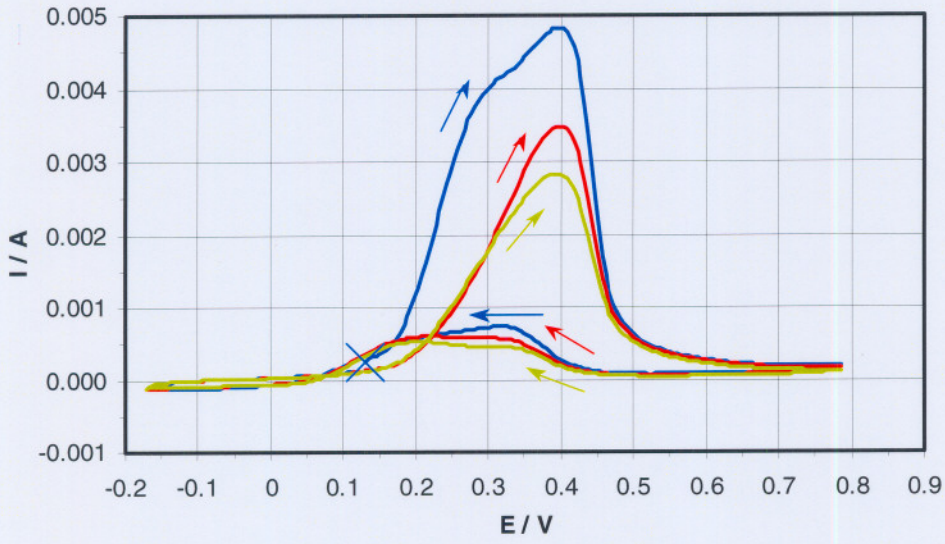

Figure 7.22: Initial direction: oxidative-reductive
Start Potential = 0.16 V, First Vertex Potential = 0.81 V, Second Vertex Potential = -0.14 V, Step potential = 0.0048 V, Scan Rate = 0.1 V/s, $[H_2SO_4]$ = 0.5 mol.dm^{-3}, N_2

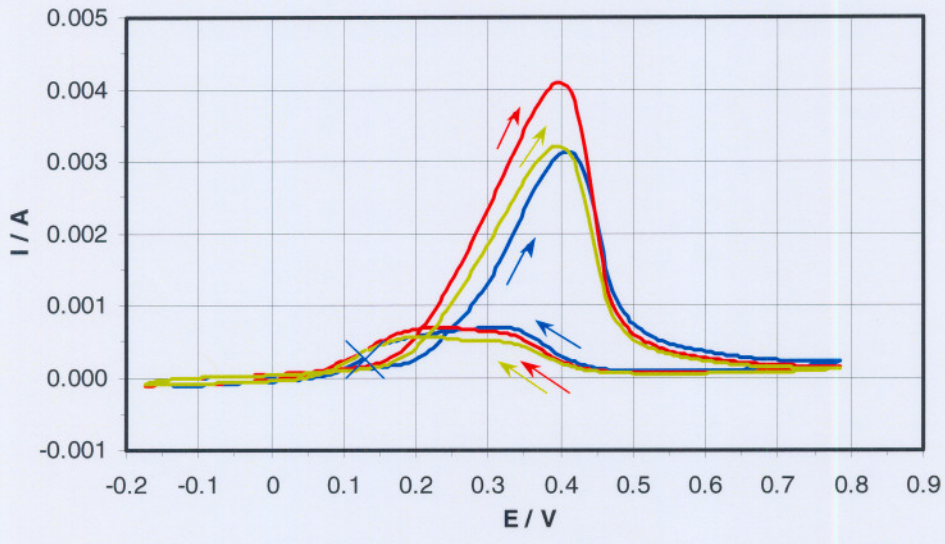

Figure 7.23: Initial direction: reductive-oxidative
Start Potential = 0.16 V, First Vertex Potential = -0.14 V, Second Vertex Potential = 0.81 V, Step potential = 0.0048 V, Scan Rate = 0.1 V/s, $[H_2SO_4]$ = 0.5 mol.dm^{-3}, N_2

From Figures 7.22 and 7.23 it is clear that the initial scan direction had a pronounced effect on the first cyclic voltammetric cycle. With a positive initial scan, two overlapping oxidation peaks are observed. In the case of an initial negative scan direction only a single oxidative peak is observed. This difference disappears for the second and third cycle. In all cases two overlapping oxidative peaks are observed when scanning from 0.81 V to – 0.14 V, which indicates that two distinctive products are formed during oxidation. These products are also formed spontaneously by the action of the acid, which will explain the double peak in the first peak in Figure 7.22.

7.2.6 PASSIVATION LAYER

During the kinetic study of the leaching of synthetic heazlewoodite pellets, it seemed that passivation of the surface area occurred after a while. Other investigators also observed this trend on metal sulphides, especially on nickel and copper sulphides (*Power, 1981 & 1982; Parker et al., 1981*). It was decided to conduct an electrochemical investigation on electrodes that were treated by acid leaching. The electrodes were once again treated as described in Paragraph 7.2.1. To see the effect of passivation, the electrode was left in the electrolyte for periods of 15 seconds, 30 seconds, 1 minute, and 2 minutes. After each period, a separate run was conducted. Each run was conducted in 0.5 mol.dm^{-3} H_2SO_4 at room temperature in the presence of N_2 gas. Results are presented in Figures 7.24 to 7.27.

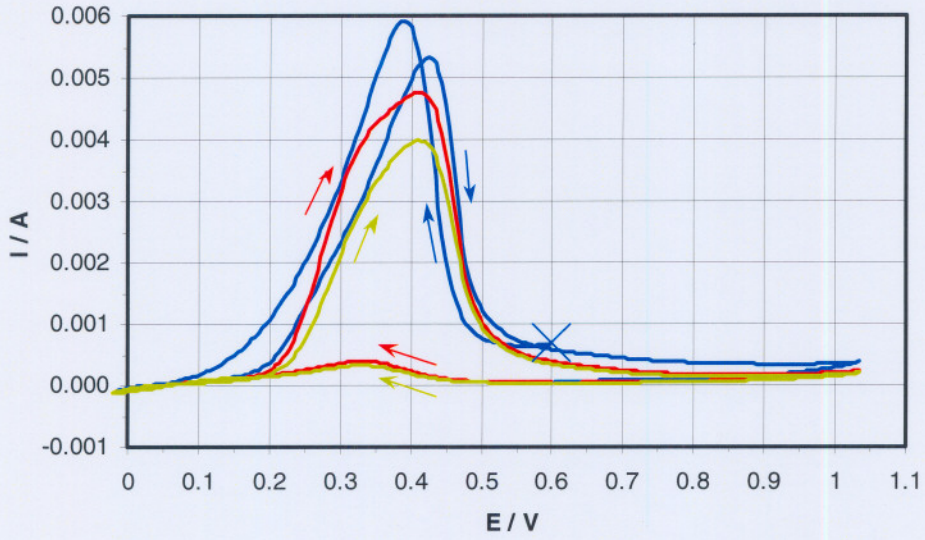

Figure 7.24: After electrode was in acid solution for 15 seconds: Start Potential = 0.63 V, First Vertex Potential = 0.01 V, Second Vertex Potential = 1.06 V, Step potential = 0.0048 V, Scan Rate = 0.2 V/s, $[H_2SO_4]$ = 0.5 mol.dm^{-3}, N_2

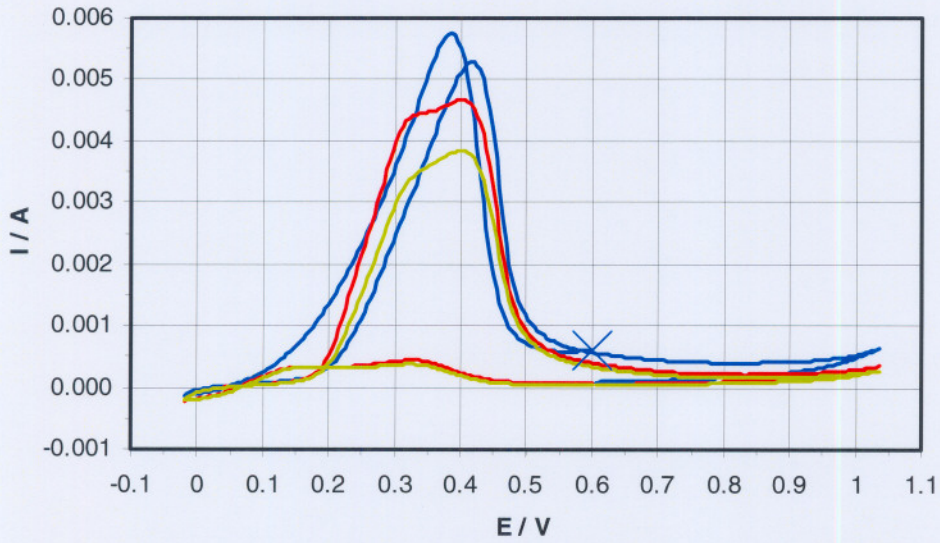

Figure 7.25: After electrode was in acid solution for 30 seconds: Start Potential = 0.63 V, First Vertex Potential = 0.01 V, Second Vertex Potential = 1.06 V, Step potential = 0.0048 V, Scan Rate = 0.2 V/s, $[H_2SO_4]$ = 0.5 mol.dm^{-3}, N_2 (Arrows as in Figure 7.24)

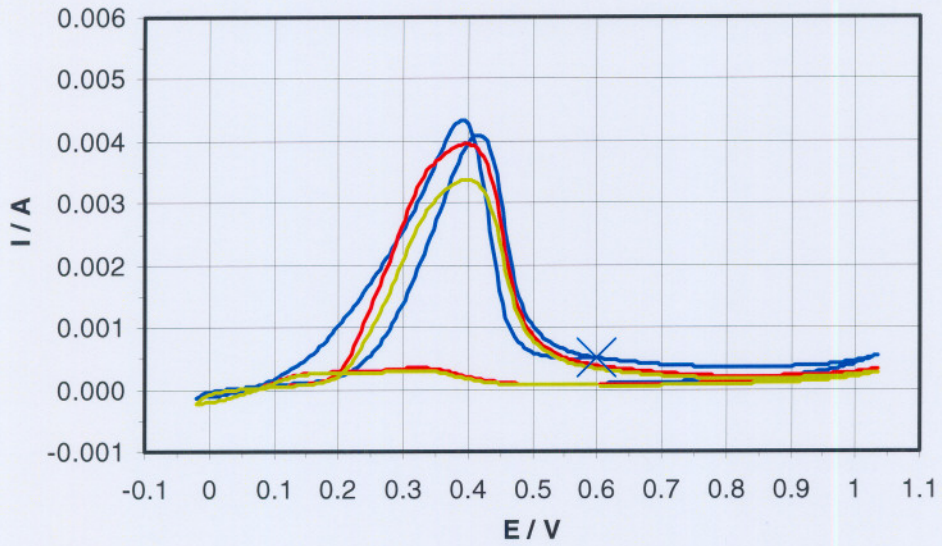

Figure 7.26: After electrode was in acid solution for 1 minute: Start Potential = 0.63 V, First Vertex Potential = 0.01 V, Second Vertex Potential = 1.06 V, Step potential = 0.0048 V, Scan Rate = 0.2 V/s, $[H_2SO_4]$ = 0.5 mol.dm^{-3}, N_2 (Arrows as in Figure 7.24)

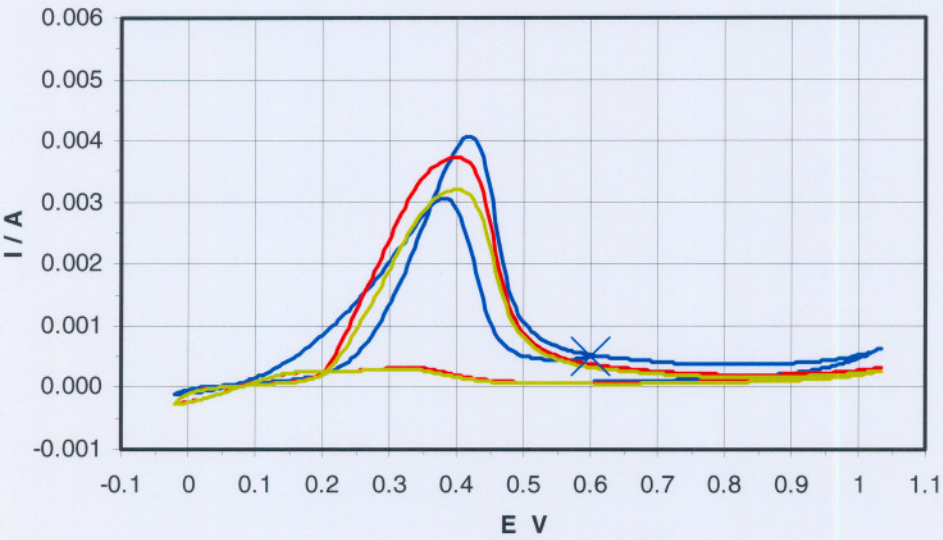

Figure 7.27: After electrode was in acid solution for 2 minutes: Start Potential = 0.63 V, First Vertex Potential = 0.01 V, Second Vertex Potential = 1.06 V, Step potential = 0.0048 V, Scan Rate = 0.2 V/s, $[H_2SO_4]$ = 0.5 mol.dm^{-3}, N_2 (Arrows as in Figure 7.24)

At the starting potential of 0.63 V, slight passivation has occurred, which causes the low current. Oxidation takes place at around 0.4 V, as is evident from the peak. Passivation is dominating at 0.01 V, as can be seen by the low

constant current. By scanning back to 1.06 V, reduction occurs around 0.45 V with deep passivation from 0.8 V up to 1.06 V.

Table 7.5 shows the maximum current values for the different runs. There is an overall decrease in the current values. This confirms the presence of a passivation layer and that the thickness of this layer probably increases with time. This layer may also become thicker as the time in the acid increases.

Table 7.5 Decreasing current values for the three cycles as a result of increasing time in electrolyte before the run was started

Forward Scan		*Backward Scan*	
E / V	*I / mA*	*E / V*	*I / mA*
0 s			
0.413	5.96	0.423	5.41
0.366	0.401	0.400	4.93
0.366	0.345	0.403	4.13
15 s			
0.390	5.92	0.424	5.32
0.331	0.399	0.410	4.76
0.331	0.327	0.410	3.99
30 s			
0.385	5.74	0.414	5.28
0.322	0.439	0.395	4.66
0.322	0.374	0.400	3.84
1 minute			
0.390	4.33	0.414	4.10
0.322	0.349	0.395	3.95
0.322	0.306	0.395	3.39
2 minutes			
0.371	3.21	0.419	4.07
0.322	0.323	0.400	3.74
0.322	0.292	0.400	3.21

7.2.7 EFFECT OF TYPE OF ACID

Similar to the kinetic leaching study, an electrochemical study was conducted to determine the effect of different acids on the electrochemical processes. The acids used were H_2SO_4, HNO_3, HCl and $HClO_4$. The acids were used in a concentration of 0.5 $mol.dm^{-3}$ and the runs were conducted under N_2 atmosphere at room temperature. Results are shown in Figures 7.28 to 7.31.

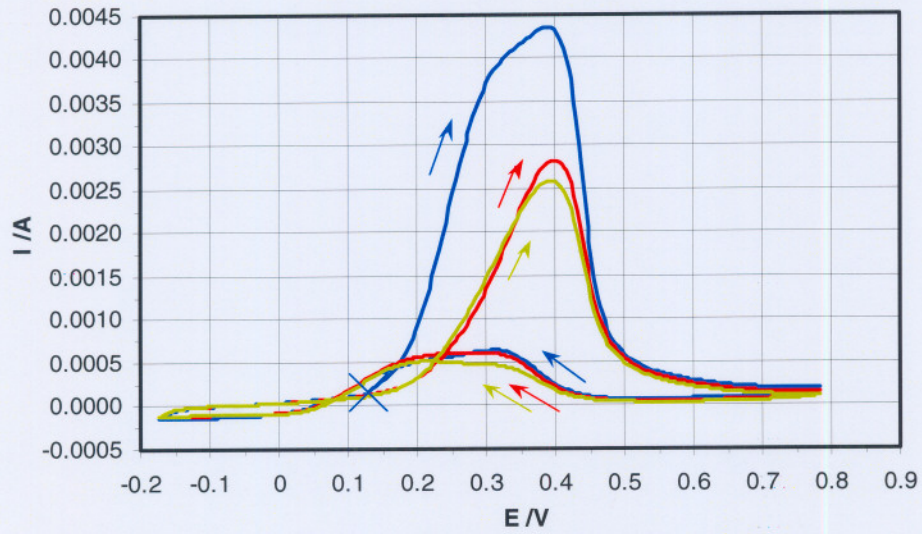

Figure 7.28: Electrolyte: 0.5 $mol.dm^{-3}$ H_2SO_4 solution Start Potential = 0.16 V, First Vertex Potential = 0.81 V, Second Vertex Potential = -0.14 V, Step potential = 0.0048 V, Scan Rate = 0.1 V/s, N_2

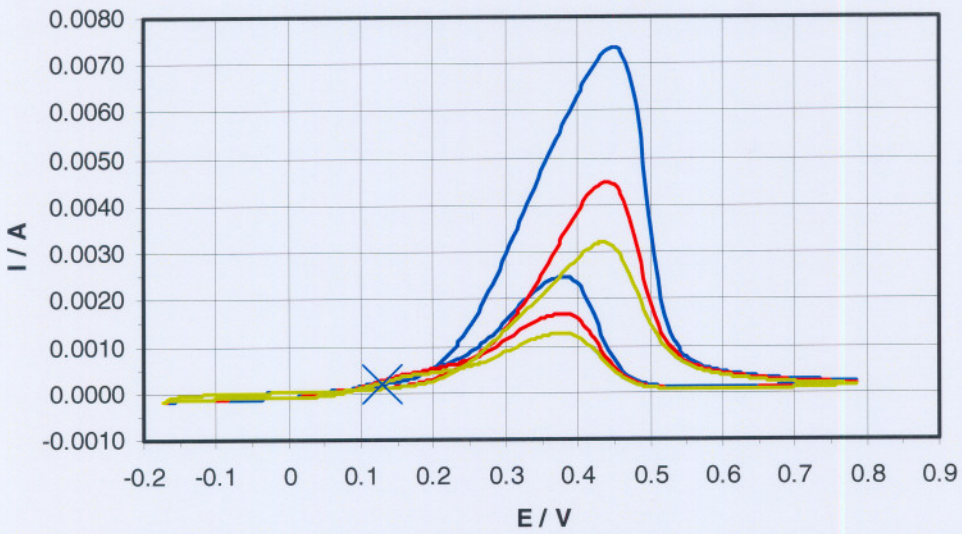

Figure 7.29: Electrolyte: 0.5 mol.dm^{-3} HNO_3 solution Start Potential = 0.16 V, First Vertex Potential = 0.81 V, Second Vertex Potential = -0.14 V, Step potential = 0.0048 V, Scan Rate = 0.1 V/s, N_2 (Arrows as in Figure 7.28)

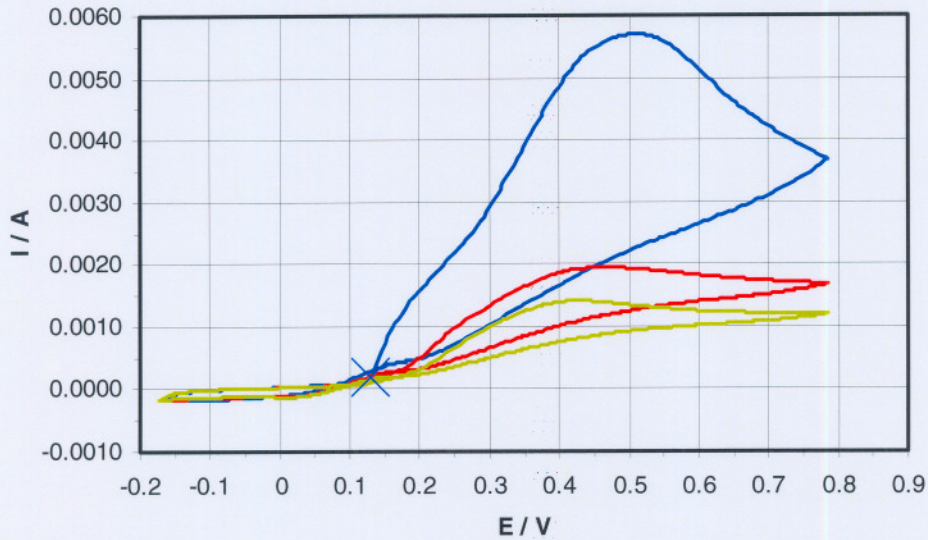

Figure 7.30: Electrolyte: 0.5 mol.dm^{-3} HCl solution Start Potential = 0.16 V, First Vertex Potential = 0.81 V, Second Vertex Potential = -0.14 V, Step potential = 0.0048 V, Scan Rate = 0.1 V/s, N_2 (Arrows as in Figure 7.28)

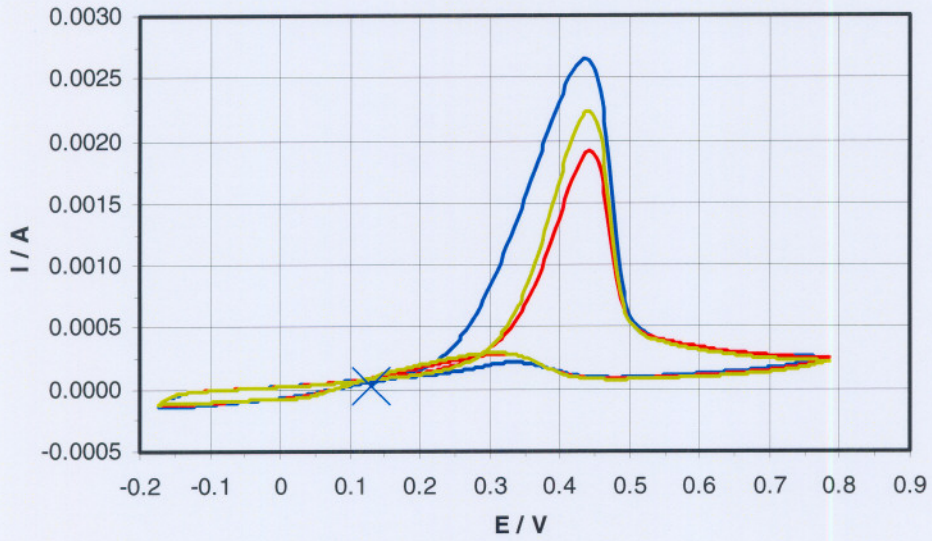

Figure 7.31: Electrolyte: 0.5 mol.dm^{-3} $HClO_4$ solution Start Potential = 0.16 V, First Vertex Potential = 0.81 V, Second Vertex Potential = -0.14 V, Step potential = 0.0048 V, Scan Rate = 0.1 V/s, N_2 (Arrows as in Figure 7.28)

Non-complexing acids appear to be quite similar, while less passivation occurred in hydrochloric acid.

7.2.8 THE INFLUENCE OF NITROGEN AND OXYGEN

The influence of nitrogen and oxygen was studied under two different scan rates, i.e. 10 mV/s and 1000 mV/s. All runs were conducted at room temperature and in a 0.5 mol.dm^{-3} sulphuric acid solution.

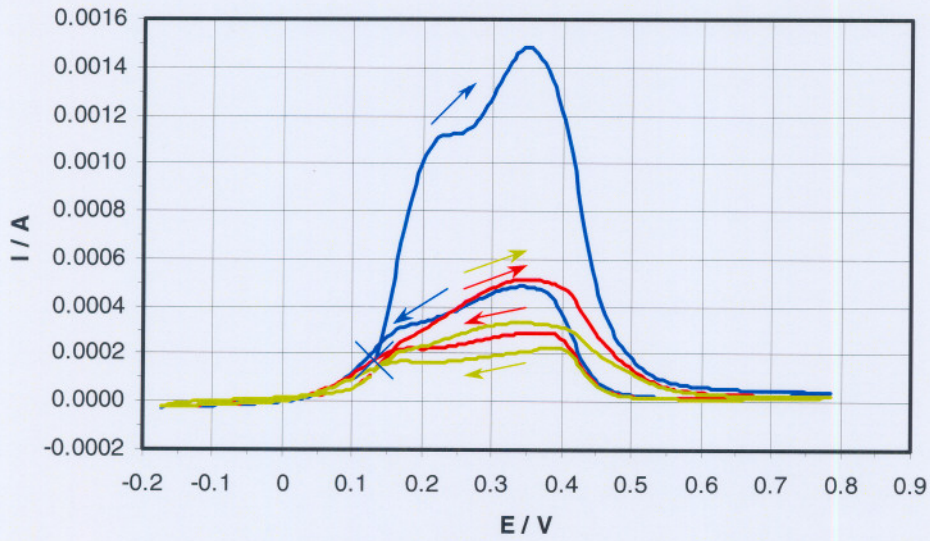

Figure 7.32: Nitrogen atmosphere
Start Potential = 0.16 V, First Vertex Potential = 0.81 V, Second Vertex Potential = -0.14 V, Step potential = 0.0048 V, Scan Rate = 0.01 V/s, [H_2SO_4] = 0.5 mol.dm^{-3}

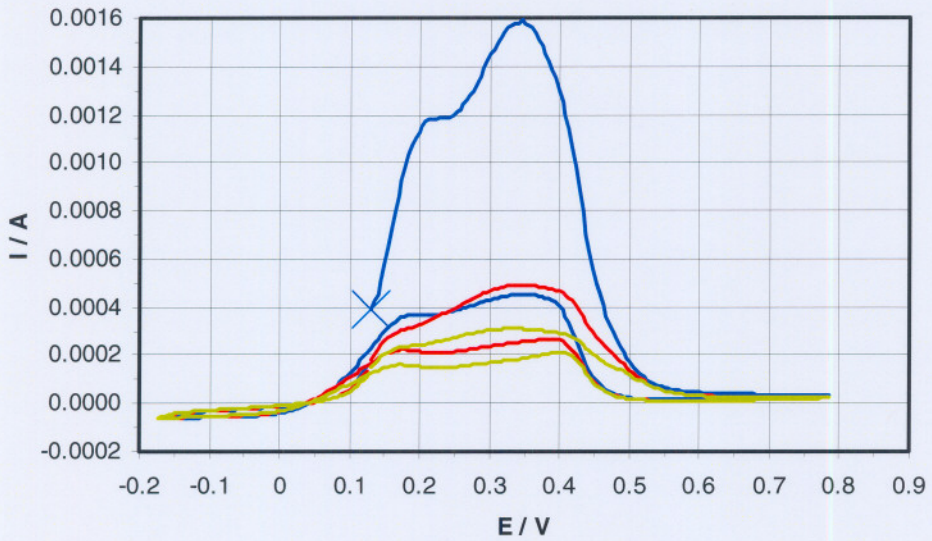

Figure 7.33: Oxygen atmosphere

Start Potential = 0.16 V, First Vertex Potential = 0.81 V, Second Vertex Potential = -0.14 V, Step potential = 0.0048 V, Scan Rate = 0.01 V/s, $[H_2SO_4]$ = 0.5 mol.dm^{-3} (Arrows as in Figure 7.32)

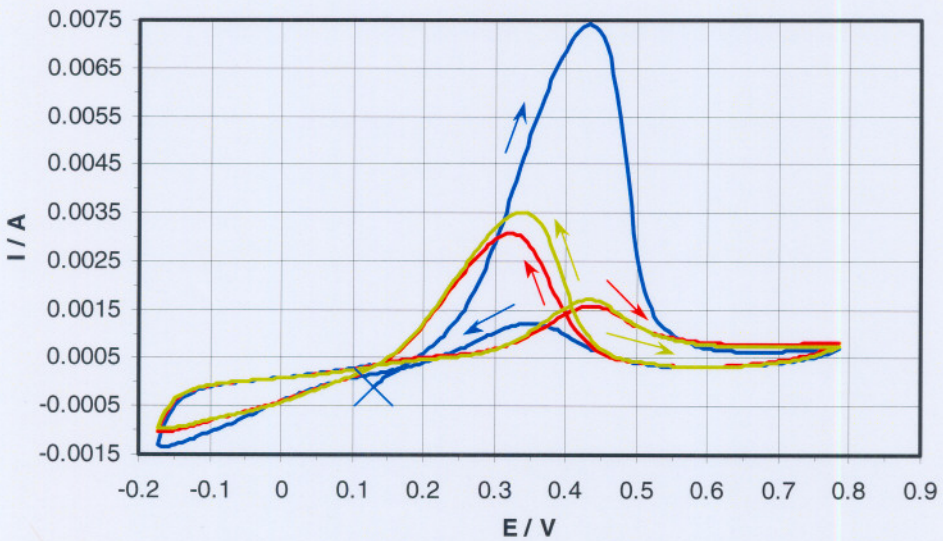

Figure 7.34: Nitrogen atmosphere

Start Potential = 0.16 V, First Vertex Potential = 0.81 V, Second Vertex Potential = -0.14 V, Step potential = 0.0048 V, Scan Rate = 1 V/s, $[H_2SO_4]$ = 0.5 mol.dm^{-3}

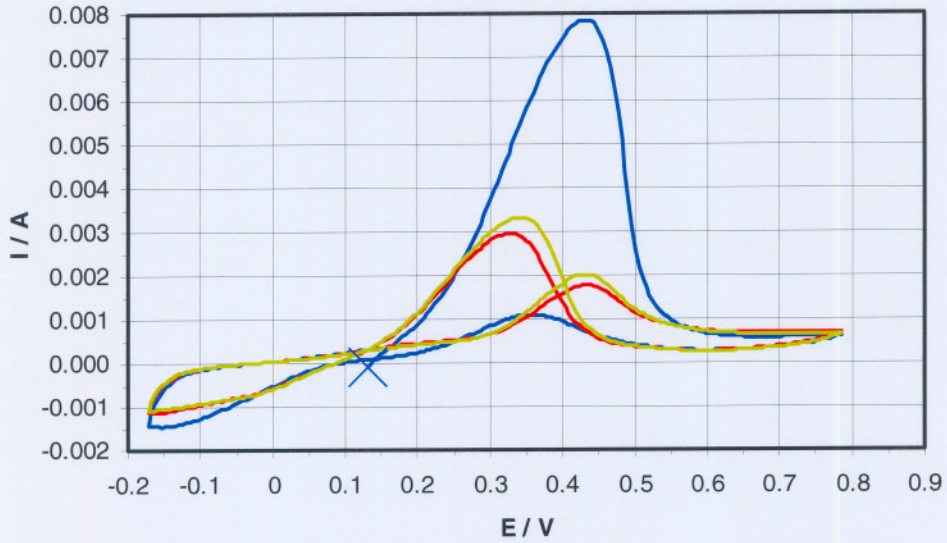

Figure 7.35: Oxygen atmosphere
Start Potential = 0.16 V, First Vertex Potential = 0.81 V, Second Vertex Potential = -0.14 V, Step potential = 0.0048 V, Scan Rate = 1 V/s,
[H_2SO_4] = 0.5 mol.dm^{-3} (Arrows as in Figure 7.34)

The appearance of distinct double peaks in the presence of oxygen indicates that chemical oxidation of the surface occurs. This reaction appears to be fast enough to cause the double peaks, even when scanning from a negative potential. At high scan rates the oxidation by oxygen seems to be too slow to cause the necessary surface composition for the appearance of the double peaks.

7.2.9 EFFECT OF CU(II) AND FE(III) IONS

The effect of Cu(II) and Fe(III) ions were studied, similarly to the thermal leaching study. The ions were added in concentrations of 0.01 mol.dm^{-3} and 0.1 mol.dm^{-3} to a 0.5 mol.dm^{-3} sulphuric acid solution. A run was conducted with 0.5 mol.dm^{-3} sulphuric acid with no Cu(II) or Fe(III) ions present, which will be used as reference (Figure 7.36). All the runs were done in 0.5 mol.dm^{-3} H_2SO_4 at room temperature and under nitrogen atmosphere.

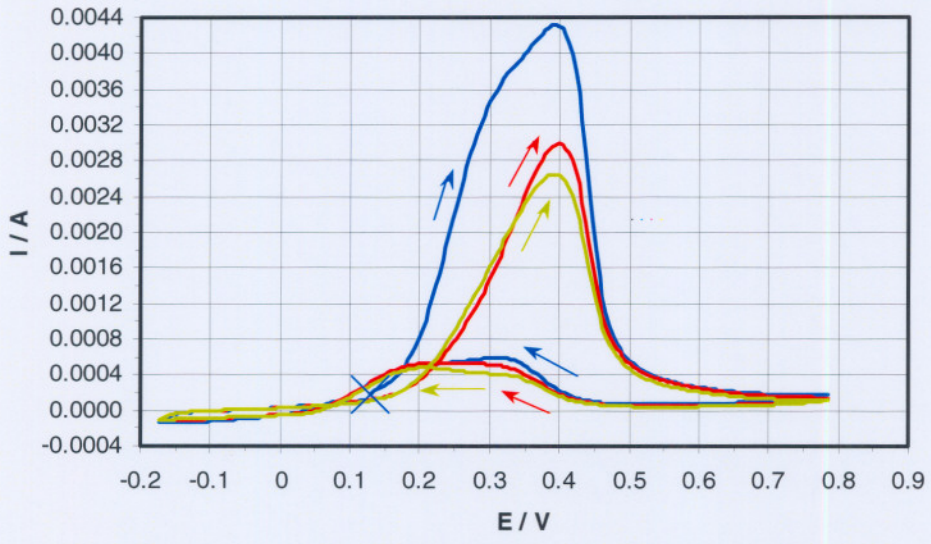

Figure 7.36: [Cu^{2+}] = 0 mol.dm^{-3}, [Fe^{3+}] = 0 mol.dm^{-3} Start Potential = 0.16 V, First Vertex Potential = 0.81 V, Second Vertex Potential = -0.14 V, Step potential = 0.0048 V, Scan Rate = 0.1 V/s, [H_2SO_4] = 0.5 mol.dm^{-3}, N_2

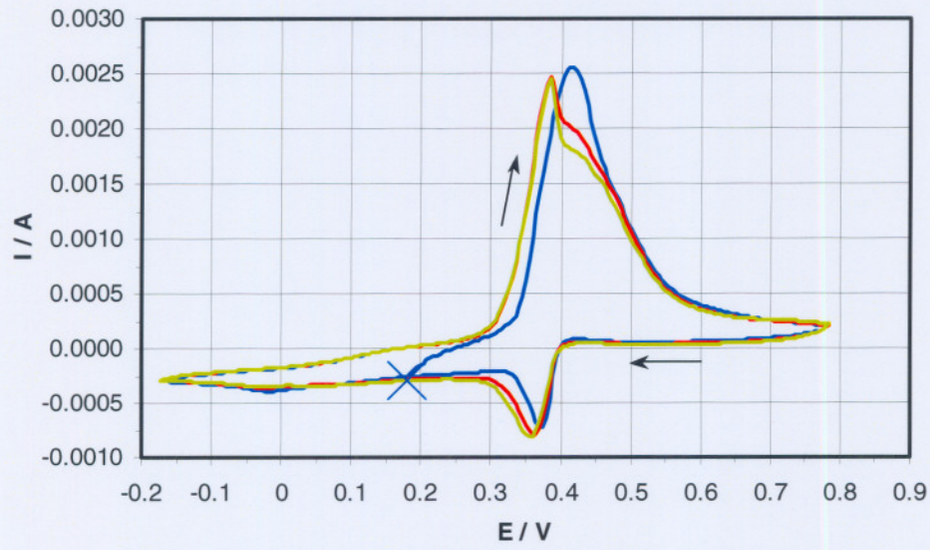

Figure 7.37: $[Cu^{2+}]$ = 0.01 mol.dm^{-3} ions in solution
Start Potential = 0.21 V, First Vertex Potential = 0.81 V, Second Vertex Potential = -0.14 V, Step potential = 0.0048 V, Scan Rate = 0.1 V/s, $[H_2SO_4]$ = 0.5 mol.dm^{-3}, N_2

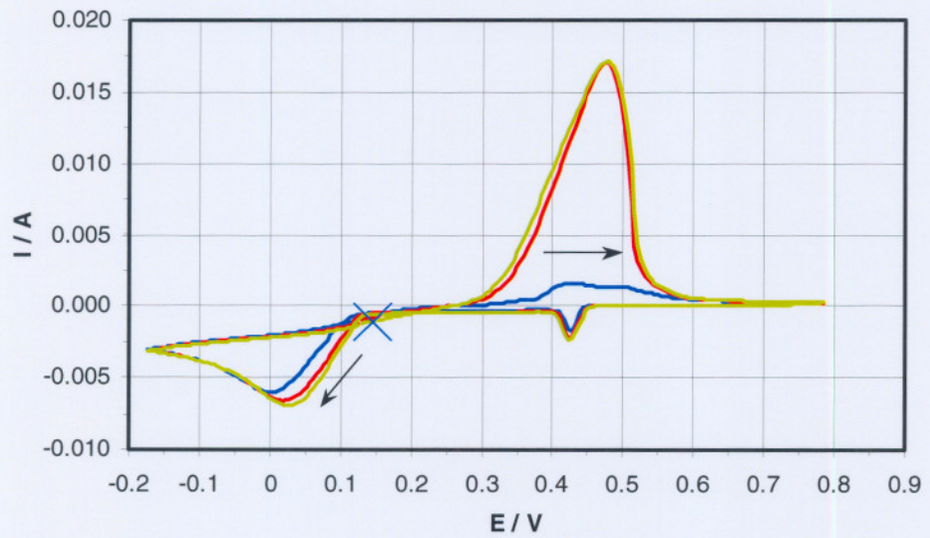

Figure 7.38: $[Cu^{2+}]$ = 0.1 mol.dm^{-3} ions in solution
Start Potential = 0.16 V, First Vertex Potential = 0.81 V, Second Vertex Potential = -0.14 V, Step potential = 0.0048 V, Scan Rate = 0.1 V/s, $[H_2SO_4]$ = 0.5 mol.dm^{-3}, N_2

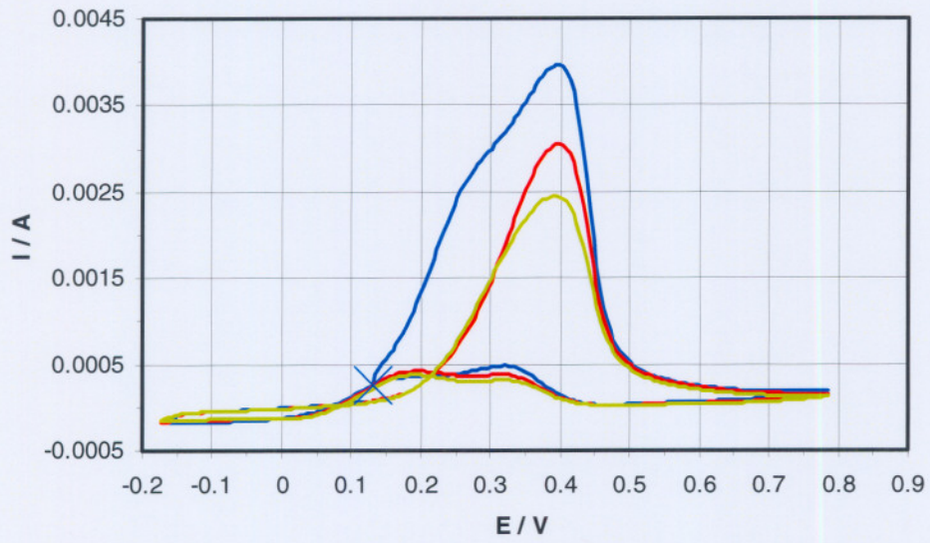

Figure 7.39: $[Fe^{3+}] = 0.01\ mol.dm^{-3}$

Start Potential = 0.16 V, First Vertex Potential = 0.81 V, Second Vertex Potential = -0.14 V, Step potential = 0.0048 V, Scan Rate = 0.1 V/s, $[H_2SO_4] = 0.5\ mol.dm^{-3}$, N_2 (Arrows as in Figure 7.36)

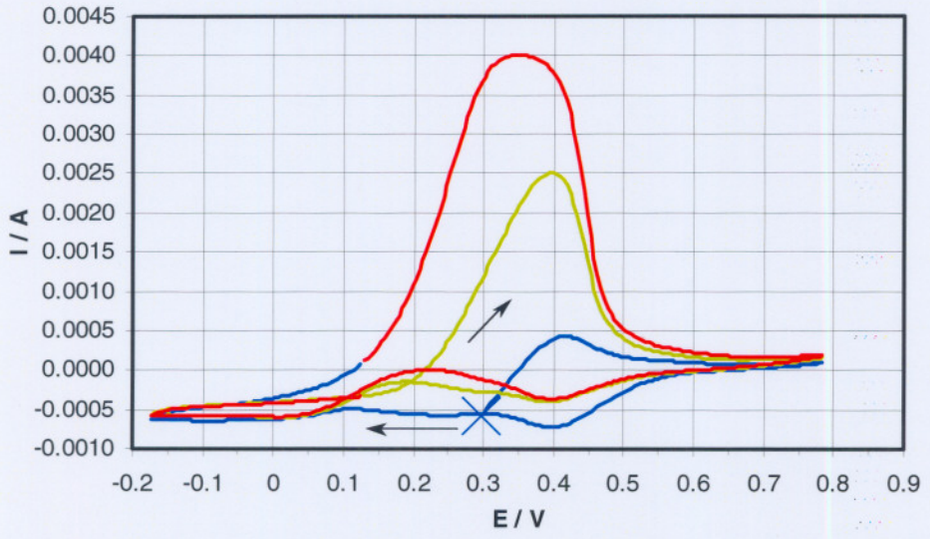

Figure 7.40: $[Fe^{3+}] = 0.1\ mol.dm^{-3}$

Start Potential = 0.33 V, First Vertex Potential = 0.81 V, Second Vertex Potential = -0.14 V, Step potential = 0.0048 V, Scan Rate = 0.1 V/s, $[H_2SO_4] = 0.5\ mol.dm^{-3}$, N_2

It appears that, at higher Cu(II) and Fe(III) concentrations, the cyclic voltammograms are dominated by the electrochemistry of the additives.
The cyclic voltammogram shape was compared with similar reported electrochemistry results from the literature. It was found that the overall shape of the cyclic voltammogram differs from those reported in literature. The addition of Fe(III) and Cu(II) resulted in cyclic voltammograms that seemed to be the combination of the electrochemistry of the electroactive species present. No distinct new peaks were identified and it appeared that the action of Fe(III) and Cu(II) cannot be readily studied by cyclic voltammetric mehods.

7.3 CHRONOPOTENTIOMETRY

The electrode preparation procedure for the chronopotentiometry part of the electrochemical study can be seen in Paragraph 6.2.2. With this electrochemical method, conducted on a rotating electrode, the potential was monitored against a normal calomel electrode (NCE). The study was conducted at different temperatures i.e. 7, 22, 30, 40, 50, 60, and 70°C.

The disc was rotating at 600 r.p.m. in a 0.5 mol.dm^{-3} sulphuric acid solution under a nitrogen atmosphere.

The electrode was initially polished *in situ* for between 20 and 30 seconds to create a new surface area. The polishing was then stopped and the chronopotentiogram was recorded for 2 minutes, since it was evident that the electrode surface became stable after about 100 seconds.

The data were compared to a model with two parallel first order reactions with the following form:

$$E_{(t)} = E_1 e^{-k_1 t} + E_2 e^{-k_2 t} + E_\infty \qquad 7.1$$

With $E(t)$ = measured potential at time t

$E(\infty)$ = equilibrium potential

k = rate constant

Because of the relation between specie concentration in solution or on the electrode surface and the potential, the potential was used as the variable in the description of the kinetics of the leaching reaction.

Results are presented in the following figures against the normal calomel electrode. The starting potential on the graph was taken just after the line stabilized and may therefore differ a bit from one chronopotentiogram to another.

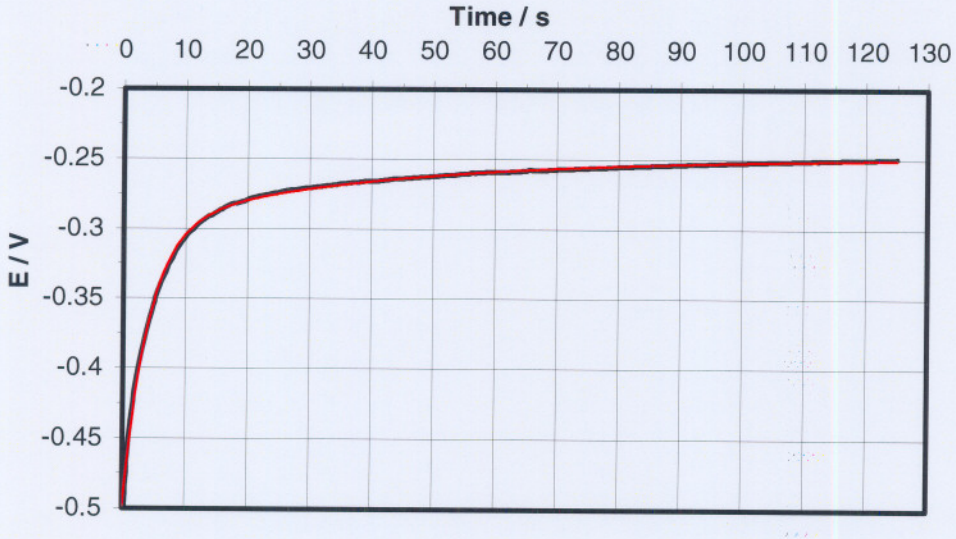

Figure 7.41:

Rotating electrode 1 in 0.5 mol.dm^{-3} H_2SO_4 at 7°C

— Experimental — Model

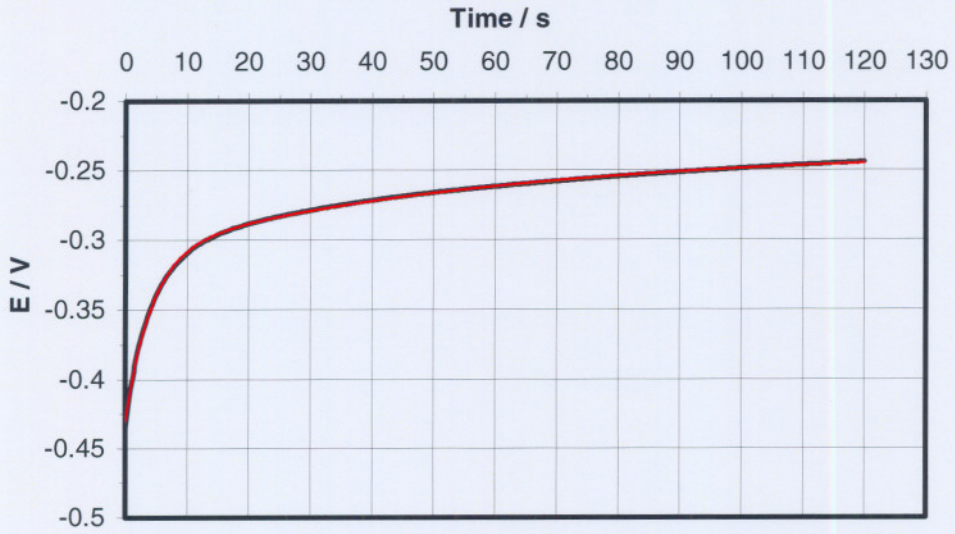

Figure 7.42:

Rotating electrode 1 in 0.5 H_2SO_4 mol.dm^{-3} at 22°C

— Experimental — Model

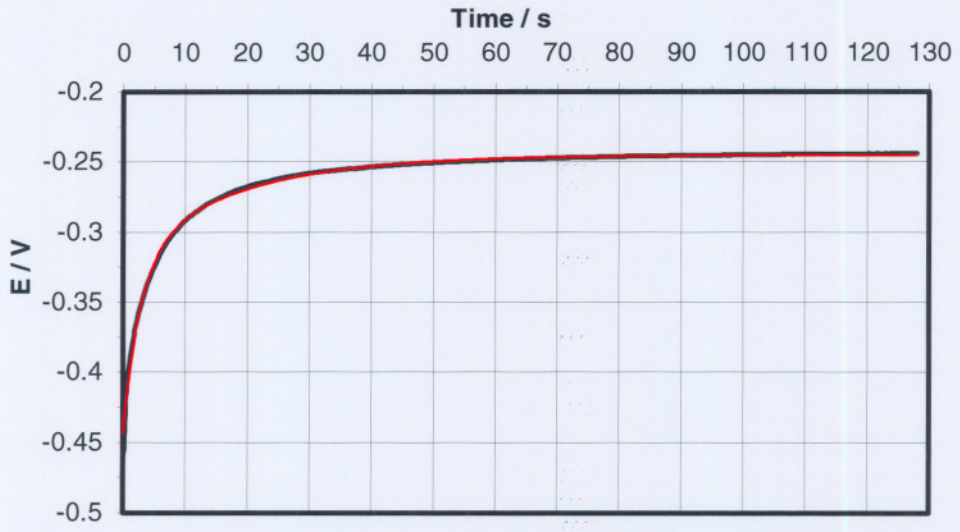

Figure 7.43:

Rotating electrode 1 in 0.5 mol.dm^{-3} H_2SO_4 at 30°C

— Experimental — Model

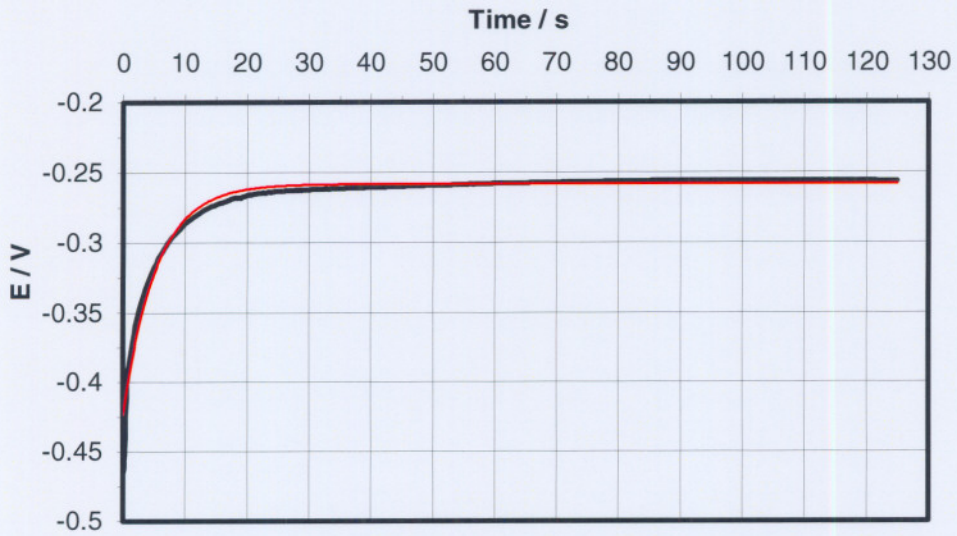

Figure 7.44:

Rotating electrode 1 in 0.5 mol.dm^{-3} H_2SO_4 at 40°C

— Experimental — Model

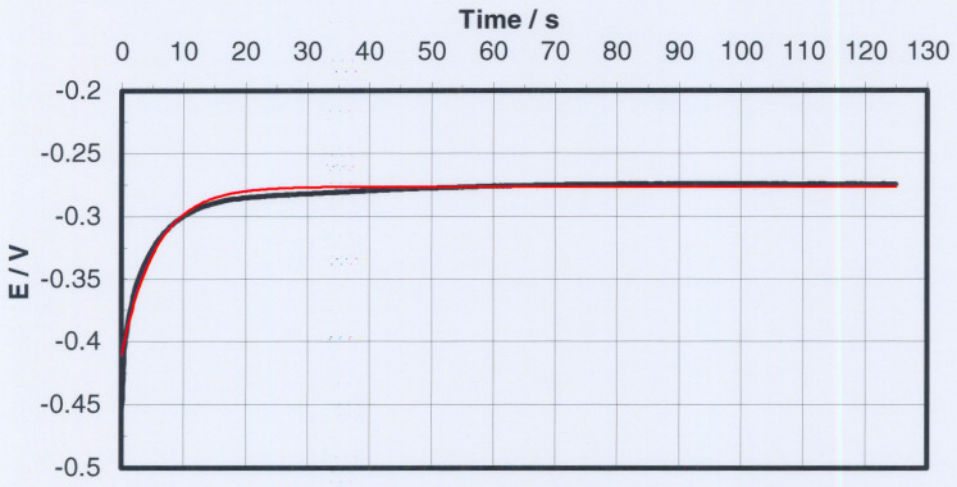

Figure 7.45:

Rotating electrode 1 in 0.5 mol.dm^{-3} H_2SO_4 at 50°C

— Experimental — Model

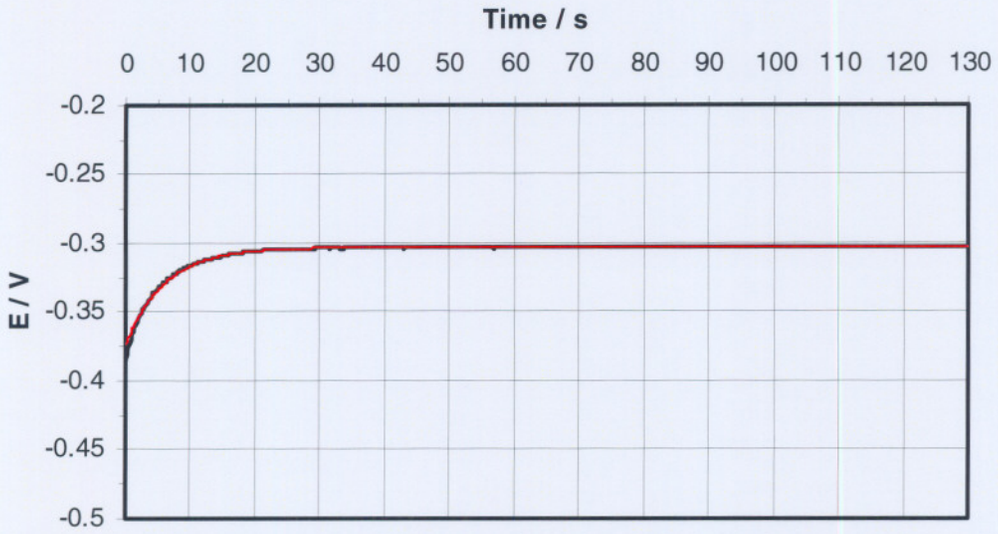

Figure 7.46:

Rotating electrode 1 in 0.5 mol.dm^{-3} H_2SO_4 at 60°C

— Experimental — Model

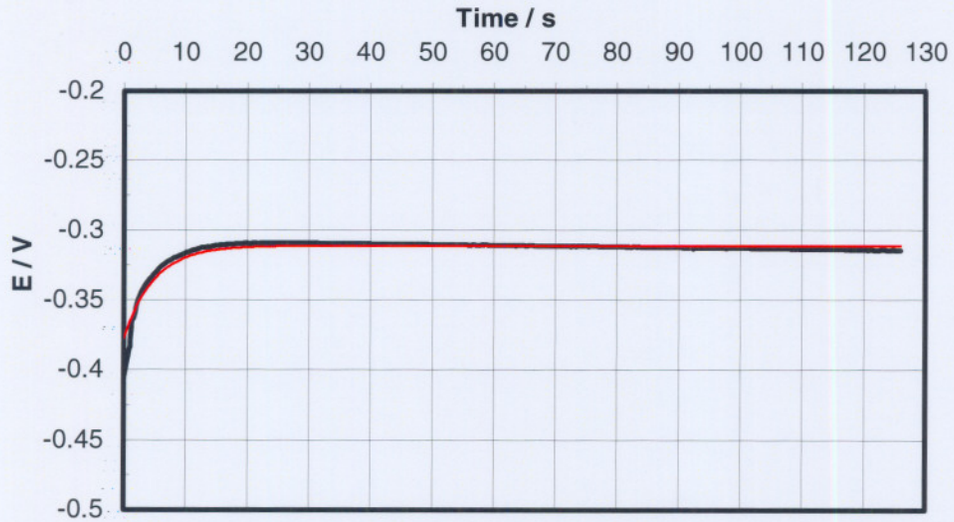

Figure 7.47:

Rotating electrode 1 in 0.5 mol.dm^{-3} H_2SO_4 at 70°C

— Experimental — Model

The general shape of the chronopotentiograms stayed the same at all temperatures. However, equilibrium was attained faster at higher temperatures. After a quick change on the fresh surface, the surface changed at a very slow rate. This is in accordance with the observations with thermal leaching where, after a rapid increase in leaching rate at the beginning, the leaching rate decreased slowly (see Figure 4.4). This may well also support the theory of a passivation layer that forms on the metal surface.

Table 7.6 Fitting parameters for equation 8.1

Temperature (°C)	E_1	E_2	E_∞	k_1	k_2
7	-0.198	-0.051	-0.248	0.246	0.027
22	-0.121	-0.072	-0.236	0.237	0.018
30	-0.046	-0.063	-0.245	0.351	0.056
40	-0.087	-9.733	-0.258	0.826	0.190
50	-0.087	-7.256	-0.276	0.826	0.181
60	-0.087	-1.44	-0.303	0.826	0.164
70	-0.087	-6.340	-0.311	0.826	0.206

Thermodynamic data can be obtained from potential measurements:

$$\Delta G = -nFE \qquad 7.2$$

$$\Delta S = nF\left(\frac{\delta E}{\delta t}\right)_P \qquad 7.3$$

$$\Delta G = \Delta H - T\Delta S \qquad 7.4$$

By plotting potential against temperature (See Figure 7.48) entropy was calculated and reported in Table 7.7. From the entropy ΔG and ΔH was also calculated.

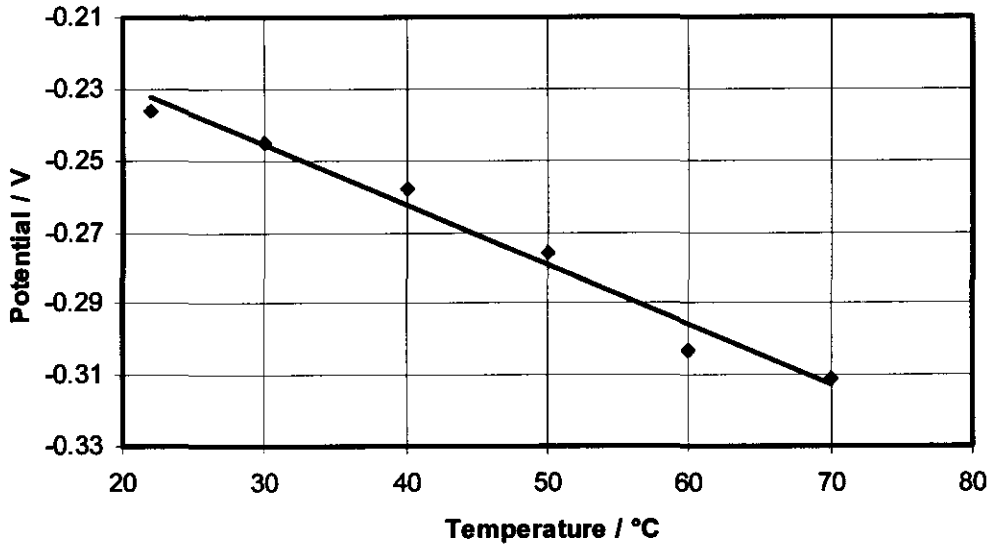

Figure 7.48 Plot of potential/V against temperature/℃

Table 7.7 Calculated thermodynamic values obtained from chronopotentiometric data

Gradient	*ΔS / (J.K^{-1}.mol^{-1})*	*ΔG / (kJ.mol^{-1})*	*ΔH / (kJ.mol^{-1})*
-0.0017	-109.35	15.32	-17.26

The calculated values fall within the range commonly encountered in electrochemistry (*Crow, 1994*).

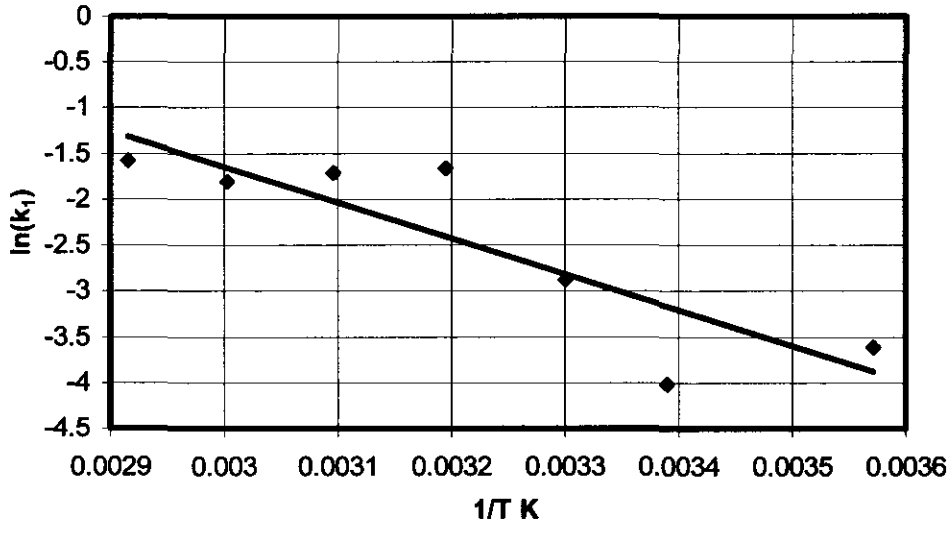

Figure 7.49 Plot of ln(k_1) against 1/T K

Table 7.8 Activation energy calculated from Figure 7.48

Gradient	*Activation energy* (E_A / *kJ.mol*$^{-1}$)
-3906 ± 991	32 ± 8

Although the value is within the range of activation energies previously measured, it cannot be used for mechanistic interpretations due to the large error.

CHAPTER 8

DISCUSSION OF RESULTS

In this chapter...

The leaching and electrochemistry results are discussed in the following paragraphs, with the aim to integrate the obtained results in order to better understand the leaching kinetics.

8.1 RELIABILITY OF RESULTS

The results obtained from the reproducibility studies, showed that the reproducibility in one pellet was fair, but from one pellet to another, it seemed that the reproducibility was poor. This was found to be true with regards to the pellets used in the leaching experiments as well as with the electrodes utilised during the electrochemistry studies. Since the pellets and electrodes were fabricated from the same Ni_3S_2 casting, the conclusion could be drawn that the casting was not homogenous. The reagents were mixed in a stoichiometric ratio and there was no indication that this ratio varied within the casting. Anisotropic crystal growth during the solidification of the molten Ni_3S_2 would probably cause the leach rate to vary for different surfaces within the pellet. In order to possibly explain and eliminate this factor, single crystal studies should be conducted. Electrochemical studies on single crystal Pt surfaces are well known and show that alternate surfaces exhibit substantial differences in electrochemical properties (*Christensen & Hamnett, 1994*). The average properties reported in this investigation should be a reliable representation of the properties for an aggregate of Ni_3S_2 crystals.

8.2 NATURE OF ACID

For the leaching and electrochemistry study, four acids were used i.e.:

- Non-complexing, oxidising: Nitric acid
- Complexing, non-oxidising: Hydrochloric acid
- Non-complexing, non-oxidising: Perchloric acid
- Industrial preference: Sulphuric acid

By looking at the leaching rates of the first hour compared between the different acids, it can be seen that an initial fast leaching rate was evident in all acids, while the dissolution rate flattened off towards the end of the leaching period. From the leaching runs, it was found that nitric acid gave the highest leaching rate, while hydrochloric acid yielded the lowest leaching rate.

Dissolution of Ni_3S_2 is partly an oxidation process, which is enhanced by the presence of oxidants. This explains why nitric acid yielded a high leaching rate, just as oxygen and iron(III) accelerated the dissolution process.

Dyson and Scott (1976) found that hydrochloric acid yielded a higher leaching rate than sulphuric acid, which seems to contradict the current study's results. *Dyson and Scott* used 5 $mol.dm^{-3}$ HCl and 2.5 $mol.dm^{-3}$ H_2SO_4 solutions, and between 97 and 99% Ni extraction was obtained within 1 to 2 hours. They reported that sulphuric acid was less satisfactory than hydrochloric acid since either more free acid remained in solution, or less nickel was extracted at a lower free acidity in the presence of sulphuric acid. The results of *Dyson and Scott* are not in conflict with the results of this study when it is taken into consideration that the $[H_3O]^+$ of 5 $mol.dm^{-3}$ HCl is much higher than that of 2,5 $mol.dm^{-3}$ H_2SO_4. Furthermore, $NiCl_4^{2-}$ complex forms at high chloride concentrations (*Cotton & Wilkonson, 1999*), while at low HCl concentration complexation is too low to bring about a pronounced effect. Perchloric acid is well known as a poor complexing and non-oxidising agent in dilute solutions, with a comparable leaching rate to that of hydrochloric acid.

The pH of 0.5 mol.dm^{-3} sulphuric acid is not substantially lower than that of 0.5 mol.dm^{-3} perchloric acid. It is not clear why sulphuric acid was found to be a better leaching agent than perchloric acid.

8.3 TEMPERATURE DEPENDANCY

Leaching experiments were conducted over the temperature range of 22 to 75°C. Calculated activation energies are shown in Table 8.1, which are compared to reported activation energies in the literature.

Table 8.1 Comparison of the activation energies for the acid leaching of nickel sulphides

Source	*Leaching system*	E_A *(kJ.mol^{-1})*	*Reported rate limiting step*
Bredenhann & van Vuuren, 1999	NiS in H_2SO_4 with $NaNO_3$	88	Surface chemical reaction changing into a diffusion controlled mechanism
Mulak, 1985	Ni_3S_2 in HNO_3	42.1 ± 0.8	Surface chemical reaction
Mulak, 1987	Ni_3S_2 in HNO_3 with Fe(III) ions	103.6 ± 4.2	Electrochemical surface reaction
Kanome et al., 1987	Ni_3S_2 in H_2SO_4	24.8	Diffusion
Filmer & Nicol, 1980	Ni_3S_2 + Ni metal Ni_3S_2 + Ni_7S_6	65 ± 5 54 ± 5	Chemical or electrochemical reaction on the surface
Current study (Initial stage)	Ni_3S_2 in H_2SO_4	28.2	(Surface chemical reaction)
Current study (Steady stage)	Ni_3S_2 in H_2SO_4	45.75	(Surface chemical reaction)

Investigations of leaching systems often indicate that surface chemical reactions are rate controlling. Criteria that support this observation are the fact that the reaction rate is proportional to reactive mineral surface area, there is

no dependence of reaction rate on agitation, the reaction rate is highly temperature dependent and there is usually no dependence of reaction rate on solution concentration of products (*Peters, 1992*). This study's leaching system seems to be supportive of the above-mentioned factors that support a chemically controlled mechanism.

With an increase in temperature between 1 and 2°C, the diffusion constant becomes between 1 to 2% higher (*Bard & Faulkner, 1980*). This translates to an activation energy of between 7 and 13 $kJ.mol^{-1}$ for diffusion controlled reactions. According to the above, the experimental activation energies of 28.23 $kJmol^{-1}$ and 45.75 $kJmol^{-1}$ are indicative of chemical processes during the rate determining step. This is in accordance with the conclusions reported by most authors (see Table 8.1).

Kato and Oki (1973) reported that the activation energy for diffusion of a nickel atom inside Ni_3S_2 relates to 1 $kcal.mol^{-1}$. This value is not comparable with 24.8 $kJ.mol^{-1}$ reported by *Kanome et al. (1987)*, who ascribed it to a diffusion controlled rate limiting step. This seems too high for a diffusion step.

8.4 INFLUENCE OF NITROGEN, OXYGEN, Fe(III) AND Cu(II) IONS

It was evident that O_2 accelerated the leaching rate of heazlewoodite in an acid medium up to three times. The following reaction equations can describe the overall leaching reactions by sulphuric acid in the presence of oxygen:

$$Ni_3S_2 + ½\ O_2 + H_2SO_4 \rightarrow NiSO_4 + 2NiS + H_2O \qquad 8.1$$

$$NiS + 2O_2 \rightarrow NiSO_4 \qquad 8.2$$

Leaching rates were found to be up to eight times faster in the presence of Fe(III) than in the case of de-aerated acid solutions. This occurred even when sub-stoichiometrical amounts of Fe(III) were present. Oxygen only slightly enhanced the leaching rate when Fe(III) was present.

$$Ni_3S_2 + 2Fe^{3+} \rightarrow 2Fe^{2+} + 2NiS + Ni^{2+} \quad 8.3$$

$$2Fe^{2+} + 2H^{+} + \tfrac{1}{2}O_2 \rightarrow 2Fe^{3+} + H_2O \quad 8.4$$

The oxidation of iron(II) ions in solution, as in equation 8.4, is slow in acid solutions. This in turn affects the oxidation of Ni_3S_2 as given in equation 8.3. Work conducted by *McKay and Halpern (1958)* showed that the kinetics of the iron(II) oxidation reaction were second order with regards to partial oxygen pressure.

It is well known that iron acts as an electron carrier and one of the proposed mechanisms can be seen in Paragraph 2.6.2.2 (*Dobrokhotov, 1959*). This still does not fully explain why the iron(III) at low concentrations in the absence of oxygen still had such a pronounced effect (see Table 4.6). It can only be assumed that iron(III) is not the sole oxidant, but that H^+ ions continue to oxidise the nickel sulphide.

The Cu(II) ions had an even greater effect on the leaching rate of the heazlewoodite. A possible initial reaction equation can be seen in reaction 8.5:

$$2Ni_3S_2 + 2CuSO_4 + H_2SO_4 + \tfrac{1}{2}O_2 \rightarrow Cu_2S + 3NiS + 3NiSO_4 + H_2O \quad 8.5$$

Another possibility may be:

$$Ni_3S_2 + Cu^{2+} \rightarrow 2NiS + Cu + Ni^{2+} \quad 8.6$$

Electrochemical data shows that Cu(II) and Fe(III) ions standard reduction potentials i.e. 0.342 V and 0.771 V, are strong enough oxidants to enhance the leaching rate of the nickel sulphide (*CRC Handbook of Chemistry and Physics, 2003*). The millerite can then be oxidised in an acid medium and in the presence of oxygen. CuS is soluble in diluted acid while Cu_2S is slightly soluble. Cu^+ is very easily oxidised in the presence of oxygen and so the probability of the formation of Cu_2S should be less than the probability of Cu

metal forming. During the scanning electron microscopy, this seemed to be the case, since a precipitate of copper metal was found on the heazlewoodite surface.

According to the Pourbaix diagram, Ni_3S_2 is oxidised at a pH of 0.4 by H^+. This implies that heazlewoodite will reduce Cu^{2+} to the Cu^0 state.

$H^+ + e^- \rightarrow ½ H_2$	$E_0 = 0,0V$	8.7
$Cu^{2+} + 2e^- \rightarrow Cu$	$E_0 = 0.34V$	8.8

Metallic copper on the Ni_3S_2 surface will cause a galvanic couple that will increase the corrosion rate on the more oxidisable conducting surface: in this case the Ni_3S_2.

8.5 ELECTROCHEMISTRY

The electrochemistry of Ni_3S_2 is dominated by irreversible oxidation-reduction processes (see Figures 7.1 and 7.2). The dissolution process is further complicated by the simultaneous occurrence of acid-base reactions. The purpose of this study was to gather information on the leaching of heazlewoodite. It was decided to do an exhaustive electrochemical investigation, but to perform electrochemistry experiments that would further the stated purpose.

8.6 PROPOSED LEACHING MODEL

Previous investigators used the shrinking-core model to describe the leaching of nickel sulphide grains. In this study, resin embedded pellets were used with only one flat surface exposed to the acid. For a simple dissolution reaction the dissolution reaction rate = rate constant x surface area. The flat surface simplifies the model in all cases to a zero order model because the surface area is constant. The shrinking-core model is applicable only to spherical particles. Therefore, the problems associated with this model with regards to

particle shape and size, distribution and surface roughness (*Velardo et al., 2002*) are avoided.

When leaching a flat surface of a thick pellet, the leaching rate will become constant once all surface layers have reached equilibrium conditions. This pseudo equilibrium will be maintained, regardless of the chemical process, until the pellet is dissolved. With small particles this is not possible, since the particles shrink at a fast rate and equilibrium is never reached.

The data obtained during this study is not directly applicable to a leaching plant because the kinetic data for the non-equilibrium situation with small particles were not investigated. Thermodynamic data i.e. activation energy as well as electrochemical data will be more reliable when the substrate stays constant.

8.6.1 QUALITATIVE DESCRIPTION OF SURFACE OXIDATION OF Ni_3S_2

The cyclic voltammograms reported in Chapter 7 can be used to describe the proposed surface changes of Ni_3S_2 during the leaching process. The peaks in the cyclic voltammograms are oxidation peaks without reduction peaks and thus conventional description of oxidation followed by reduction will not be used.

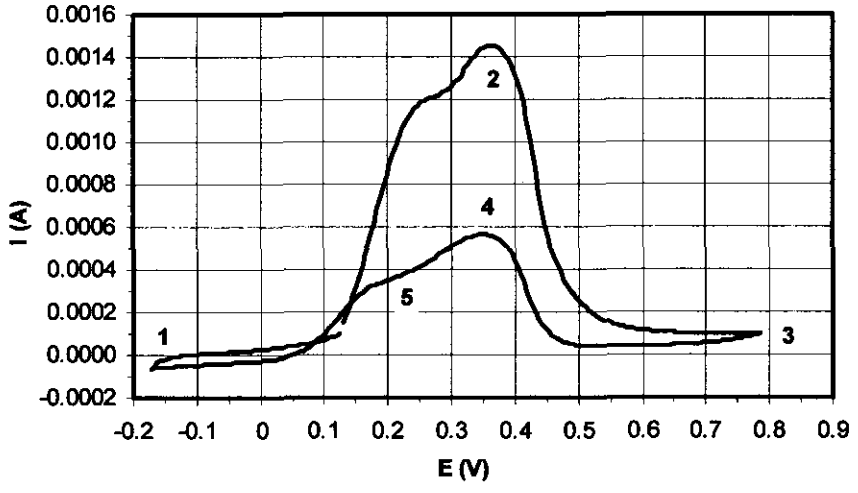

Figure 8.1 Example of a typical cyclic voltammograms of Ni_3S_2 in dilute H_2SO_4

A qualitative description of numbers 1 to 5 of the cyclic voltammogram in Figure 8.1 can be seen in Table 8.2.

Table 8.2 Qualitative description of Figure 8.1

Number	*Sketch*	*Description*
1		At this potential the surface is active and consists of unmodified Ni_3S_2. The potential is too negative to cause oxidation.
2	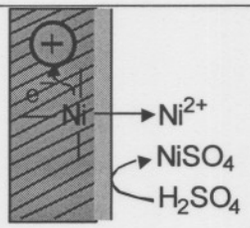	Oxidation is now taking place. An inactive phase may start to form. Rapid chemical dissolution is occurring. The appearance of two oxidation peaks on cyclic voltammograms is indicative that two distinctive phases are formed at the surface.
3	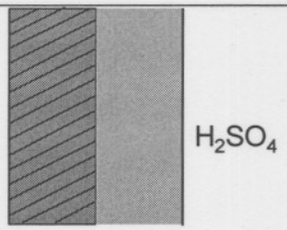	An inactive phase is now dominating on the surface and the chemical dissolution of the surface has become very slow.
4	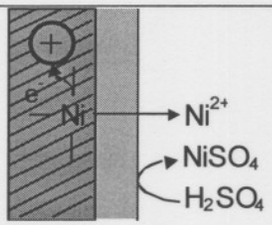	The potential is too low to keep the inactive phase intact and the inactive layer is dissolving slowly in the acid. The oxidation and chemical dissolution process increases again but the surface does not reach the same conditions as at point 2.
5	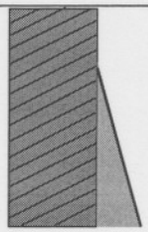	The potential is so low that the oxidation process is occurring slowly. The inactive phase is still dissolving and the unmodified surface starts to reappear.

8.6.2 QUALITATIVE DESCRIPTION OF THE LEACHING PROCESS

The acid leaching process in the absence of additional oxidants will be described as an acid-base reaction and an oxidation reaction by H^+.

Overall leaching reaction:

$$Ni_3S_2 + 3H_2SO_4 \rightarrow 3NiSO_4 + 2H_2S + H_2 \qquad 8.9$$

The reaction does not occur in a single step, but an inactive sulphur rich phase is formed on the nickel sulphide surface.

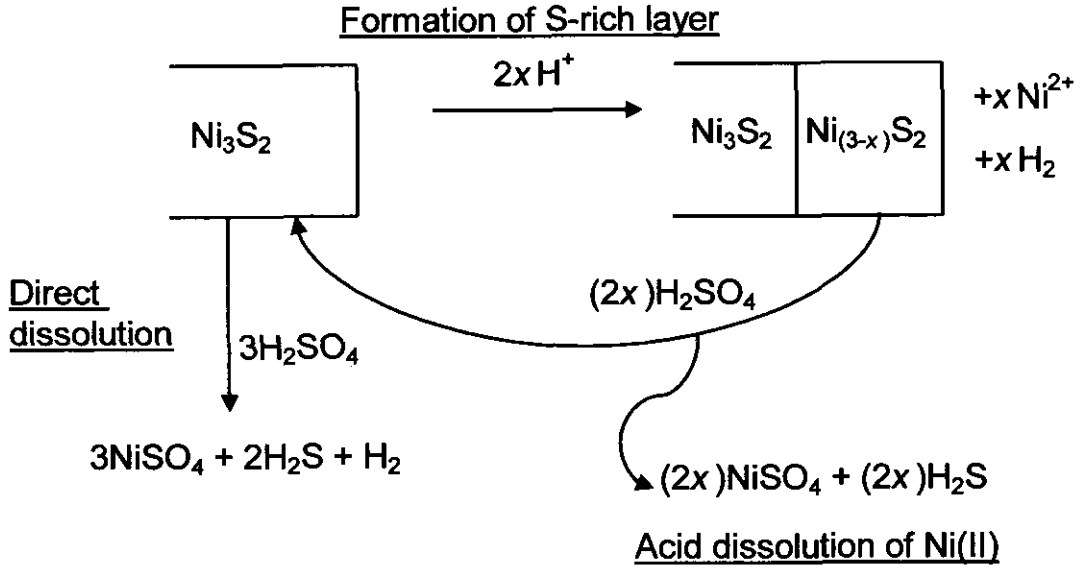

Figure 8.2 Proposed empirical model for the leaching process

This model is in accordance to the major features of the experimental observations.

The initial fast leaching rate occurs while the inactive sulphur rich layer is still thin. Once this layer has reached its equilibrium thickness, the leaching rate becomes constant. Oxidants will enhance the oxidation rate resulting in a faster direct oxidation, as well as a thicker inert layer. In the electrochemical

oxidation this inert layer could nearly halt the dissolution. No chemical oxidant was found that could oxidise the Ni_3S_2 to the same degree.

8.7 CONCLUSIONS

A similar model for the thermal leaching and electrochemistry of Ni_3S_2 describes the experimental observations successfully. The major properties of the leaching process are:

- The leaching reaction is a combination of oxidation and acid-base reactions.
- A less active surface layer inhibits the reaction.
- The hydronium ion is sufficient to oxidise the nickel sulphide, but additional oxidants enhance the leaching rate.
- A too high oxidation potential may lead to deactivation of the nickel sulphide surface.
- The reaction rate is controlled by surface reactions and not by diffusion through the solvent or the solid surface layer on the nickel sulphide.
- The leaching leads to surface roughening.
- The leaching rate is influenced by the orientation of the nickel sulphide crystals.

Previous electrochemical investigators measured over a wide potential range. However, in this study it was found that the dissolution rate determining processes are controlled over a small potential range of 0.25 – 0.55 V. When attempting to improve existing leaching processes or developing new leaching technology, it should be taken into consideration that small changes in oxidants may have a large influence on the leaching rate.

8.8 RECOMMENDED FUTURE WORK

From the results obtained by this thermal leaching and electrochemical studies, the following test work can be recommended:

1. Single crystal studies on nickel sulphide. This eliminates the formation of different crystal planes, which will prevent the leaching rate to vary between these planes, as was proposed in this study.
2. Study of the different phases formed during the leaching of Ni_3S_2 and the influence of these phases on the reaction rate and mechanism.
3. Include copper sulphide and platinum group metals in the nickel sulphide to better represent the commercially used nickel-copper matte.

APPENDIX I

LIST OF MINERALOGICAL TERMS

CHEMICAL FORMULA	*MINERALOGICAL TERM*
Ni_3S_2	Heazlewoodite
NiS	Millerite
Ni_3S_4	Polydymite
Ni_7S_6	Godlevskite
Cu_2S	Chalcocite
CuS	Covellite
$Cu_{1.8}S$	Digenite
$CuFeS_2$	Chalcopyrite
$Cu_{1.96}S$	Djurleite
$Fe_{1-x}S$	Pyrrhotite
FeS	Troilite

BIBLIOGRAPHY

Aral, K., Sunada, S., Iwata, M. and Izaki, T., *J. Japan Inst. Metals*, 1982, **45 (8)**, 787

Atkins, P.W., **Physical Chemistry**, Oxford University Press, New York, 6th Ed., 1998

Bard, A.J., and Faulkner, L.R., **Electrochemical Methods. Fundamentals and Applications**, Wiley & Sons. 1980

Betova, I., Bojinov, M., Kinnunen, P., Laitinen, T., Pohjanne, P. and Saario, T., Electrochimica *Acta*, 2002, **47**, 2093

Bojinov, M., Fabricius, G., Kinnunen, P., Laitinen, T., Mäkelä, K., Saario, T. and Sundholm, G., *Electrochimica Acta*, 2000, **45**, 2791

Bredenhann, R. and van Vuuren, C.P.J., *Minerals Engineering*, 1999, **12 (6)**, 687

Christensen, P.A. and Hamnett, A., **Techniques and mechanisms in electrochemistry**, 1st Ed., Blackie Academic. 1994, 263

Cotton, F.A. and Wilkinson, G., **Advanced Inorganic Chemistry**, 6th Ed., Wiley & Sons, 1999, 837

CRC Handbook of Chemistry and Physics, 84th Edition, CRC Press, 2003

Crow, D.R., **Principles and applications of electrochemistry**, 4th Ed., Blackie Academic & Professional, 1994, 162

Dobrokhotov, G.N., *Journal of Applied Chemistry of the USSR*, 1959, **32**

Dutrizac, J.E. and Chen, T.T., *Canadian Metallurgical Quarterly*, 1987, **26(4)**, 265

Dyson, N.F. and Scott, T.R., *Hydrometallurgy*, 1976,**1**, 361

Filippou, D., Konduru, R. and Demopoulos, G.P, *Hydrometallurgy*, 1997, **47**,1

Filmer, A.O. and Nicol, M.J., *Journal of the South African Institute of Mining and Metallurgy*, 1980, 415

Garrels, R.M. and Christ, C.L., **Solutions, Minerals, and Equilibria**, Harper and Row, 1965

Gerlach, L., Pawlek, F. and Rictesel, H., *Erzmetall*, 1970, **23**, 486

Ghali, E., Subrahmanyam, D.V., Legault, J. and Tremblay, R., *Surface Technology*, 1979, **8**, 195

Greenwood, N.N. and Earnshaw, A., **Chemistry of the Elements**, 2nd Ed., Butterworth-Heinemann, 1997, 1145

Hackl, R.P., Dreisinger, D.B., Peters, E. and King, J.A., *Hydrometallurgy*, 1995, **39**, 25

Hillrichs, E. and Bertram, R., *Hydrometallurgy*, 1983,**11**,181

Hillrichs E and Bertram R, *Hydrometallurgy*, 1983,**11**, 195

Hofirek, Z., The chemistry of the nickel-copper matte leach process at Rustenburg Refiners, *Internal report*, 1988

Hofirek, Z. and Kerfoot, D.G.E., *Hydrometallurgy*, 1992, **29**, 357

Hofirek, Z. and Nofal, P.J., *Hydrometallurgy*, 1995, **39**, 91

Jha, M.C., Carlberg, J.R. and Meyer, G.A., *Hydrometallurgy,* 1983, **9**, 349

Kanome, O., Abe, H., Okuwaki, A. and Okabe, T., *Hydrometallurgy,* 1987, **19**, 1

Kato, T. and Oki, T., *Japan Institute of Metals Journal,* 1973, **37**, 1338

Lorenzen, L., *Chemical Engineering in the new South Africa,* 1991, **1(B5)**, 1

Marcus, P. and Protopopoff, E., *Corrosion Science*, 1997, **39(9)**, 1741

McKay, D.R. and Halpern, J., *Transactions of the Metallurgical Society of AIME*, 1958, 301

Meng, X. and Han, K.N., *Minerals and Metallurgical Processing*, 1993, 128

Mulak, W., *Hydrometallurgy*, 1983, **11**, 79

Mulak, W., *Hydrometallurgy*, 1985,**14**, 67

Mulak, W., *Hydrometallurgy*, 1987, **17**, 201

Nicol, M.J. and Scott, P.D., *Journal of the South African Institute of Mining and Metallurgy,* 1979

Nicol, M.J., *Hydrometallurgy: Research, Development and Plant Practice,* 1983

Okuwaki, A., Kanome, O. and Okabe, T., *Metallurgical Transactions B.* 1984, **15B**, 609

Parker, A.J., Paul, R.L. and Power, G.P., *J. Electroanal. Chem.,* 1981, **118**, 305

Perry, R.H. and Green, D., **Perry's Chemical Engineers' Handbook** , 6th Ed., McGraw – Hill. 1984, 4

Peters, E., *Metallurgical Transactions B,* 1976, **7B**, 505

Peters, E., *Trends in Electrochemistry,* 1977, 267

Peters, E., **Hydrometallurgy: Theory and practice course notes,** (Rustenburg Base Metals Refinary, Library), 1992, Chapter IV

Plasket, R.P. and Romanchuk, S., *103rd Annual General Meeting of the AIME, Dallas,* 1974

Pourbaix, M., **Atlas of electrochemical equilibria in aqueous solutions,** Pergamon Press, 1966

Power, G.P., *Aust. J. Chem,* 1981, **34**, 2287

Power, G.P., *Electrochimica Acta,* 1982, **27(3)**, 359

Provis, J.L., Van Deventer JSJ, Rademan JAM and Lorenzen L, *Hydrometallurgy*, 2003, **2139**, 1

Rademan, J.A.M., Lorenzen, L. and Van Deventer, J.S.J., *Hydrometallurgy,* 1999, **52**, 231

Rieger, P.H., **Electrochemistry**, 2nd Ed., Chapman & Hall, New York, 1994, 60

Robinson, D.J., **An introduction to the Chemistry and Refining of the Platinum Group Metals, Course Notes**, ANGLO AMERICAN PLATINUM CORPORATION, 2001

Scherer, J., Ocko, B.M. and Magnussen, O.M., *Electrochimica Acta,* 2003, **00**, 1

Scott, P.D. and Nicol, M.H., *Trends in Electrochemistry,* 1976, 303

Scott, P.D. and Nicol, M.J., The kinetics and mechanism of the non-oxidative dissolution of some iron sulphides in aqueous acidic solutions. *National institute for Metallurgy Report No. 1858*, 1976

Sinev, L.A., Soboleva, T.R. and Sharmo, E.A., *Izv. Vyssh. Ucheb. Zaved. Tsvetn. Metall.*, 1975, **4**, 35

Skoog, D.A., Holler, F.J. and Nieman, T.A., **Principles of Instrumental Analysis**, 5th Ed., Saunders College Publishing, 1998

User Manual for General Purpose Electrochemical Systems, Version 4.2, Eco Chemie B.V. Utrecht, 1995

Velardo, A., Giona, M., Adrover, A., Pagnanelli, F. and Toro, L., *Chemical Engineering Journal,* 2002, **90**, 231

Wagner, C. and Traud, W., *Electrochem.*, 1938, **44**, 391

BEDANKINGS

Hiermee betuig ek my opregte dank en waardering aan:

- ons Hemelse Vader sonder Wie niks moontlik is nie en Wie my gedra het in die moeilike asook die goeie tye;

- my ouers, vir hulle nimmereindigende liefde en ondersteuning en omdat hulle in my glo;

- Quintus, vir al sy aanmoediging, liefde en ondersteuning;

- dr. G. Lachmann en prof. D. Bruinsma vir die leiding en onvoorwaardelike hulp;

- Anglo Platinum wat die studie 'n moontlikheid gemaak het, asook vir die finansiële ondersteuning;

- my vriende en familie vir hulle ondersteuning en liefde;

- die studente en personeel by die Skool vir Chemie en Biochemie vir hulle vriendskap en ondersteuning.

YOLANDÉ ZAAYMAN

2004-11-05